A VAP-33 homologue: a possible role in intracellular signalling and membrane structure in neurons

Susan Middleton

A thesis submitted for the degree of Doctor of Philosophy

The University of Edinburgh

2005

Declaration

I declare that this thesis was composed entirely by myself and the work on which it is based is my own, with the following exceptions noted below and acknowledged in the text:

BiP northern blot was carried out by Dr Paul Skehel (University of Edinburgh)

Cross-linking of VAPB and VAPBP56S was carried out by Dr Paul Skehel (University of Edinbugh)

Abstract

VAMP/synaptobrevin-associated protein of 33kDa (VAP33) was first identified in *Alplysia californica*. There are two mammalian homologues of VAP33 named VAPA and VAPB both of which are ubiquitously expressed and have been found to associate with the endoplasmic reticulum (ER) (Skehel et al. 2000). We have evidence that wild type VAPA and VAPB behave differently in Triton X-114 and that VAPB may not be integral to the ER. These proteins are type II membrane proteins and have a N-terminal Major Sperm Protein (MSP) domain, a coiled-coil domain and a transmembrane domain. Deletion of the yeast VAPA homologue, SCS2, disrupts the regulation of the inositol biosynthesis system and the Unfolded Protein Response (UPR) from the ER. Also in *Caenorhabditis elegans* the MSP is involved in structural motility and has an Eph receptor-dependent signalling function during oocyte maturation. This raises the interesting possibility that in addition to a structural role, the VAP proteins may also provide a signalling function. The MSP domain of the protein may be of particular importance for such signalling activity. Specifically, we have found that when the VAPA MSP domain alone is expressed in neurons it aggregates, activates components of ER stress pathways, and induces apoptosis via caspase 3. It is possible, therefore, that VAP proteins may activate intracellular signalling pathways through regulated interactions of their MSP domains, and that aggregations of MSP-containing polypeptides may disrupt these systems. A yeast two-hybrid screen was carried out using the MSP domain of VAPA and several potentially positive interacting proteins have been identified including ATF6 and DnaJ, which corroborate this hypothesis.

These results have clinical implications as a missense mutation in the VAPB gene has recently been identified as being associated with an atypical form of amyotrophic lateral sclerosis (ALS8) (Nishimura et al. 2004). The P56S VAP-B mutation lies within the highly conserved MSP domain. P56 is conserved in all VAP proteins. The X-ray structure of the nematode MSP has been solved and the P56S substitution is predicted to affect the multimerization state of the protein. Wild type VAP-A and B are expressed in motor neurons but do not accumulate at the synaptic junction. We introduced the P56S mutation into mouse VAP-B and expressed it as a GFP-fusion in primary neurons. The substitution has a profound effect on the sub-cellular distribution of the protein, causing accumulation of membrane associated protein aggregates. Such a dramatic change in the sub-cellular distribution would most likely disrupt the normal function of the protein. The P56S substitution is unlikely therefore to represent a normal functioning polymorphism further supporting the proposal that the mutation in the VAP-B gene is the cause of disease in the ALS affected Brazilian family.

Acknowledgements

Firstly, I would like to thank my supervisor Paul Skehel for all his instruction, support, patience and wisdom over the last three years. I would also like to thank Jeanette, Aidrien and Lorna for their help and support at various times during this project. The members of the diminishing fourth floor also deserve thanks for their encouragement and support.

Finally I would like to thank my mum and my friends for keeping me sane through this whole thing.

Index of Figures

Chapter 6

Index of Tables

List of abbreviations

Aβ	Amyloid β
ALS	Amyotrophic lateral sclerosis
Apaf-1	Apoptosis Protease Activating Factor 1
Apo E	Apolipoprotein E
APP	β Amyloid prcursor protein
AR-JP	Autosomal recessive juvenile parkinsonism
ATF6	Activating transcription factor 6
BAK	Bcl-2 homologous antagonist/killer
BAP-31	B-cell leukaemia 2 associated protein of 31 kDa
Bcl-2	B-cell leukaemia 2
Bet-1	Blocked early in transport 1
BFP	Blue Fluorescent Protein
Bid	BH3 interacting domain death agonist
Bim	Bcl2 interacting mediator of cell death
BoNT	Botulinium Neurotoxin
Ca^{2+}	Calcium ion
Caspase	Cysteine dependent aspartate specific proteases
CHOP	C/EBP-homologous protein
COPI	Coatamer complex protein I
DTT	Dithiothreitol
DAG	Diacyl glycerol
DIABLO	Direct IAP binding protein with low pI
eIF2α	eukaryotic Initiation Factor α
EM	Electron microscopy
EOR	ER overload response
ER	Endoplasmic reticulum
ERAD	Endoplasmic reticulum associated degradation
Erp57	Endoplasmic reticulum protein 57
GFP	Green Fluorescent Protein
GLUT-4	Glucose transporter 4
GRP78/BiP	Glucose regulated protein of 78 kDa
GRP94	Glucose regulated protein of 94 kDa
GTP	Guanine triphosphate
HAC	homocysteine and cysteine
HCV	Hepatitis C Virus
HEK	Human embryonic kidney
INO	Inositol
IP_3	Inositol phosphate
IRE1	Inositol-requiring 1
JNK	c-Jun N terminal kinase
KDEL	Lys-Asp-Glu-Leu
LRP	Low-density lipoprotein receptor-related protein
MAM	Mitochondria associated endoplasmic reticulum membrane

mCu	mitochondrial Calcium ion uniporter
MFP1	Membrane Fibre Protein 1
MFP2	Membrane Fibre Protein 2
mNCE	mitochondrial Sodium ion/calcium ion exchanger
MOSPD	Motile sperm domain containing protein
MPOP	Membrane Phosphoprotein
MPP^+	1-Methyl-4-phenylpyridinium
mPTP	mitochondrial Permeability transition pore
MSP	Major Sperm Protein
NEM	N-ethylmaleimide
NSF	N-ethylmaleimide sensitive fusion protein
6OHDA	6-hydroxy-dopamine
OMM	Outer mitochondrial membrane
OPI	Overproduction of inositol
OSBP	Oxysterol binding protein
PA	Phosphatidic acid
PACS2	Phosphofurin acidic cluster sorting protein 2
PaPD	periplasmic chaperone
PC	Phospatidyl Choline
PDI	Protein disulphide isomerase
PE	Phosphatidyl ethanolamine
PERK	Protein kinase receptor-like endoplasmic reticulum kinase
PS	Phosphatidyl Serine
PS1	Presenilin 1
RER	Rough Endoplasmic reticulum
Sar1	Secretion associated Ras
SCS2	suppressor of choline sensitivity 2
Sec	Secretory pathway protein
SER	Smooth Endoplasmic reticulum
SERCA	Smooth Endoplasmic Reticulum calcium ion exchanger
SM	Sphingomyelin
SMAC	Second mitochondria-derived activator of caspase
SNAP	Synaptosomal associated protein
SNARE	Soluble N-ethylmaleimide sensitive protein attachment protein receptor
SP	Site protease
TeNT	Tetanis Toxin Tetanus
tER	Transitional Endoplasmic reticulum
t-PA	Tissue plasminogen activator
TRAF	Tumor necrosis factor receptor associated factor
Trex	Tetracycline Repressor
UCHLI	Ubiquitin C-terminal hydrolase L1
UPR	Unfolded protein response
VAMP	Vesicle associated membrane protein
VAP	Vesicle associated membrane protein associated protein
VCIP135	Valosin-containing protein (p97)/p47 complex-interacting protein p135

XBP1	X-box binding protein 1

TABLE OF CONTENTS

5. VAPA and VAPB

6. The VAP family and motor neuron degeneration

1. Introduction

1.1 The endoplasmic reticulum

The endoplasmic reticulum (ER) is involved in protein, lipid and sterol synthesis, post-translational modification of proteins and protein and lipid transport. It is a large organelle occupying more than 50% of cellular membranes and greater than 10% of the cell volume (Figure 1.1). There are three separate specialized areas in the ER. The rough ER (RER) has ribosomes and is specialized for protein synthesis. It also couples protein synthesis to protein translocation into the lumen through the translocon. The transitional ER (tER) has specialized cup-shaped ER cisternae from which newly synthesized proteins exit via COPII vesicles (Barlowe et al., 1994). Smooth ER (SER) is dedicated to Ca^{2+} storage and lipid and sterol synthesis. It is enlarged in cell types where increased Ca^{2+} sensitivity is needed such as skeletal muscle cells and neurons.

The peripheral ER is made up of cisternal sheets, linear tubules, polygonal reticulum and 3-way junctions (Dreier et al., 2000). In neurons the ER protrudes into both axons and dendrites and has been morphologically identified in synaptic terminals and in postsynaptic densities (Broadwell et al., 1983). The cytoskeleton, in particular microtubules, plays a major role in the cellular organization of the ER membrane. Microtubule dynamics have been studied using time-lapse microscopy and they employ

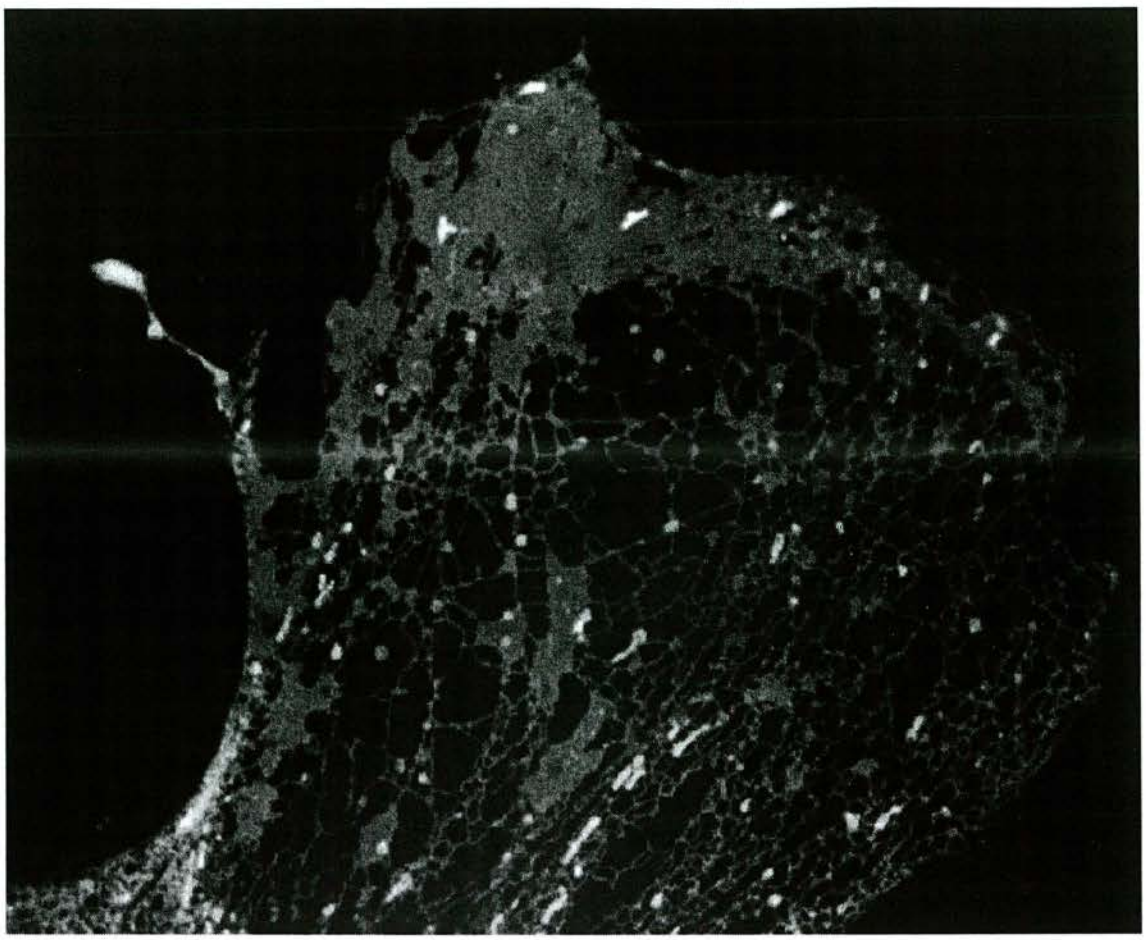

Figure 1.1 The Endoplasmic Reticulum. This figure shows the stained endoplasmic reticulum from a 3T3 fibroblast recorded via confocal microscopy (Terasaki et al., 1986).

three different mechanisms. New ER tubules can be pulled out of existing tubules by motor proteins such as kinesin migrating along microtubules. Secondly, the polymerizing tips of microtubules may pull newly forming tubules along. Finally, ER tubules may associate with the sides of microtubules via motor proteins as they slide along other microtubules (Waterman-Storer et al., 1998). The cytoskeleton contributes to ER dynamics but it is not necessary for ER maintenance, as when the cytoskeleton is disrupted by addition of nocozadole the ER remains intact (Dabora et al., 1988).

1.1.1 Lipid composition of the ER membrane

There are 3 types of eukaryotic membrane lipids. They are the glycerolipids, which are based on glycerol and include diacyl glycerol (DAG), phosphatidic acid (PA) and phosphatidyl choline (PC). The sphingolipids are based on a C18 sphingoid base and include ceramide and sphingomyelin (SM). The sterols such as cholesterol are based on a planar four-ring structure. The lipid content of different organelles within the cell is quite different. For instance the plasma membrane is rich in sterols, sphingolipids and saturated glycerolipids, which promote bilayer rigidity and impermeability due to their packing density. The plasma membrane has an asymmetric lipid distribution with the aminophospholipids concentrated on the cytoplasmic side and the sphingolipids concentrated on the exoplasmic side (Figure 1.2). The ER membrane, however, shows symmetric lipid distribution and primarily contains unsaturated glycerolipids that make the membrane flexible and facilitates incorporation of newly synthesized protein (Zachowski et al., 1993).

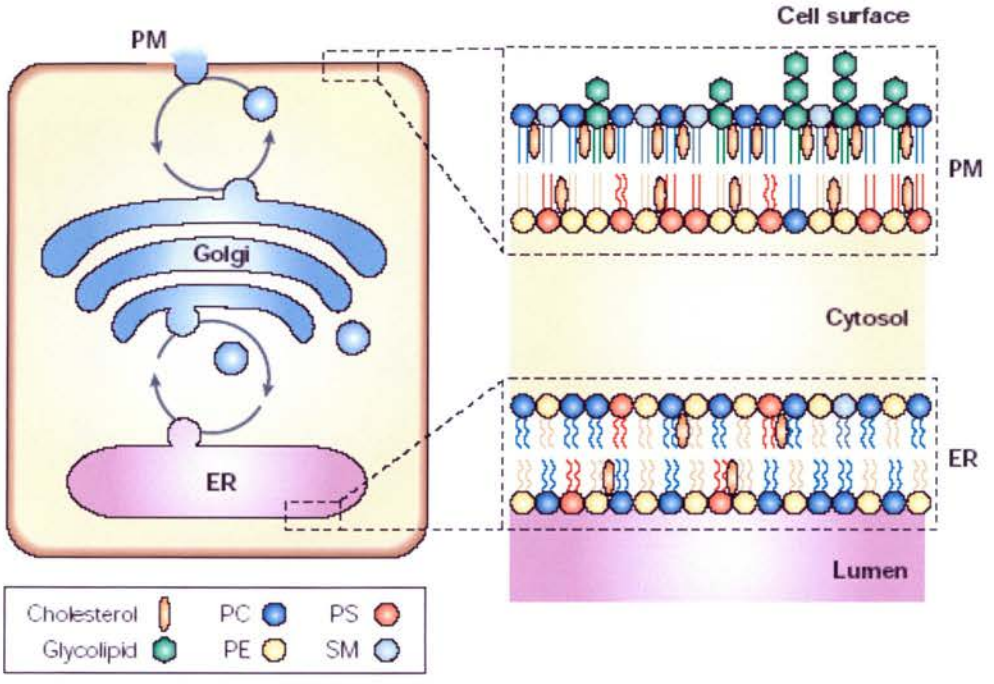

Figure 1.2. Diagram showing the major lipid content of the plasma membrane and the ER membrane (Holthuis and Levine, 2005).

1.1.2 Protein composition of the ER membrane

Most membrane proteins are shared between RER and SER. However, several proteins involved in translocation or processing newly synthesized proteins are enriched in RER as shown by the fractionation of liver cells (Kreibich et al., 1978). Landmark proteins from yeast tER include the COPII subunits Sec12, Sec23, Sar1 and Sec16 (Sonderholm et al., 2004). Epoxide hydrolase is a classical marker of SER (Galteau et al., 1985).

1.1.3 The ER as a calcium store

The ER is, as a rapidly exchanging Ca^{2+} store, able to release Ca^{2+} ions upon stimulation. A high concentration of free Ca^{2+} (0.2-2mM) is maintained in the lumen. This high free Ca^{2+} concentration is a key factor in maintaining protein synthesis and processing. Important Ca^{2+} binding proteins in the ER lumen are calreticulin, and the glucose regulated proteins GRP78 and GRP94. Besides being a Ca^{2+} signaling organelle, the ER is involved in post-translational modification of proteins. Folding of proteins is controlled by several enzymatic systems, including peptidyl prolyl isomerases and gylcosylation enzymes (glycosidases and mannosidases) (Chevet et al., 2001). These systems are controlled by several families of chaperones such as, glucose-regulated proteins (GRP78, GRP94), lectin-like chaperones (Calreticulin, calnexin and calmegin) and protein disulphide isomerases (PDI, Erp57).

1.2 ER biogenesis

Newly formed ER is derived from the outer nuclear membrane. In UT-1 cells where both the level of HMG CoA reductase and the amount of crystalloid ER are regulated by cholesterol, the membrane of the smooth ER cisternae has been identified as the precursor of the crystalloid ER tubule. The cytoskeleton is not necessary for formation of this tubular network in vitro and thus is presumed not to have a role in ER biogenesis. ER network formation in extracts requires ATP and GTP and is N-ethylmaleimide (NEM) sensitive (Dabora et al., 1988). Inhibition of network formation by GTPγS and NEM suggests that a Rab protein and/or a protein similar to the NEM sensitive fusion protein (NSF) may be involved. ER network reformation requires the NEM-sensitive AAA ATPase, p97 and the adaptor protein p47. NSFα and γSNAPs mediate the first fusion event and the second process involves the p97/p47/VCIP135 complex and induces fusion of the connected ER tubules to form three-way junctions (Kano et al., 2005). A role for p97/p47 in the in vitro formation of the tER has also been suggested (Roy et al., 2000). tER sites are relatively stable structures and are not generated in response to protein synthesis and transport even though they undergo fission and fusion in mammalian cells (Watson et al., 2005).

1.3 The ER membrane forms contact sites with other organelles

The ER forms close contacts, named ER contact sites, with other organelles including the trans Golgi network (Ladinsky et al., 1999), endosomes (Haj et al., 2002), peroxisomes

(Geuze et al., 2003), the plasma membrane (Li et al., 2004) and mitochondria (Wang et al., 2000).

1.3.1 The ER membrane and the plasma membrane

Contact sites between the ER and plasma membranes are found in all cell types. This may be so that lipids can traffic bidirectionally between the ER and plasma membrane independently of the secretory pathway. Three bridging complexes have been identified as being important in the formation of these contact sites. In both mammals and yeast the translocon of the RER interacts directly with the plasma membrane exocyst, which is a large complex of proteins required for polarized exocytosis in eukaryotic cells (Guo et al., 2004). VAMP associated protein A (VAPA) can form bridging complexes with peripheral membrane proteins on the plasma membrane as well as at other sites (Loewen et al., 2003). In phagocytes, which engulf large bodies, the plasma membrane must grow rapidly. Under these extreme circumstances extra membrane is provided by the ER mediated by an ER vesicular Soluble N-ethylmaleimide sensitive protein Attachment protein REceptor (vSNARE) homologous to Sec 22 (Becker et al., 2005).

1.3.2 The ER membrane and the mitochondrial membrane

The ER and mitochondria are also closely associated with each other. They are physically linked in many cell types and they co-regulate some important functions including apoptosis, lipid trafficking and regulation of Ca^{2+} (Levine et al., 2004). The ER

compartment that interacts with the mitochondria is called the mitochondria associated ER membrane (MAM). The MAM is enriched in lipid synthases and has less ribosomes compared with RER (Vance et al., 1990). The enrichment of lipid synthases is compatible with one of the clearest functions of the MAM, which is to participate in lipid traffic to and from the mitochondria (Flippin et al., 2003). For example some of the phosphatidyl serine (PS) synthesized in the ER is transferred to the mitochondria where it is decarboxylated to phosphatidyl ethanolamine (PE) and then transported back to the ER (Voelker et al., 2000). There is emerging evidence that the ER and mitochondria can have shared membrane proteins (Miyazaki et al., 2005, van Herpen et al., 2005). For instance PACS-2 binds to the proapoptotic protein Bid in both ER and mitochondria (Simmen et al., 2005).

1.3.3 The ER and peroxisomes

The ER is involved in peroxisome biogenesis but peroxisomal proteins are made on cytoplasmic ribosomes and post translationally inserted (Tabak, 2003). Peroxisomes are ubiquitous single membrane bound organelles involved in many metabolic pathways, which produce hydrogen peroxide. The subsequent decomposition of this toxic compound by catalase is a fundamental peroxisome process (Kovacs et al., 2002).

1.3.4 The ER and the Golgi apparatus

The Golgi apparatus is a series of flattened cisternal membrane structures, which do not fuse in a continuous manner but are closely juxtaposed in a stack-like fashion. The Golgi is a polarized structure with a cis face, which exchanges proteins and lipids with the ER, and a trans face, which communicates with the plasma membrane and compartments of the endocytic pathway (Schweizer et al., 1988). EM tomography shows that the contact between an ER domain and a Golgi stack is as close as that between the stacks of Golgi itself (Ladinsky et al., 1999). As secretory material passes through the Golgi from the ER in a cis to trans manner it is post-translationally modified in a sequential manner (Griffiths et al., 1986). Post-translational modifications such as glycosylation, sulphation and phosphorylation of proteins, proteoglycans and sphingolipids occur in the Golgi lumen (Neutra et al., 1966, Palade et al., 1975). The trans-Golgi is particularly involved in a number of post-translational modifications, for example sialylation, tyrosine sulphation and proteolytic processing. This requires substrates, such as nucleotide sugars, nucleotide sulphates and ATP to be transported into the lumen of the Golgi from the cytosol. Transport of these substrates into the Golgi lumen occurs via antiport with the corresponding nucleoside monophosphate (Hirschberg et al., 1987). Glucosyltransferases and other enzymes involved in post-translational modifications represent a significant proportion of the resident membrane protein in the trans-Golgi. Other groups of Golgi resident proteins include retrieval receptors, matrix and cytoskeletal binding proteins and components of the vesicular transport machinery.

1.4 Major membrane transport routes in mammalian cells

There are two major routes of transport in mammalian cells. The first is named the biosynthetic route where proteins synthesized in the RER are transported to the cis-Golgi via the intermediate compartment. The proteins then undergo post-translational modifications and are transported to the median and trans-Golgi network. They are then transported to the plasma membrane in vesicles and either, interact with receptors there or are secreted via exocytotic mechanisms into the extra cellular medium (Pfeffer et al., 2003). The second route is the endocytic pathway, which starts with the invagination of the plasma membrane. A bud is then formed and is scissioned from the plasma membrane. This endocytic vesicle is internalized and carries proteins, lipids, nutrients and ligands bound to their receptors into the cell. The cargo is either transported to the lysosyme to be degraded or to the late endosomes where ligands and their receptors are dissociated and the receptors are recycled to the plasma membrane (Gruenberg et al., 1995).

The coatamer proteins are involved in vesicle formation and the vesicular and target Soluble N-ethylmaleimide sensitive protein Attachment protein REceptors (v and tSNAREs) are involved in vesicle membrane fusion. v and tSNAREs assemble from opposing membranes allowing the fusion of intracellular membranes along both the biosynthetic and endocytic pathways (Sollner et al., 1993). Coatmer proteins are responsible for vesicular transport between the ER and Golgi. COPII vesicles are involved in the main export route from the tER to the Golgi (Barlowe et al., 1994). Retrograde transport between the Golgi and ER involves the KDEL receptor and COPI

vesicles (Figure 1.3). The KDEL receptor retrieves KDEL motif luminal ER proteins from post ER compartments (Stornaiuolo et al., 2003). The retrieval of these proteins involves COPI vesicles (Presley et al., 2002). Movement of COPI and COPII vesicles between the transitional ER and the Golgi is postulated to be via microtubule interactions (Young et al., 2005).

Membrane fusion requires the assembly of the SNARE complex, which is composed of one SNARE motif provided by the donor membrane vSNARE and three SNARE motifs provided by two or three acceptor membrane tSNAREs. Different cell types have their own complement of SNAREs. The neuronal synaptic vSNARE synaptobrevin 2, also called Vesicle Associated Membrane Protein (VAMP) 2, and tSNAREs syntaxin 1 and SyNaptosomal Associated Protein of 25 kDa (SNAP-25), are proteolysed by the light chains of the clostridial neurotoxins [tetanus neurotoxin (TeNT) and botulinum neurotoxin (BoNT)] that block neurotransmitter release. It was by use of these neurotoxins (Partanello et al., 1993) and via association with NSF, αSNAP and βSNAP that these SNAREs were found to be involved in neurotransmitter release (Sollner, 1993). SNAREs can also be involved in a number of other cellular processes. For instance TeNT insensitive VAMP (TI-VAMP or VAMP-7) is involved in apical transport in epithelial cells (LaFont et al., 1999) and in neurite outgrowth (Martinez-Arcas et al., 2000).

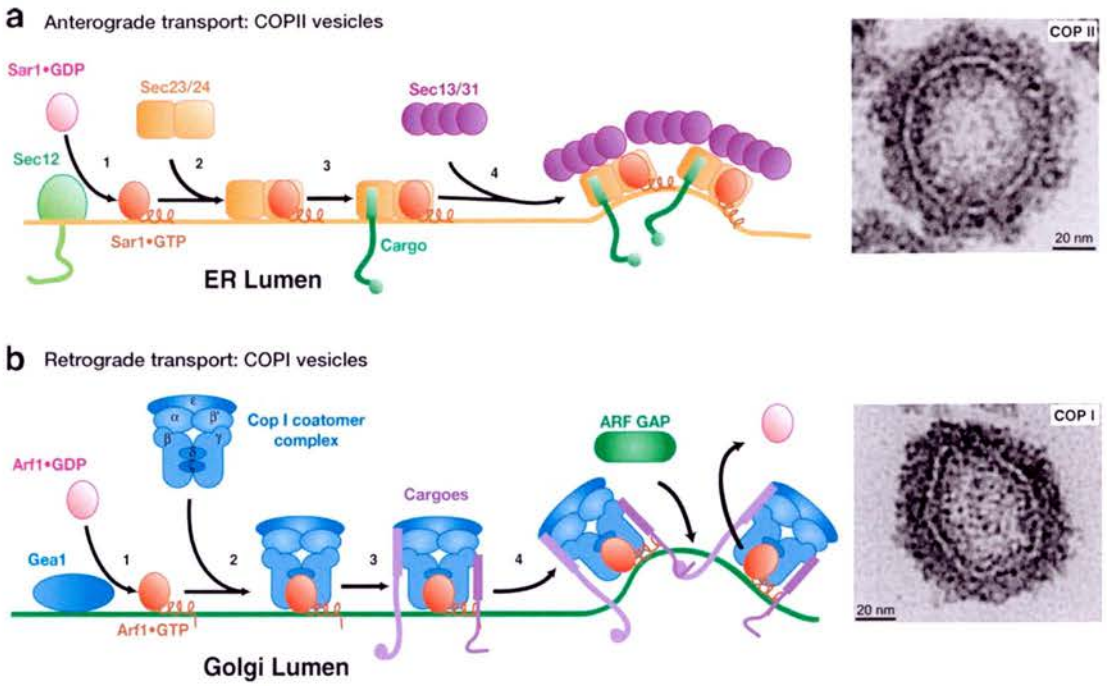

Figure 1.3. Forward and retrograde transport between the transitional ER and Golgi network is mediated by COPII and COPI vesicles (Lee et al., 2004).

1.5 The ER and apoptosis

Apoptotic cell death can be initiated by a variety of factors including perturbation of intracellular homeostasis or the ligation of plasma membrane death receptors. Apoptosis is a normal cellular response in development where cells, which are no longer required, are induced to undergo cell death. It can also be activated inappropriately, and as such, underlies the pathology of many neurodegenerative diseases. In the apoptotic death response the cell undergoes nuclear and cytoplasmic condensation with blebbing of the plasma membrane. The cell then breaks up into membrane-enclosed fragments, known as apoptotic bodies, which are recognized and engulfed rapidly by neighbouring cells or macrophages. The major proteins involved in apoptosis are the cysteine-dependent, aspartate-specific proteases (caspases) and the B-cell leukemia 2 (Bcl-2) family members. The caspases are the executioners of the apoptotic pathway and when they are activated they destroy key components of the cellular infrastructure and activate cellular factors, which damage the cell. Bcl-2 proteins act as regulators of this cell death response. Pro-apoptotic Bcl-2 proteins can homo-oligomerise and form pores in the mitochondrial membrane, releasing factors, which can activate the caspases. There is increasing evidence that the ER plays an important role in the initiation of apoptosis.

1.5.1 Bcl-2 proteins as regulators of apoptosis on the ER

To be designated as a Bcl-2 family member, a protein must possess at least one of the conserved Bcl-2 homology (BH) domains and have an effect on apoptosis. There are three subfamilies of Bcl-2 related proteins. These are the anti-apoptotic subfamily (eg.

Bcl-2, Bcl-X_L), the multi-domain pro-apoptotic subfamily (eg. BAK, BAX) and the pro-apoptotic BH_3-only subfamily (eg. Bim, Bad). The anti-apoptotic family has all four BH domains and the multi-domain pro-apoptotic family has all but the BH_4 domain. The three dimensional structure of Bcl-X_L, Bid, Bax and Bcl_w are more similar than predicted from their primary sequence alignments. Each protein has two central hydrophobic helices surrounded by amphipathic helices in a structure that resembles the pore-forming domain of the bacterial diphtheria toxin. Consistent with the known structures there is good in vitro evidence that some of these proteins can form pores or channels in lipid bilayers. Thus a combination of protein: protein interactions and pore/channel formation are thought to constitute the main molecular mechanisms of Bcl-2 activity (Desagher et al., 2000).

BH_3-only proteins can either directly or indirectly activate BAX or BAK, inducing their intramembranous homo-oligomerisation, which results in permeabilisation of the outer mitochondrial membrane (OMM) and release of intermembrane space proteins, including cytochrome c and SMAC/DIABLO (Wei et al., 2000, Du et al., 2000). The ER Ca2+ level is crucial in controlling the fate of the cell in response to certain stimuli, such as ceramide, arachidonic acid and oxidative stress. Genetic or pharmacological reduction of steady state ER Ca^{2+} levels is associated with resistance to apoptosis-induced by ceramide (Zundel et al., 1998). The ER checkpoint controlled by Bcl-2 family members resides upstream of the mitochondrion (Figure 1.4). It regulates apoptosis by modulating mitochondrial Ca^{2+} uptake. Ca^{2+} ions may communicate death signals from the ER to the mitochondria either directly by increasing mitochondrial Ca^{2+} concentration or indirectly

cell-intrinsic pathways through calcineurin activation. In either case Ca^{2+} signals generated by inositol 3,4,5 phosphate (IP_3) receptor mediated release of Ca^{2+} from the ER lumen are important. The apoptotic switch in mitochondrial Ca^{2+} signaling can be mediated by the pro-apoptotic protein tcBid, which increases the magnitude of mitochondrial Ca^{2+} signals by selectively permeabilising the OMM (Csordas et al., 2002). Ca^{2+} also activates cell intrinsic death pathways directly by activating calcineurin, which dephosphorylates and activates the pro-apoptotic Bad (Wang et al., 1999) or induces Bik (Jiang et al., 2001). The anti-apoptotic Bcl-2 associates with calcineurin in neurons and can dock calcineurin with IP_3 receptors to block IP_3-mediated Ca^{2+} release from the ER (Erin et al., 2003).

Members of the reticulon family are predominantly localized in the ER. These proteins upregulate the ER localization of Bcl-2 and Bcl-X_L, resulting in inactivation of their anti-apoptotic activity (Tagami et al., 2000). A Bcl-2 variant (Bcl-2/cb5) exclusively targeted to the ER prevents apoptosis induced by Myc activation and by tunicamycin and brefeldin A (Hacki et al., 2000). Bax inhibitor 1 protein, an apoptosis suppressor, also localizes specifically to the ER (Xu et al., 1998). Bcl-2 associated protein 31 (BAP-31), a 28kDa integral membrane protein, contains a cytosolic domain, which interacts preferentially with pro caspase 8, Bcl-X_L and Bcl-2 (Ng et al., 1997). Recently, a new member of the BH_3-only family, Spike, was isolated. It was found in the ER where it inhibits the formation of a complex between BAP-31 and Bcl-X_L (Mund et al., 2003).

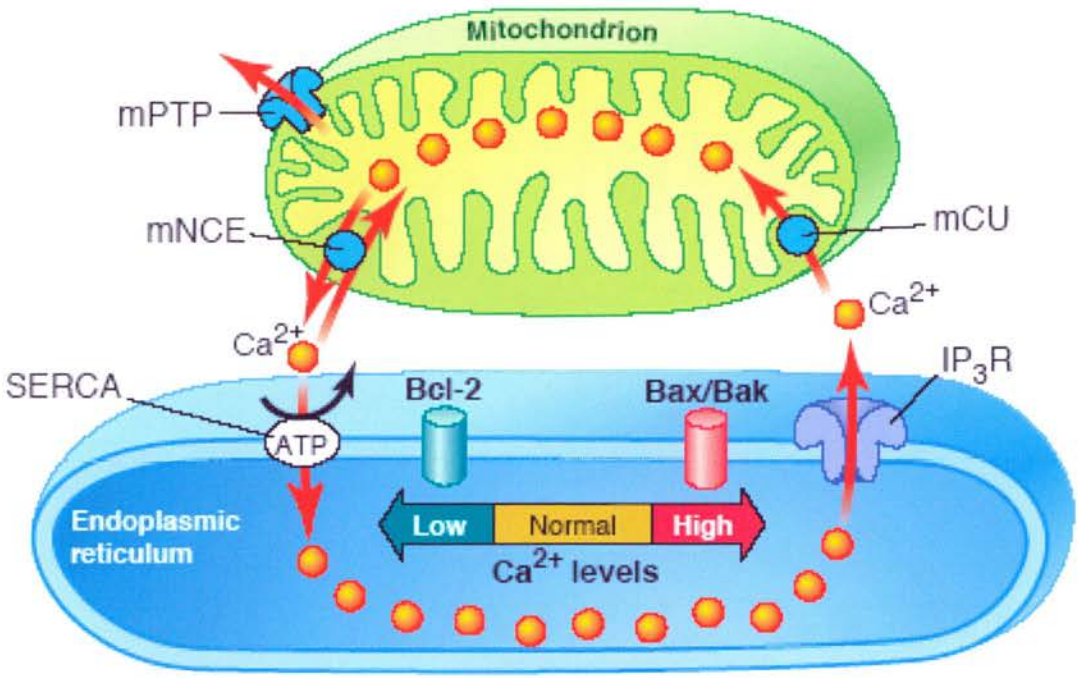

Figure 1.4. The ER and mitochondria in apoptosis (Demaurex et al., 2003). Under normal conditions, Ca^{2+} continuously cycles between the ER and mitochondria. Ca^{2+} is pumped into the ER by Ca^{2+} ATPases (SERCA), and released by IP_3–gated channels (IP_3R). Ca^{2+} enters mitochondria by a Ca^{2+} uniporter (mCU) and is released by a Na^+/Ca^{2+} exchanger (mNCE). The **mitochondrial permeability transition pore (mPTP) is important in regulating ion balance.** The ER Ca^{2+} load reflects the balance between Bcl-2 and Bax/Bak proteins.

1.5.2 Caspases as effectors of apoptosis at the mitochondria

Cytochrome c is a member of the mitochondrial electron transport chain that is required for the generation of ATP. In addition to its role in cellular energetics, cytochrome c is an important trigger of the caspase cascade. Cytochrome c mediated activation of cell death pathways occurs if it is released from the mitochondria into the cytoplasm. In the cytoplasm cytochrome c binds Apaf-1 to form the apoptosome. The apoptosome is a molecular complex consisting of cytochrome c, Apaf-1, ATP and procaspase-9 and activates caspase-9 by cleaving procaspase-9 (Lui et al., 1996).

Caspases are the major executioners of the apoptotic pathway. They exist as latent precursors, procaspases, which, when activated, initiate the death pathway by destroying key components of the cellular infrastructure and activating factors that damage the cell. Procaspases are composed of p10 and p20 subunits and an N-terminal recruitment domain. Active caspases are heterotetramers consisting of two p10 and two p20 subunits derived from two procaspase molecules. Caspases with a long N-terminal pro-domain are initiators of apoptosis (upstream) such as caspases 2, 8, 9 and 10, or are involved in cytokine production like caspases 1, 4, 5, 11, 12, 13. Caspases with a short prodomain include caspase 3, 6 and 7 and are apoptotic effector proteins (downstream), and caspase 14, which is involved in cytokine maturation (Shi et al., 2002).

1.5.3 Specific ER pathways associated with apoptosis

The mammalian ER also has three compensatory pathways, which are activated when it is overloaded with unfolded proteins. These pathways are the ER stress response, the ER overload response (EOR) and the ER associated degradation pathway (ERAD). The ER stress response leads to upregulation of chaperone proteins to assist in protein folding and a decrease in translation of other proteins through its main effector proteins IRE1, PERK and ATF6 (Kaufman et al., 2002). If the backlog of unfolded proteins cannot be cleared then the ER stress response activates apoptosis via caspase-12 and CHOP-mediated pathways (Yoneda et al., 2001). The EOR is manifested by activation of the transcription factor NF-κB, which in turn activates various pro-inflammatory proteins and cell adhesion molecules (Pahl et al., 1995). The ERAD pathway targets unfolded proteins in the ER for ubiquitination and degradation by the 26S proteasome in the cytosol (Kostova et al., 2003).

1.6 The ER and neurodegeneration

Defects in any of the ER pathways linked to apoptosis appear to be important in many neurodegenerative diseases. In diseases where there are protein aggregates formed, such as Alzheimer's disease, Parkinson's disease, Huntington disease, early onset dystonia and amyotrophic lateral sclerosis (ALS), these aggregates lead to the apoptotic death of specific subsets of neurons.

1.6.1 Alzheimer's disease and neurodegeneration

Alzheimer's disease is a progressive degenerative disease of the brain in the elderly. The histopathological signs of Alzheimer's disease include the presence of neuritic plaques and neurofibrillary tangles. The neuritic plaques mostly consist of β amyloid (Aβ) peptide and the neurofibrillary tangles are intracellular aggregates of hyperphosphorylated microtubular tau protein. The formation of plaques is an early event in the pathogenesis of Alzheimer's disease that then initiates the formation of neurofibrillary tangles (Gotz et al., 2001). The three main genes related to disease pathogenesis are the β amyloid precursor protein (APP) gene, presenilin 1 (PS1) and presenilin (PS2). When mutated these genes cause early-onset familial Alzheimer's disease in 5% of all cases of Alzheimer's disease. There are also four other genes, which have polymorphisms that may be risk factors for Alzheimer's disease. They are apolipoprotein E (apo E), α-2 microglobulin, low-density lipoprotein receptor-related protein (LRP) and very low-density lipoprotein receptor (Shastry et al., 1999). The expression of PS1 mutants linked to familial Alzheimer's disease in human neuroblastoma SK-N-SH cells increases susceptibility to ER stress induced by tunicamycin or calcium ionophores and upregulates BiP mRNA. The same findings were observed in primary neuronal cultures from PS1 mutant (I213T) knock in mice (Katayama et al., 1999).

1.6.2 Parkinson's disease and neurodegeneration

Parkinson's disease is characterized by muscular rigidity, postural instability and resting tremor. It involves the degeneration of dopaminergic neurons in the substantia nigra. The clinical hallmark of Parkinson's disease is the deposition of intracytoplasmic inclusion bodies (Lewy bodies) in neurons. Heritable forms of the disease are caused by mutations in three genes (Shastry et al., 1999) α synuclein, parkin and ubiquitin C-terminal hydrolase L1 (UCHL1). The Parkinson's disease mimetics 6-OHDA, MPP^+ and rotenone specifically activate ER stress pathways in cultured neuronal cells (Ryu et al., 2002). Autosomal recessive juvenile parkinsonism (AR-JP) is caused by mutations of the parkin gene. Parkin is an E3 ubiquitin ligase that specifically recognizes its substrate protein, promoting its ubiquitination and subsequent degradation in the ERAD pathway (Takihashi et al., 2003). There is also genetic evidence implicating ER stress in rare forms of Parkinson's disease (Shimura et al., 2000).

1.6.3 Huntington disease and neurodegeneration

Huntington disease is an autosomal dominant polyglutamine disorder. The affected individuals exhibit involuntary, jerky movements and alterations in memory and mood. In Huntington disease there is a selective loss of striatal neurons. It is caused by expansion of $[CAG]_n$ tracts in the huntingtin gene. This induces oxidative and ER stress, and proteosomal and mitochondrial dysfunction (Meriin et al., 2002). Aggregation or inclusion body formation in Huntington disease has actually been suggested to reduce

neuronal cell death. It has been discovered that the more diffuse forms of the protein Huntingtin are the ones more likely to cause apoptosis (Arrasate et al., 2004).

1.6.4 Early-onset torsion dystonia and ER membrane inclusions

Early-onset torsion dystonia is an autosomal dominant movement disorder beginning in childhood and manifesting as contracted, twisted postures throughout life. Roughly 60% of cases have an in frame GAG deletion in Torsin A resulting in the loss of a glutamic acid residue. Torsin A is highly expressed in the dopaminergic neurons of the substantia nigra and the dystonia is thought to arise from a disturbance in dopamine signaling (Hewett et al., 2000). Wild-type Torsin A is expressed on the ER but the mutant protein accumulates in multi-layered concentric membrane whorls in the cytoplasm, frequently accompanied by flattening of the neuron cell body and loss of the neurites. The whorls stain for Torsin A and PDI and appear to cleave from the ER. Unexpectedly, the Torsin A protein is not a grossly misfolded protein that produces membrane inclusions by eliciting an ER stress response. Instead, inclusion formation requires the addition of an N-linked glycan to a specific residue in the ATP binding region of mutant Torsin A (Bragg et al., 2004).

1.6.5 Amyotrophic lateral sclerosis and neurodegeneration

Amyotrophic lateral sclerosis (ALS) is a neurodegenerative disease caused by progressive loss of motor neurons (Figure 1.5) in the brain and spinal cord. Amyotrophy

is the neurogenic atrophy of muscle and lateral sclerosis refers to the hardness of the spinal cord at autopsy, due to proliferation of astrocytes and scarring of the lateral columns of the spinal cord. The degeneration normally begins focally and then spreads and involves both corticospinal (Figure 1.6) (upper) and spinal (lower) motorneurons (Brooks, 1994). Lower motor neuron degeneration results in symptoms such as muscle denervation, loss of tendon reflexes and fasiculations, and these are followed by muscle atrophy. Fasiculations are visible twitches of muscle that can be seen under the skin. They result from involuntary but synchronous contractions of all of the muscles in a motor unit. They are characteristic of slowly progressive diseases of the motor neuron itself and are rarely seen in peripheral neuropathies. Corticospinal degeneration results in additional focal spasticity (Swash, 1999). When corticospinal symptoms occur alone, the syndrome is referred to as progressive bulbar palsy whereas if only lower motor neurons are involved the syndrome is called progressive spinal muscular atrophy. The disease progresses rapidly, in typical ALS, and leads to paralysis and death in 3-5 years.

Both environmental and genetic factors have been implicated in the pathology of ALS and familial forms of the disease have only been found to account for roughly 10% of the cases.

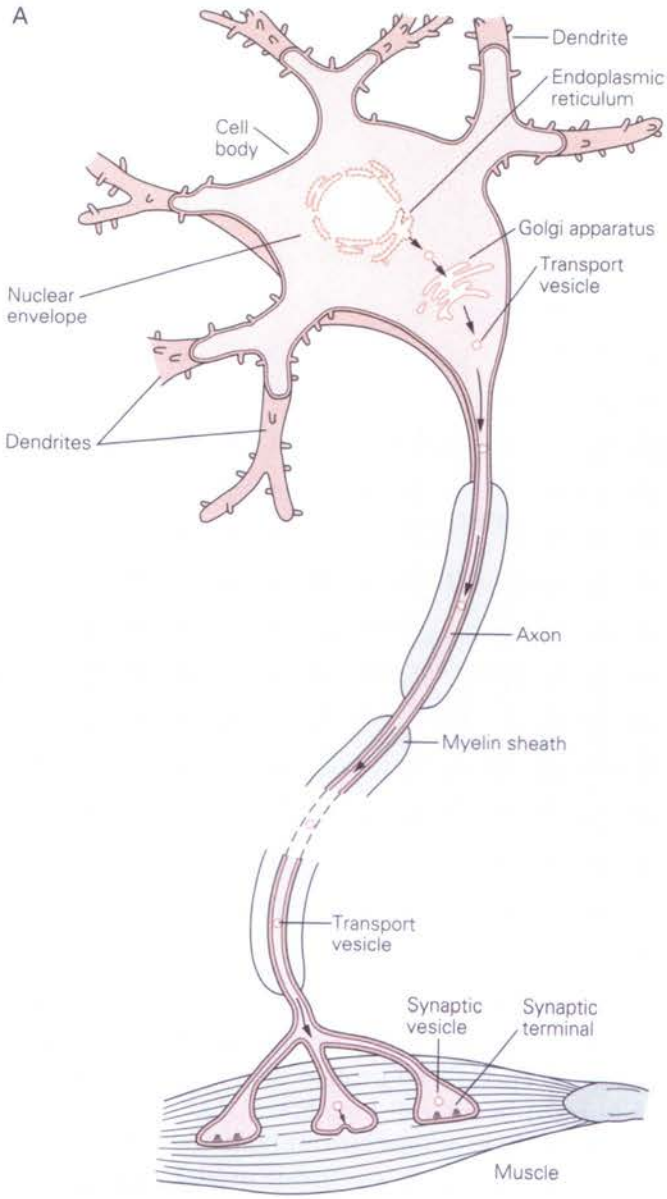

Figure 1.5 General layout of a motor neuron (Kandel et al., Principles of Neural Science, 4th Edition). Motor neurons are located in the ventral horn of the spinal cord and have long axons, which synapse onto a group of muscle fibres known as a motor unit. They have large cell bodies and their nucleus is distinctive because of its large and prominent nucleolus. Dendritic spines are found on motor neurons, which process excitatory and inhibitory synaptic inputs.

Figure 1.6 Areas involved in motor activity in the brain and spinal cord (Pinel, Biopsychology, 5th Edition). The Dorsolateral and Ventromedial tracts both initiate in the cerebral cortex. The motor neurons activated by the Ventromedial tracts project to proximal muscles of the trunk and limbs whereas the motor neurons activated by the Dorsolateral tracts project to distal muscles.

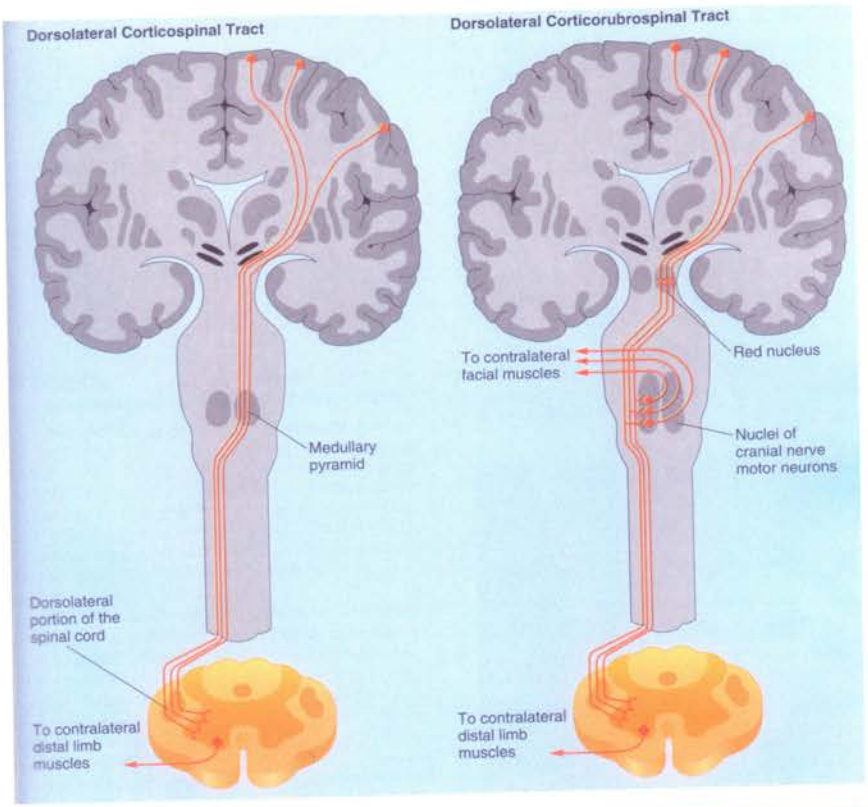
Dorsolateral Corticospinal Tract
Medullary pyramid
Dorsolateral portion of the spinal cord
To contralateral distal limb muscles
Dorsolateral Corticorubrospinal Tract
To contralateral facial muscles
Red nucleus
Nuclei of cranial nerve motor neurons
To contralateral distal limb muscles

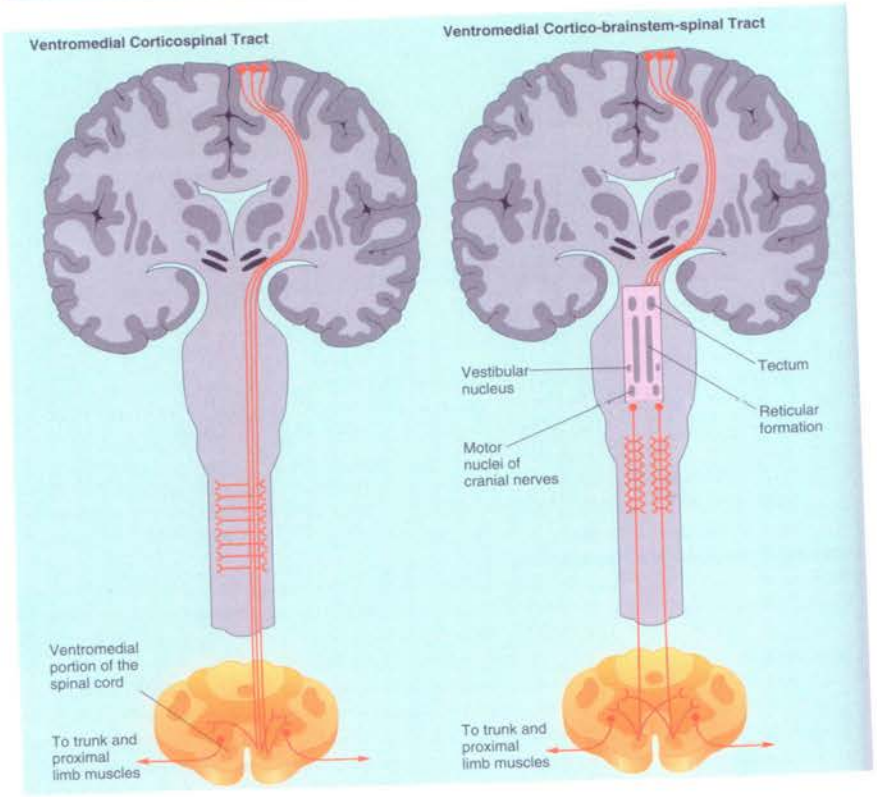
Ventromedial Corticospinal Tract
Ventromedial portion of the spinal cord
To trunk and proximal limb muscles
Ventromedial Cortico-brainstem-spinal Tract
Vestibular nucleus
Tectum
Reticular formation
Motor nuclei of cranial nerves
To trunk and proximal limb muscles

One of the most consistent cases for the involvement of environmental factors in disease progression has been found among the Pacific Islanders of Guam. In Guam an abnormally high percentage of the islanders have a Parkinsonian-Dementia complex plus ALS type symptoms. This has been found to be caused by the ingestion of cycasin from the indigenous cycad plant. Cycasin decreases neuronal DNA repair, causes an upregulation of Tau mRNA and an increase in excitatory neurotoxicity (Esclaire et al., 1999). Other putative environmental factors include a history of trauma to the brain and spinal cord, strenuous physical activity, exposure to radiation, electrical shocks, welding or soldering materials, and employment in paint, petroleum, or dairy industries. But none of these have been reported consistently (Gubbay et al., 1985).

As previously mentioned, familial or genetic (FALS) factors account for 5-10% of ALS cases (Kudkowicz et al., 1997). In 1993 the cytosolic copper-zinc superoxide dismutase (SOD1) was shown to have mutations specifically linked to the development of ALS. SOD1 is a 153 amino acid metalloenzyme with high expression in nervous tissue, liver and erythrocytes. It catalyses the conversion of superoxide to molecular oxygen and hydrogen peroxide (Rosen et al., 1993). Since 1993 more than 100 different mutations in all 5 exons of the SOD1 gene have been identified as being associated with ALS (Cudkowicz et al., 1997). Knock out models in mice, which express no SOD1, have no ALS phenotype suggesting that it is not a loss of SOD1 enzymatic activity, which leads to motor neuron degeneration (Reaume et al., 1996). Dominant SOD1 mutations are thought to act as gain of function mutations (Kunst et al., 1997). Several hypotheses have been put forward as to how the ubiquitously expressed SOD1 can mediate selective

motor neuron death. There have been reports that SOD1 mutant mice display increased oxidative stress (Kruman et al., 1999), that there is increased glutamate release leading to glutamate-mediated excitotoxicity (Leigh et al., 1996, Raiteri et al., 2005), that they display increased ER stress (Tobisawa et al., 2003, Wootz et al., 2004), that mutant SOD1 sequesters the antiapoptotic protein Bcl-2 (Pasinelli et al., 2004) and that there is an accumulation of ceramides and cholesterol esters in the spinal cord (Cutler et al., 2002), all leading to motor neuron cell death.

There have been several other genes linked to various forms of ALS. Autosomal recessive ALS (ALS2) has been linked to mutations in the Alsin gene. Symptoms in this form of the disease begin in the 1st or 2nd decade and continue for 15-20 years. Alsin is expressed in the brain and spinal cord and has a PH and guanine-nucleotide exchange factor (GEF) domain. The mutations found in this gene are truncation mutations therefore this is predicted to result in a loss of function of Alsin. It is thought that Alsin may act as a regulator of GTPases and modulate microtubules, membrane organisation and trafficking in neurons (Hadano et al., 2001). When the truncated form of Alsin was expressed in monkey Cos-7 cells it resulted in enlargement and accumulation of early endosomes, impairment of mitochondria trafficking and fragmentation of the Golgi apparatus. It was also found to have a centrosomal localisation in SK-N-SH and SW13 cells, which suggests that it may be involved in producing microtubules (Millecamps et al., 2005). Juvenile ALS (ALS4) is a rare autosomal dominant form of the disease characterised by distal muscle weakness and atrophy. ALS4 has been mapped to the STEX gene and encodes a novel 302.8kDa protein, which contains an RNA/DNA

helicase domain. Motor neuron degeneration may be due to a dysfunction in helicase activity or other steps in RNA processing (Chen et al., 2004).

Therefore the ER is an important organelle in the pathogenesis of many diseases. Neurons in particular seem to be sensitive to disturbances in protein folding, especially with the onset of old age.

1.7 The VAMP-Associated Protein (VAP) family and the ER

VAP was first identified as a VAMP/synaptobrevin-associated protein in a yeast two-hybrid screen in *Aplysia californica*. Antibodies raised to the VAP protein were shown to block neurotransmitter release in *Aplysia* (Skehel et al., 1995). Since then VAP homologues have been identified in yeast (Kagiwada et al., 1998), *drosophila* (Pennetta et al., 2002), mice (Skehel et al., 2000), rats (Soussan et al., 1999) and humans (Weir et al., 1998). There are two homologues of VAP in mammalian cells, VAPA and VAPB, and human cells also have a splice variant of VAPB called VAPC (Nishimura et al., 1999). VAPA and VAPB have three domains a Major Sperm Protein (MSP) domain, named for its homology to the major sperm protein of *C. elegans*, a coiled-coil domain, and a transmembrane tail (Figure 1.7). VAPC contains the MSP domain and 24 amino acids, which are not found in VAPA or VAPB.

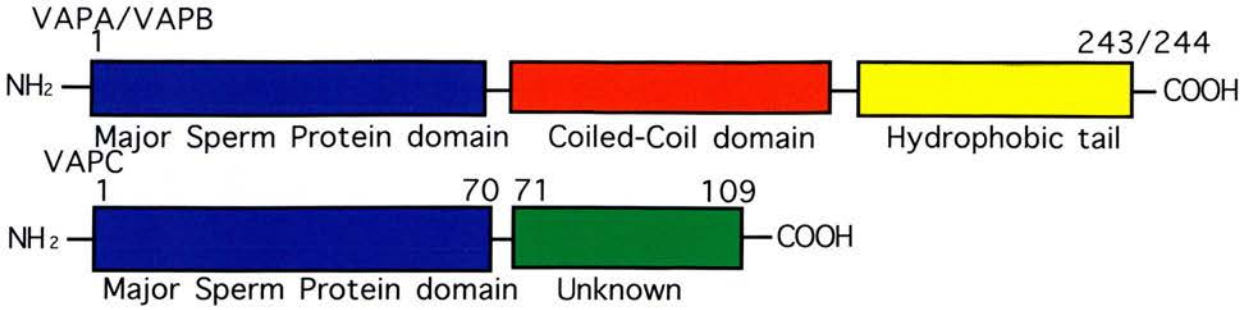

Figure 1.7. Cartoon of VAPA/VAPB and VAPC showing their major domains.

The VAP proteins are type II membrane proteins mainly expressed on the endoplasmic reticulum (ER) (Skehel et al., 2000) and Golgi (Soussan et al., 1999) in mammalian cells and yeast (Kagiwada et al., 1998). Mouse VAPA does not co-localise with VAMP/synaptobrevin at synaptic structures, but expression overlaps with lower levels of VAMP/synaptobrevin in the cell body of neurons. VAPA also associates with microtubules and intracellular vesicles in mice. Therefore it is likely that VAPA participates in delivery of proteins and lipids to synaptic terminals via its interaction with VAMP/synaptobrevin rather than a direct involvement in synaptic exocytosis (Skehel et al., 2000). Rat VAPB antibodies were found to inhibit retrograde intra Golgi transport and to result in the accumulation of COPI vesicles (Soussan et al., 1999).

Human VAP proteins have also been shown to interact with VAMP/synaptobrevin along with a variety of other v and tSNAREs, such as syntaxin 1a, bet1, sec22, αSNAP and NSF. However they do not bind to syntaxin 17, a tSNARE involved in smooth ER traffic or to the plasma membrane tSNARE SNAP-25 (Weir et al., 2001). As VAPA is not found in synaptic structures one hypothesis is that the VAP proteins act as a protein chaperone for the SNARE and fusion proteins so that they cannot inappropriately interact before they localize correctly. As sec22 is a component of the SNAREpin required for retrograde transport to the ER (Burri et al., 2003) and bet1 is involved in ER to Golgi transport (Zhang et al., 2001) it is plausible that disruption of VAP function would indirectly disrupt transport between the Golgi and ER. The possibility does, however, remain that the VAP proteins are directly involved in fusion events in retrograde transport from the Golgi to the ER.

The VAP proteins have also been identified as interacting with a number of other proteins (Table 1.1). There is also some evidence that VAPA co-localizes with occludin at the tight junction of epithelial cells (Lapierre et al., 1999). Drosophila VAPA is expressed at larval neuromuscular junctions where it regulates synaptic bouton budding in a dose-dependent manner. It is postulated to regulate division of boutons at synaptic terminals by stabilizing and directing the microtubule cytoskeleton during budding (Pennetta et al., 2002).

VAP	INTERACTING PROTEIN	VAP INTERACTION DOMAIN	CELLULAR OR BIOLOGICAL CONSEQUENCE
VAPA/B	VAMP	COILED COIL	PREDICTED CHAPERONING ABILITY
VAPA	SYNTAXIN 1A	COILED COIL	PREDICTED CHAPERONING ABILITY
VAPA	Bet1	COILED COIL	PREDICTED CHAPERONING ABILITY
VAPA	sec22	COILED COIL	PREDICTED CHAPERONING ABILITY
VAPA	αSNAP	COILED COIL	PREDICTED CHAPERONING ABILITY
VAPA	NSF	COILED COIL	PREDICTED CHAPERONING ABILITY
VAPA	OCCLUDIN	UNKNOWN	UNKNOWN
VAPA	VAMP2	COILED COIL	INDIRECT ACTION ON GLUT4 TRANSLOCATION TO THE PLASMA MEMBRANE
VAPA/B	NS5A OF HCV	C-TERMINAL 3RD	ANCHOR OR RECEPTOR ON ER
VAPA/B	NS5B OF HCV	MSP	ANCHOR OR RECEPTOR ON ER
VAPA	OSBP1	MSP	PREDICTED EFFECT ON ER STRUCTURE/ BIOGENESIS
VAPA	ORP1	MSP	UNKNOWN
VAPA	ORP2	MSP	UNKNOWN
VAPA	ORP3	MSP	PREDICTED EFFECT ON ER STRUCTURE/ BIOGENESIS
VAPA	ORP4	MSP	UNKNOWN

VAPA	ORP6	MSP	UNKNOWN
VAPA	ORP7	MSP	UNKNOWN
VAPA/B	ORP9	MSP	PREDICTED EFFECT ON ER STRUCTURE/ BIOGENESIS
VAPB	NIR1	MSP	UNKNOWN
VAPB	NIR2	MSP	PREDICTED EFFECT ON ER STRUCTURE/ BIOGENESIS
VAPB	NIR3	MSP	PREDICTED EFFECT ON MICROTUBULE ORGANISATION

Table 1.1 VAP interacting proteins.

1.8 VAPA and insulin signaling

In muscle and fat cells insulin causes rapid recruitment of intracellular vesicles containing the GLUT4 glucose transporter to the plasma membrane, thus causing an increase in glucose entry into the cell. GLUT4 incorporation into the plasma membrane requires the participation of VAMP-2, syntaxin-4 and synaptosome-associated protein of 23kDa (SNAP-23) in 3T3-l1 adipocytes (Figure 1.8). VAMP-2 is also involved in GLUT4 arrival at the surface of L6 myoblasts expressing Myc-tagged GLUT4 (Tamori et al., 1998). VAPA co-localises with VAMP-2 in L6 myoblasts and 3T3-L1 adipocytes and partially co-localises with GLUT4 in L6 myoblasts. Cells expressing exogenous VAPA showed roughly 60% less GLUT4-myc on their surface after insulin treatment relative to insulin stimulated but untransfected or empty vector transfected controls. However if VAPA was coexpressed with VAMP-2-GFP then the levels of GLUT4 on the plasma membrane returned to control levels when stimulated. When the cells were treated with VAPA antibody the insulin stimulated GLUT4 translocation was inhibited to a significant extent but the basal level of GLUT4 on the plasma membrane was unaffected. Therefore it is likely that the exogenous VAPA may limit the amount of endogenous VAMP-2 able to mediate GLUT4-myc fusion with the plasma membrane. It may be that the disruption of VAPA is interfering with VAMP-2 due to interrupted protein chaperoning function or it may have a direct ability to assist in the initiating step in GLUT4 transport. (Foster et al., 2000).

Insulin stimulated GLUT4 incorporation into the plasma membrane appears to fail in insulin resistance accompanying several forms of diabetes (Klip et al., 1990, King et al.,

1992). If combined with pancreatic β cell dysfunction this leads to persistent hyperglycemia and its associated complications such as eye, nerve and kidney disease. The loss of an XBP-1 allele predisposes mice to diet induced peripheral insulin resistance and type II diabetes (Ozcan et al., 2004). As XBP-1 is a factor involved in the ER stress response the link between ER stress and diabetes has been studied. In obese (ob/ob) and high fat diet (HFD) mice there is increased PERK phosphorylation in liver extracts compared with lean controls. There was also an increase in GRP78/BiP mRNA not due to increased levels of glucose alone. ER stress inhibits insulin action in liver cells mediated by an IRE1α and JNK dependent protein kinase cascade. $PERK^{-/-}$ mice have been found to exhibit a phenotype resembling type I diabetes resulting from pancreatic islet destruction soon after birth (Harding et al., 2001). PERK mutations also cause a rare inherited form of type I diabetes in mice (Delphine et al., 2000).

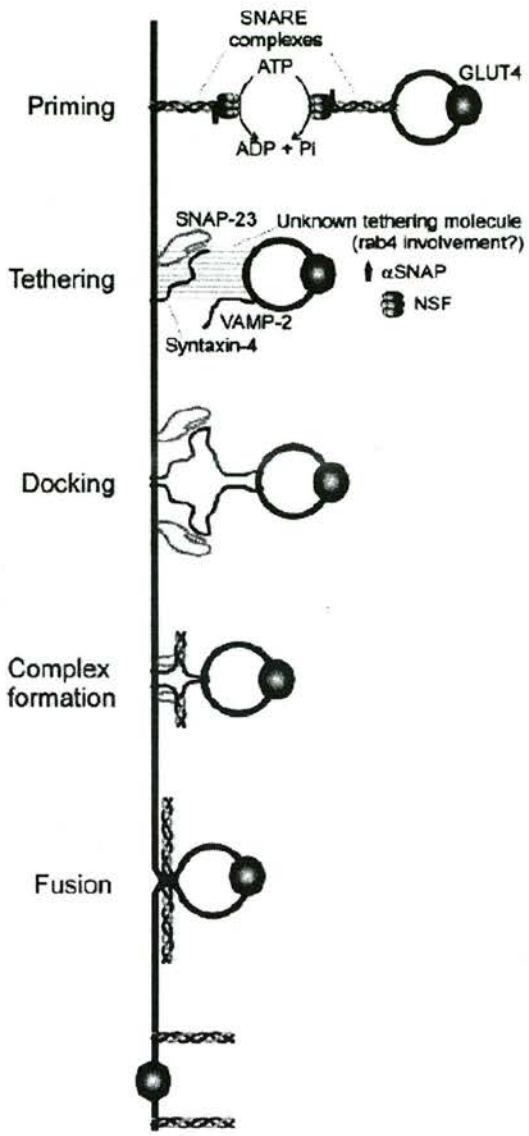

Figure 1.8 Steps in vesicle docking and fusion applied to the glucose transporter 4 (GLUT-4) system (Foster et al., 2000).

1.9 VAPA and Hepatitis C Virus (HCV)

HCV is a member of the *Flaviviridae* family and a positive-sense, single-stranded RNA virus (Choo et al., 1991). The viral genome encodes a single polyprotein of about 3010 amino acids, NH2-C-E1-E2-p7-NS2-NS3-NS4A-NS4B-NS5A-NS5B-COOH, which is proteolytically processed by viral and host proteases (Lohmann et al., 1996). There are structural (core (C), E1 and E2) and nonstructural proteins (NS2-NS5B). NS3 is a serine protease and has RNA helicase activities (Tai et al., 1996), suggesting its potential role in viral RNA synthesis. NS5B is a RNA dependent RNA polymerase (Poch et al., 1989). NS5A is a phosphoprotein (Tanji et al., 1995) and contains a putative nuclear localization signal that can target a heterologous reporter gene product to the nucleus. The N-terminus truncated, but not the full-length, NS5A is a potent transcriptional activator (Kato et al., 1997). It has recently been shown that NS5A has potential BH1, BH2 and BH3 sites and interacts with Bax to inhibit apoptosis (Chung et al., 2003).

VAPA has been shown to interact with NS5A and NS5B with the MSP domain binding to NS5B and the C-terminal 3rd of VAPA interacting with NS5A (Tu et al., 1999). The VAPA protein acts as an anchor or receptor for these HCV proteins to localize them to the ER membrane where they can carry out HCV replication and translation. Small interfering (si) RNA-mediated down regulation of VAPA in Huh-7 cells blocked HCV replication and translation (Zhang et al., 2004). When NS5A is hyperphosphorylated this interrupts its interaction with VAPA and this negatively regulates viral RNA replication (Evans et al., 2004). There is also some evidence to suggest that VAPA can localize with HCV to lipid rafts and that it has a role in HCV and encephalomyocarditis virus (EMCV)

internal ribosomal entry site (IRES)-mediated translation (Gao et al., 2004). It has been suggested that VAPA may be a cellular factor playing a role in regulating the switch between replication and translation of HCV RNA.

In order to ensure viral replication and survival, the HCV proteins modify the host ER stress response. NS5A inhibits the double stranded RNA dependent eIF2α kinase PERK and prevents its dimerisation (Gale et al., 1997). As cells expressing NS5A have lower levels of eIF2α phosphorylation this increases translation initiation and alters ER stress pathways (Tardif et al., 2004). Cells expressing HCV replicons can also activate the UPR via ATF6 (Tardif et al., 2002). NS5A can activate the EOR after disturbing intracellular $Ca2^{+}$ levels leading to the activation of NFκB and STAT-3 (Gong et al., 2001). It is possible that the effects of NS5A on ER stress pathways may be in part mediated via its interaction with VAPA.

1.10 Thesis aims

The aim of this thesis is to study the MSP domain of the mammalian VAP proteins in greater detail. Especially in its potential roles in the ER stress response and in some forms of familial Amyotrophic Lateral Sclerosis (ALS). In order to carry out this aim a variety of techniques, such as, a yeast two hybrid screen with VAPA MSP and a VAPA MSP domain inducible stable cell line will be used, along with characterization of the VAPB mutant VAPBP56S.

2. METHODS

2.1 Yeast 2 hybrid protein interaction screen

DupLEX-A^{TM} YEAST TWO-HYBRID SYSTEM. This is a Lex-A-based version of the yeast two-hybrid system originally developed by Fields and Song. In the Lex-A system the DNA binding protein is the *E. coli* Lex-A protein and the activation protein is the acid blob domain B42. The DNA binding protein and the activation protein cannot activate reporter expression on their own but when they are brought together via two interacting proteins they activate reporter gene expression.

The MSP domain of VAPA (containing the coding sequence for amino acids 1-101) was cloned into the yeast bait vector pGilda. The bait vector pGilda-MSP, or one of the control vectors pRHFM1 or pSH17-4 was then transformed into the yeast strain EGY48 along with the reporter plasmid, pSH18-43. This was done in order to determine whether the bait vector autoactivated the reporter plasmid. pGilda-MSP was then transformed into the yeast along with pJK101 to test if it could bind to the LexA operators in the nucleus when activated by galactose. The pGilda-MSP bait plasmid did not autoactivate the SH18-34 reporter plasmid therefore the yeast containing the bait and reporter plasmids was subjected to a large-scale lithium acetate transformation with the LexA JG4-5 library plasmid. A yeast colony containing the pGilda-MSP and pSH18-34 was picked and grown up overnight in YNB(glu)-his-ura medium at 30°C. This overnight culture was then diluted to OD_{600} 0.1 in YPD medium and grown for a further 4 hr. The cells were then harvested by spinning at 1500g for 5 min, washed in 30ml of distilled H_20

(dH_20) and spun again. The supernatant was poured off and the pellet resuspended in 1.5ml LiOAc. 30 50µl aliquots were made and 50µg of carrier DNA and 1µl of JG4-5 library plasmid were added. Then 300µl of LiOAc/PEG was added to each tube and the tube inverted and incubated at 30°C for 30 min. 40µl DMSO was added to each tube and then they were mixed by inversion and heat shocked at 45°C for 20 min. 0.6µl of dH_2O was added to each tube, they were mixed by inversion and plated onto 30 24x24 cm YNB(glu)-his-ura-trp plates. $5x10^6$ clones were calculated to have been obtained via a 100mm titration plate and these were harvested with a sterile microscope slide and frozen in 50% glycerol aliquots. An aliquot of yeast was then grown in minimal YNB(gal)-his-leu-trp-ura medium until there were approximately $4x10^7$ cells (calculated via a titration of viable cells). These cells were then plated onto YNB(gal)-his-leu-trp-ura plates to gain potential positive transformants and clonies were picked at 48 and 72hrs. 115 potential positive transformants were gained and these were tested on X-gal plates. Overall 40 colonies were obtained which were blue and therefore true positives. DNA was isolated from the positives by growing each colony in 2 ml of YNB(glu)-trp medium at 30°C overnight. 1.5ml of each was centrifuged in eppendorf tubes for 10s at maximum speed. The supernatant was poured off, the pellet was vortexed to resuspend it in the residual liquid, then 200µl of plasmid rescue solution was added. 100µl of phenol (tris-sat pH 8.0) and 100µl of 24:1 chloroform:isoamyl alcohol (Gibco) was added along with 0.3g of acid-washed glass beads and this was vortexed vigorously for 2 min. This mixture was centrifuged at 14K rpm in a microcentrifuge for 5 min at room temperature. 200µl was removed from the top (aqueous) layer and transferred to a clean eppendorf tube. 20ml of 3M NaOAc (Sigma) was added, the solution was vortexed, and then 440µl of 95%

ethanol was added. The solution was centrifuged for 20 min at 14K rpm in a microcentrifuge, the supernatant pipetted off and discarded. Then it was washed with 70% ethanol and the supernatant discarded, the pellet vacuum dried and resuspended in 5µl of sterile distilled water. 1µl of the DNA was used to transform the *E. coli* KC8 cells and they were plated onto ampicillin LB (Sigma) plates. Colonies were restreaked onto – trp plates and those that grew were harvested by miniprep and sequenced.

All materials obtained from Q-BIOgene unless otherwise stated.

Yeast medium - YNB-ura-his-leu-trp (or other selective medium):

6.7 g yeast nitrogen base w/o amino acids

0.6 g -his-ura-trp-leu (or other selective) dropout mix

20 g glucose (or 20 g galactose + 10 g raffinose for gal/raff media) (Sigma)

20 g agar (if for plates) (Sigma)

Add 1 liter of distilled water and autoclave for 20 minutes.

For plates, cool to 50°C before pouring

Yeast selective X-gal media - 6.7 g yeast nitrogen base without amino acids

0.6 g -his-ura-trp-leu dropout mix

20 g glucose (or 20 g galactose + 10 g raffinose for gal media) (Sigma)

20 g agar (Sigma)

900 ml distilled water

Autoclave and cool to 65°C

In a separate bottle, autoclave 7 g of sodium phosphate (dibasic) and 3 g of sodium phosphate (monobasic) in 100 ml of distilled water (Sigma)

Mix the two solutions, add 0.8 ml of 100 mg/ml 5 bromo-4-chloro-3-indolyl-

beta-D-galactopyranoside (X-gal) in N,Ndimethyl formamide, and pour plates

2.2 Cell line characterisation experiments

2.2.1 Calcium phosphate transfection of HEK293 cells

HEK293 cells were maintained in DMEM supplemented with 10% FBS and 1% penicillin/streptomycin (Invitrogen) at 37°C in 5% CO_2. For transfection with the plasmids HEK cells were plated at 40-60% confluency. A solution of 1.25mM calcium chloride, 1μg of plasmid DNA, and N,N-bis(2-hydroxyethyl)-2-aminoethanesulfonic acid (BES) buffered saline, pH 6.95 (Sigma) in culture medium, was then added. This gave a calcium phosphate precipitate, which initiated DNA entry into the cells. HEK cells were incubated for four hours at 37°C in 5% CO_2. The solution was then removed and replaced with fresh culture medium.

BES-Buffered Saline (2X) - 280 mM NaCl

Filter sterilize and store at -20°C

1.5mM Sodium Phosphate Dibasic (Na2HPO4)

50mM BES, pH 6.95

2.2.2 Dissection and preparation of rat E19 primary hippocampal cultures

Hippocampi of E19 rat embryos were dissected. The hippocampi were transferred to a 35mm dish containing 2ml of Hank's/Hepes Solution and 200μl of Trypsin and 20μl of DNAse solution were added. The dish was placed into the incubator at 37°C for 20 minutes. After 20 minutes at 37° C, 5 ml of the growth medium was added to the dish.

This was transferred to a tube and made up to 10 ml by adding growth medium. The hippocampi were allowed to settle down to the bottom of the tube. The solution was removed and the cells were washed once more with 10 ml of growth medium. The hippocampi were then centrifuged at 1200rpm for 5min and the solution was removed and 2ml of growth medium and 20µl of DNAse were added. The cells were triturated with a fire polished Pasteur pipette. The cells were counted and plated down in 6 well PLL coated plates at the appropriate concentration (usually 100.000 to 800.000 cells per well). The day after the preparation the old media was removed and replaced with 1.5ml of serum free medium.

All materials are obtained from Invitrogen unless otherwise stated.

HDMEM - 25mm Hepes buffered Dulbeccos mod. medium (500ml) + 5ml Pen-strep

HEBSS - Hepes buffered Calcium and Magnesium free Earls BSS pH 7.3

EBSS - (Earls BSS) + 10mM Hepes (that is 238mg Hepes for 100ml HBSS): pH 7.3

L-15 - (Leibovitz) medium with L-Glutamine W/ L-Amino Acids.

Add 5ml of Pen-strep to a 500ml bottle of L – 15.

Hanks /Hepes solution - HBSS 500ml + 1.19g Hepes (PH to 7.3 and Filtered)

Trypsin Solution - Dissolve 100mg Trypsin in 10ml of Ca^{2+}/Mg^{2+} free PBS

Filter to sterilise and stock in 200µl aliquots in the freezer

DNAse solution - 5mg DNAse (Sigma) dissolved in 1ml of PBS

Growth Medium - 500ml BME

50ml Horse Serum

5ml Pen-strep

8ml of a 32.5% Glucose Solution (in water, sterile)

5ml Sodium Pyruvate 100 mM solution

5ml N2 supplement

Filter through a 0.2μm sterile filter.

Serum free medium - 500ml BME

5 ml Pen-strep

8 ml of a 32.5% Glucose Solution (in water, sterile)

5 ml Sodium Pyruvate 100mM solution

5 ml N2 supplement

10 ml B27 supplement

Filter through a 0.2μm sterile filter.

PLL solution stock solution - 10mg/ml in distilled water. Further dilution 200μl to 40ml.

Fibronectin stock solution - 1mg/10ml. Further dilution 1ml to 10ml

2.2.3 Nucleofection of HEK293 cells and primary hippocampal cultures

Using the Cell line Nucleofector™ Kit (Amaxa biosystems). The supplemented Nucleofector solution V was pre-warmed to room temperature and culture medium was pre-warmed to 37°C. For HEK293 cell nucleofection 6 well plates were prepared by adding 1ml of culture medium to the required number of wells. The cells were grown to the required confluency and harvested by trypsinisation. For primary cultured cell

suspension hippocampal cells were nucleofected before plating. An aliquot of detached cell suspension was taken and the cells were counted to determine the cell density. The required number of cells (10^6 cells per nucleofection sample) was centrifuged at 200xg for 10 minutes. The supernatant was discarded and the pellet was resuspended in Nucleofector solution V to a final concentration of 10^6 cells/100µl. 100µl of cell suspension was mixed with 5µg of DNA (in 5µl of H_2O). The nucleofection sample was transferred into a cuvette, placed into the Nucleofector and electroporated, using the appropriate program. 500µl of culture medium was added to the cuvette and the sample was transferred to the prepared 6 well plates using the plastic pipettes provided. Cells were then incubated in a 37°C/5% CO_2 incubator for 24 hours before being imaged.

2.2.4 Cell imaging and immunofluoresense

Live cells were split into 6 or 12 well plates and transfected with green fluorescent protein (GFP) or red fluorescent (DS.Red) fusion constructs via calcium phosphate transfection or nuclefection. After 12-48 hours these cells were imaged using an Olympus IX70 fluoresense microscope with a 40X objective. Cells were objectively screened under phase to determine whether they were healthy. They were then screened to identify those that had lower levels of overexpression and only those cells that had approximately 30-70% overexpression as determined by fluorescence levels were imaged.

For confocal microscopy cells were seeded at an appropriate density on coverslips coated with poly-D-Lysine. Growth medium was aspirated, replaced with fixative and incubated at room temperature for 15-20min. The fixative was aspirated, perm/quench added and

then immediately aspirated and replaced with fresh permeating and quenching solution (perm/quench). Cells were incubated in perm/quench for 10-15 minutes. The perm/quench was aspirated and replaced with PGAS and incubated for 5 minutes. The primary antibody was diluted in PGAS and added to the coverslip. The coverslip was incubated in a humidified chamber for 1 hour. The coverslip was then washed in PGAS and then the secondary antibody was added and incubated in a humidified chamber for 1 hour. The coverslip was washed in PGAS and then was washed 3 times in PBS. The coverslip was attached to the slide with a drop of mowiol 4-88 and stored in the dark for at least 4 hours before being imaged on the BioRad Radiance 2000 confocal microscope with 60X oil immersion lenses.

All materials are obtained from Sigma unless otherwise stated.

Fixative – 3% paraformaldehyde (PFA) and 0.1% gluteraldehyde in phosho-buffered saline (PBS).

Perm/quench – 50mM NH_4Cl and 0.2% saponin in PBS.

PGAS – 0.2% gelatin, 0.02% saponin, and 0.02% NaN_3 in PBS.

2.2.5 TUNEL staining

Using the Oncogene DNA fragmentation detection kit for Terminal deoxynucleotidyl transferase-mediated dUTP-biotin nick end labelling (TUNEL) of DNA fragments. HEK and primary hipoocampal cultured cells were fixed as above. When the coverslips were removed from PGAS they were covered with 50-100µl of Proteinase K for 5min to remove exogenous protein from the cells. They were then washed 3 times in PBS. The samples were covered in 50µl of 3% H_2O_2 for 5min to inactivate endogenous peroxidases and then rinsed once in PBS. The coverslips were then incubated with 100µl of the

supplied buffer to equilibrate the samples at the correct pH for 10min. The equilibration buffer was gently removed and the cells were treated with 57μl TdT labelling reaction mix and 3μl TdT enzyme and incubated for 1.5hr in a humidified chamber at 37°C. The coverslips were removed from the chamber, excess liquid was blotted off and 100μl of the supplied buffer to end the reaction (Stop buffer) was applied for 5min. The Stop buffer was removed with a PBS rinse and the coverslips were treated with 100μl of the supplied blocking buffer for 10min. The blocking buffer was carefully removed and the samples were treated with 100μl of 1X conjugate for 30min. The coverslips were washed in PBS and then 100μl of 3,3'-diaminobenzidine tetrahydrochloride (DAB) solution was added for 15min. The cells were rinsed with dH_2O and the coverslips were attached to the slide with a drop of mowiol and stored in the dark for at least 4 hours before being imaged with oil immersion lenses.

2.2.6 Creation of an inducible stable cell line

Using the Trex System from Invitrogen based on tetracycline inducible expression via repression of transcription in the absence of tetracycline. The MSP domain of VAPA fused to the carboxy terminus of GFP was ligated into pcDNA4/TO. This plasmid was then treated with the restriction endonuclease ScaI, which cleaved the plasmid and increased the efficiency of genomic integration, and transfected into HEK cells stably expressing pcDNA6/TR using the calcium phosphate method. Cells were left to grow for 48hrs post-transfection. The growth medium was aspirated and they were then treated with 50μg/ml zeocin in fresh growth medium. The selective medium containing zeocin was replenished every 3-4 days until zeocin resistant colonies were detected. 24 zeocin-

resistant colonies were picked and put into a 24 well plate. These colonies were grown for a further 48 hours and then tested with 1μg/ml tetracycline to check inducible gene expression. 4 colonies were found have good inducible expression and these colonies were grown up further and then frozen down or expanded for further experimentation.

All materials obtained from Invitrogen unless otherwise stated.

Growth medium – DMEM

10% Foetal Bovine serum

1% Penicillin/Streptomycin

2.2.7 DNA laddering

Cells were grown to confluence, trypsinised, washed and counted. 10^6 cells were pelleted and the supernatant was discarded. Cells were resuspended on ice in 20μl of lysis buffer and pipetted to ensure complete lysis. They were then incubated at 55°C for 1 hour. The cell debris was pelleted at 14,000rpm in a tabletop microfuge and 5μl of 20mg/ml RNase A was added to the supernatant. This was incubated at 55°C for 1 hour. The sample was centrifuged briefly to pellet any further cell debris and the supernatant was collected. The supernatant was heated to 70°C for 2 minutes and mixed with 10μl of loading buffer. This was run on a 2% agarose gel containing 0.5μg/ml ethidium bromide at 40V for 2 hours and visualised under UV light.

All materials obtained from Sigma unless otherwise stated.

Lysis buffer – 50mM Tris-HCl (pH 8)

10mM EDTA

0.5% SDS

0.5mg/ml proteinase K

2.2.8 Propidium iodide cell viability assay

Cells were plated and grown to 20-40% confluency. A 50X stock solution of 250ml/ml of propidium iodide (Sigma) solution was prepared in distilled water. The desired amount of cell culture medium was made up with 1X propidium iodide. The medium on the cells was carefully aspirated and replaced with the medium containing propidium iodide. The cells were incubated for 20 min at 37°C and then imaged. Viable cells were detected on a fluorescent microscope as those, which excluded the propidium iodide.

2.2.9 Northern blotting

HEK293 cells were calcium phosphate transfected with Green Fluorescent Protein (GFP), Blue Fluorescent Protein (BFP), MSP-GFP/TO, VAPA-GFP, and tPA-GFP. The cells were lysed in 1ml Trizol reagent (Invitrogen) and incubated for 5min at room temperature to permit complete dissociation of the nucleoprotein complexes. 0.2ml of chloroform was added and the tubes were shaken by hand for 15s and then incubated at room temperature for a further 3 minutes. The samples were spun at 12K x g for 10min at 4°C. The aqueous phase was moved to a clean eppendorf tube and 0.5ml isopropyl alcohol was added. The samples were incubated for 10min at room temperature and then spun at 12K x g for 10min at 4°C. The supernatant was removed and the RNA pellet was washed with 1ml of 75% ethanol, vortexed and centrifuged at 7,500 x g for 5min at 4°C.

The supernatant was carefully removed and the RNA was air-dried for 10min. The RNA was then resuspended in DEPEC H_2O for 10min at 60°C and the optical density of the RNA was measured via spectrophotometeric analysis. 2µl of each RNA sample was suspended in a mixture of 2µl 10X MOPs, 4µl formaldehyde, 10µl formamide and 1µl ethidium bromide. The samples were incubated at 85°C for 10min, transferred to ice for 10min and 2µl of formaldehyde gel loading buffer was added. The RNA was subjected to electrophoresis on a 1.5% agarose gel containing 1X MOPs at 125V. The RNA was transferred from the gel to a nylon membrane (Hybond-N) using a turboblotter. The BiP hybridisation probe (encoding the entire BiP cDNA) was made using the Prime-it Random Primer labelling Kit (Stratagene) and was labelled using [α-^{32}P] dCTP. For the hybridisation of the BiP probe to the mRNA on the membrane the Hybridisation Buffer with 50% formamide was preheated to 65°C and the membrane was prehybridised in this solution for 1hr. 50µl of the BiP probe was then added to 10ml of the Hybridisation Buffer and the membrane was incubated with this solution overnight at 65°C. The membrane was washed twice with 2X SSC containing 1% SDS for 5min at room temperature and then washed twice with 0.5X SSC containing 1% SDS for 5min at 65°C. The membrane was imaged using a phospho-imager.

All materials obtained from Sigma unless otherwise stated.

Formaldehyde gel loading buffer - 62.5% Formamide

9.25% Formaldehyde

1.25x MOPS Buffer

50 µg/ml Bromophenol Blue (BPB)

50 µg/ml Xylene Cyanol (XC)

10X MOPS - 0.4M Morpholinopropanesulfonic acid (free acid)

0.1M Sodium acetate

10mM EDTA

adjust to pH 7.2 with NaOH

store dark in fridge

20 x SSC - 3M NaCl

0.3M Sodium Citrate

2.2.10 BioRad protein assay

Prior to western blotting samples were subjected to a protein assay to ensure that a standard amount of protein (10-20μg) was loaded in each well. The BioRad dye reagent concentrate was diluted 1:4 and filtered. Five dilutions of BSA protein standard (BioRad) were prepared in the range 0.2 to 0.9 mg/ml. Five dilutions of the protein sample to be used in western blotting were also prepared. 100μl of each standard and sample solution were added to a test tube. 5ml of diluted dye reagent was then added to each test tube, the samples were vortexed and incubated at room temperature for 5 minutes. The absorbance of the samples and standards at 595nm was then measured and the concentration of the sample solutions was determined by comparing the absorbance levels to that of the standards.

2.2.11 Western blotting

Samples were suspended in SDS loading dye and run on a 10% or 4-20% SDS gel at 125V in Tris-Glycine running buffer. They were then transferred to a pvdf (Hybond-P) membrane in CAPS buffer at 25V for 16 hours. The pvdf membrane was then incubated in 5% non-fat milk for 1hr at room temperature. The membrane was incubated with the

appropriate primary antibody (VAPA (Skehel et al., 1995), VAPB (GeneTex), GFP (molecular probes), phosphPERK (Cell Signalling Technology), caspase 3 (Cell Signalling Technology) or HA (Upstate)) for 1hr. The membrane was washed twice in PBS plus 0.1% Tween20 for 5 minutes and then incubated for 1hr in the appropriate secondary antibody (Goat anti-rabbit or Donkey anti-sheep). The blot was then washed three times in PBS plus 0.1% Tween20 for 10 minutes. ECL detection buffer was added to the blot, which was then exposed on Kodak film and analysed.

All materials obtained from Sigma unless otherwise stated.

SDS loading Dye (2X) – 80mM Tris (pH 6.9)
2% SDS (Bio-Rad)
100mM DTT
10% Glycerol (Bio-Rad)
0.004% bromophenol blue

10% Resolving Gel – 4ml 20% acrylamide (Bio-Rad)
2.5ml resolving buffer (pH 8.8)
3.3ml dH_2O
200µl 10% APS (Bio-Rad)
5µl Temed (Bio-Rad)

Stacking Gel – 0.5ml 20% acrylamide (Bio-Rad)
1.3ml stacking buffer (pH 6.8)
3.2ml dH_2O
40µl 10% APS (Bio-Rad)
5µl Temed (Bio-Rad)

Tris-Glycine Running buffer (10X) – 30g Trizma

140g Glycine

50ml 20% SDS (Bio-Rad)

dH_2O to 1litre

CAPS transfer Buffer (50X) – 0.5M CAPS (pH 11.5)

2.3 DNA preparation, PCR and Cloning of VAP cDNA

2.3.1 Amplification of mouse cDNA library

Using the GENETRAPPER® protocol (adapted from Hanahan et al., 1991) for semi-solid amplification of plasmid cDNA libraries. 2 litres of 2X LB were prepared. 200mls were removed and used to make the 2X LB glycerol. 5.4g of SeaPrep agarose were added to the 1.8 litres of 2X LB and this was autoclaved. The LB agarose was then cooled to 37°C and 200μg/ml of ampicillin (Invitrogen) was added. 4×10^5 - 6×10^5 colonies from the original mouse brain cDNA library were added and then incubated for 1 hour in an ice bath. The colonies were then incubated in a gravity flow incubator at 30°C for 40–45 hours without disturbance. The colonies were removed from the incubator and spun at 8000 rpm for 20 minutes at room temperature. The supernatant was poured off and the colonies resuspended in 100 ml of 2X LB glycerol (12.5%). The colonies were split into aliquots and stored at -70°C.

All materials are obtained from Sigma unless otherwise stated.

2 X LB - 20 g Tryptone (Fisher)

10 g Yeast Extract

10 g NaCl

Bring to 1,000 ml H_2O.

2 X LB Glycerol (12.5%) - 175 ml 2 X LB

25 ml Glycerol (100%)

Filter sterilise and store for up to two months at room temperature.

2.3.2 Spectrophotometric quantitation of nucleic acids

Nucleic acid concentrations were determined by measuring the UV absorbance at 260nm of diluted samples (Beckman DU-7 spectrophotometer). Assuming the molecular weight of a nucleotide pair is 660 Daltons, an OD_{260} absorbance of 1 is equivalent to 50µg/ml for double stranded DNA, 40µg/ml for RNA and 33µg/ml for 20mer oligonucleotides (Sambrook *et al.,* 1989).

2.3.3 The polymerase chain reaction (PCR)

The polymerase chain reaction (PCR) allows amplification of a specific DNA fragment *in vitro.* Extension of the annealed primers with a DNA polymerase from the thermophilic bacterium *Thermus aquaticus* (Taq) or *Pyrococcus furiosus* (Pfu) polymerase, for increased fidelity, in the presence of deoxynucleotides result in amplification of the target DNA. The standard PCR conditions described by Ashworth (1993) were used. Each 50µl reaction contained the following components:

5µl of 10x PCR buffer (150mM Tris-HCl pH 8.8, 600mM KCl, 22.5mM, $MgCl_2$),

1.25µl of 10mM dNTPs ,

1µl (10pmol) of each of two primers,

1Unit of Taq or pfu DNA polymerase

water and 50ng template DNA to a total volume of 50µl.

A single working stock of PCR components, minus template DNA, was made to reduce reaction variation. The template, added last to reduce chances of cross-contamination, was plasmid DNA (~1-10ng), genomic DNA (~50ng) or cDNA libraries (~1-5µl). All sets of reactions included a sample, lacking template DNA as a negative control. The PCRs were carried out on a programmable thermocycler (Robocycler or ABI9700). Generally, the samples underwent 30 cycles of:

(a) denaturation at 94°C for 0.5 min.

(b) annealing at 50-55°C for 0.5 min.

(c) extension at 72°C for 1 min.

followed by 5 min. at 72°C.

In most cases the products of the PCR reaction were treated with restriction enzymes and ligated into the plasmid vectors EGFP-C1, pcDNA4/TO or monomeric DS.Red-C1. These vector constructs were then introduced into chemically competent TOP10F bacteria.

2.3.4 Primer list (Invitrogen custom primers)

Name	Sequence	Construct/vector
	5' 3'	
VAPB1	GCGAATTCCATGGCGAAGGTGGAACAG	Full-length VAPB
VAPB2	GGGTGATCAGCGGCCGCCCCTACAAGGCAATCTTCCCT	Full-length VAPB

Pointmut1	TCCCACTGTTGGACCGCACACAGTA	VAPAP56S
Pointmut2	TACTGTGTGCGGTCCAACAGTGGGA	VAPAP56S
Pointmut3	TACTGCGTGCGGTCCAACAGTGGGG	VAPBP56S
Pointmut4	CCCCACTGTTGGACCGCACGCAGTA	VAPBP56S
VAPB5	GACGGATCCCTACATCGCCTTCCTCAC	VAPB/VAPBP56S without tail
VAPB6	GCGAATTCCGCAAAACCGGAAGACCTT	VAPB coiled-coil with tail
VAPC1	GACGGATCCGCTAAGGCCCTCCTCCTT	VAPC
VAPB7	GACGGATTCCTATTTTGCCTCCTTCCA	VAPB MSP
Yeast1	CTGAGTGGAGATGCCTCC	pJG4-5
Yeast2	GCCGACAACCTTGATTG	pJG4-5
417	CGTCAGCAGAGCTTCACCATTG	pGilda
483	AAAGGATCCGCTCTGGCGGCCACTGGGAAG	VAPB tail with Bam H1 site

2.3.5 Digestion of DNA with restriction endonucleases

DNA was digested with restriction enzymes using the manufacturer's recommended 10x restriction buffers and digestion temperatures (New England Biolabs). Routinely, 1μg of plasmid DNA was digested for 1 hour at 37°C in a total volume of 10μl of 1x restriction buffer using between 5-10 units of restriction endonuclease, such that the volume of restriction enzyme did not exceed one tenth of the reaction volume.

2.3.6 Gel electrophoresis of DNA

Agarose gel electrophoresis was used to size or separate DNA fragments within the range 50bp-20kb. Electrophoresis was carried out using a horizontal gel electrophoresis

apparatus according to the manufacturer's operating instructions. Gels were made from 0.8-2.0% agarose melted in 1x TAE buffer (40mM Tris-HCl, pH7.8; 20mM sodium acetate; 1mM EDTA, pH8.0) containing 0.5μg/ml ethidium bromide solution. The melted agarose was cast in a horizontal gel tray after cooling to 60°C with a suitably positioned comb to form slots in the gel. The gel, once solidified, was submerged in 1x TAE buffer with 0.5μg/ml ethidium bromide. DNA solutions (0.1μg-10μg) were resuspended in loading buffer (0.25% w/v bromophenol blue; 100mM EDTA; 30% glycerol) and loaded into the wells of the gel. The samples were electrophoresed at 65V in parallel with double-stranded DNA size markers DNA was visualised using short- or long-wave ultraviolet light.

2.3.7 Gel extraction of DNA (Qiagen)

The DNA band was visualised under long wavelength (365nm) ultra-violet light and excised from the agarose gel using a clean, sharp scalpel. The agarose containing the DNA band was placed in an eppendorf tube 3 volumes of buffer QXI plus 2 volumes of dH_2O were added to the tube. The Qiaex II was vortexed for 30s and then 10μl were added. This was then incubated at 50°C for 10min and vortexed every 2min. The solution was then centrifuged at full speed in a tabletop microfuge for 30s and the supernatant discarded. The pellet was resuspended in 500μl of buffer QXI and then centrifuged for 30s and washed twice in 500μl of solution PE (70% ethanol). The pellet was air dried for 10-15min and then resuspended in 20ml of dH_2O and incubated at 50°C for 5min. The suspension was then centrifuged for 30s and the supernatant containing the DNA was pipetted into a clean tube.

2.3.8 Introduction of DNA into chemically competent bacteria

One 50 μl vial of One Shot® cells (Invitrogen) for each transformation was thawed on ice. 1μl of DNA or ligation mix was added to the cells and the vial was incubated on ice for 30min. The vial was then incubated at 42°C in a pre-heated water bath for 30s and placed back on ice. 250μl of SOC medium was added to the vial and it was incubated at 37°C for one hour in a rotary shaker-incubator. 10-50μl of each vial was spread onto plates containing either the appropriate antibody selection.

2.3.9 Miniprep of bacterial plasmid DNA (Qiagen)

An overnight culture of a single bacterial colony was grown in 2ml Luria-Bertani (LB) medium at 37°C in a rotary shaker-incubator. 1.5ml of the bacterial culture was pipetted into an eppendorf tube and centrifuged at 14K rpm in a tabletop microfuge. The supernatant was pipetted off and discarded and the pellet was resuspended in 250μl of buffer P1 containing RNase A to remove RNA contamination. The bacterial cells were then lysed in 250μl NaOH/SDS (buffer P2) for 5min. The lysate was neutralized by the addition of 350μl of buffer N3 and the high salt concentration of this buffer allowed the chromosomal DNA and denatured proteins to precipitate leaving the plasmid DNA. The suspension was then centrifuged at 14K rpm for 10 min. The supernatant was added to the Qiaprep column and drawn through using a vacuum manifold. 0.5ml of buffer PB followed by 0.75ml of buffer PE were added to the column and washed through. The column was then centrifuged for 1min at 14K rpm to remove residual PE. Finally 50μl of buffer EB was added to the column, it was incubated at room temperature for 1min and then centrifuged for 1min to elute the DNA into a fresh eppendorf tube.

2.3.10 DNA sequencing

Sequencing was carried out using the ABI PRISM Dye Terminator Cycle Sequencing Ready Reaction Kit based upon fluorescent chain termination. The sequencing reaction was set up with 8.0μl of Terminator Ready Reaction Mix (ABI PRISM) 0.1μg/ml of double stranded DNA or 30ng/ml of PCR product, and 3.2pmole of primer in a final reaction volume of 20μl. The sequencing reaction was then placed in the Applied Biosystems GeneAmp PCR system 9700. The reaction was kept at 96°C for 30s, 50°C for 15s and 60°C for 4 min and this was repeated for 25 cycles. The reaction was then cooled to 4°C. The sequencing reaction was ethanol precipitated by adding 2μl 3M sodium acetate (pH 4.6) and 50μl of 95% ethanol. This was vortexed and then spun at 20000 rpm for 40 min at 4°C. The ethanol was aspirated and replaced with 70% ethanol and spun for a further 10 min. The 70% ethanol was aspirated and the pellet was left to air dry. The sample was resuspended in 25μl of template suppression reagent (P/N 401674), vortexed, and spun. The sample was then heated at 95°C for two min to denature the DNA, vortexed and spun again. Samples were then loaded into the ABI PRISM 310 Genetic Analyser for sequencing.

2.4 Protein localisation and multimerisation experiments

2.4.1 Chemical cross-linking of protein

HEK cells were nucleofected with VAPB-GFP or VAPBP56S-GFP and incubated overnight at 37°C. They were then treated with 100mM to 250mM disuccinimidyl

suberate (DSS) (Pierce) for 10min. The cells were lysed in SDS loading dye and samples were used for western blotting.

2.4.2 Triton X114 extraction (adapted from Bordier, 1981)

Cells were grown to the desired confluency (10^7 cells/cm^2), trypsinised and then harvested. The cells were then homogenised in 5ml of ice-cold 20mM Hepes (pH7.4), 320mM sucrose plus protease inhibitors (Boeringer). This was then centrifuged at 1500 rpm for 10 min at 4°C. The supernatant was decanted into another tube leaving the P1 pellet (consisting of cellular membranes such as the plasma membrane and nuclear membrane). The supernatant or post nuclear fraction was centrifuged for a further 30 min at 20000 rpm to give the P2 (consisting of cellular membranes such as ER, Golgi and intracellular vesicles) and S2 layers. The S2 layer was centrifuged for a further 90 min at 100000 rpm to give the P3 (possibly consisting of aggregated protein) and S3 (consisting of soluble protein) layers. The P2 layer was resuspended in resuspension buffer and incubated for 10 min on ice (or until cleared). The resuspended P2 was layered on to 300ml of sucrose cushion and then incubated at 30°C for 3 min. This was then centrifuged at 300g for 3 min. The upper aqueous layer was removed and kept. 150ml of 10% Triton X114 was centrifuged at 14000 rpm in a bench top centrifuge to remove the remaining detergent phase.

All materials obtained from Sigma unless otherwise stated.

Resuspension buffer – 10mM Hepes pH 8.0 with KOH

400mM KCl

1.0% Triton X114 (BDH)

Sucrose cushion – 6%(w/v) Sucrose

10mM Hepes pH 8.0

400mM KCl

0.06% Triton X114 (BDH)

3. Yeast-two Hybrid Screen to identify MSP domain interacting proteins

3.1 Background

VAPA and VAPB have three domains, the N-terminal MSP domain, a coiled-coil domain and a hydrophobic tail domain (Nishimura et al., 1999). The coiled-coil domains of VAPA and VAPB have been shown to interact with a variety of SNARE and fusion proteins (Weir et al., 2001). However, a full screen of proteins interacting with the MSP domains of these proteins has yet to be carried out. The MSP domain of the VAP proteins shares a high level of homology with the major sperm protein first identified in nematodes. The major sperm protein folds into an Ig-like domain, which is structurally related to the periplasmic bacterial protein chaperone (PaPD).

In nematodes this protein has been shown to be involved in sperm locomotion in a role analogous to that of actin in higher eukaryotic organisms. MSP forms filaments in nematode sperm due to various interaction domains, which see it first form dimers and then filamentous multimers (Baker et al., 2002). The formation of these filaments pushes a vesicle formed from the plasma membrane forward at the leading edge of the lamellipod causing sperm locomotion (Italiano et al., 1996). Other proteins involved in the polymerization of MSP include a 48kDa membrane phosphoprotein (MPOP) (LeClaire et al., 2003) and two MSP fibre proteins (MPF1 and MPF2) (Buttery et al., 2003).

More recently, MSP has been implicated in oocyte maturation and sheath cell contraction in *Caenorhabditis elegans* (Miller et al., 2001). *C. elegans* oocytes are surrounded by sheath cells, which they are coupled to via gap junctions. Sheath cell contraction drives ovulation. VAB-1, a protein-tyrosine kinase is the only Eph receptor in *C. elegans* and it negatively regulates oocyte M-phase entry. MSP acts as an antagonist of the VAB-1 Eph receptor to give MAPK activation and oocyte meiotic maturation. It also antagonizes the CEH-18 pathway, which acts in parallel with VAB-1 (Miller et al. 2003). However on sheath cell membranes it may act as an agonist of the VAB-1 receptor and thus increase sheath cell contraction. In order for MSP to regulate oocyte maturation it has to be released from the sperm. However, sperm lack the cellular components required for classical protein secretion, such as the ER, Golgi and ribosomes. Kosinski et al., have recently discovered that spermatids and spermatozoa in *C. elegans* release MSP by a novel vesicle-budding mechanism. Using TEM they visualized double membraned vesicles containing MSP. These vesicles appeared to be labile and fuse to generate lipid whorls as they disintegrate and release their contents (Kosinski et al., 2005).

Proteins, which contain MSP domains, are found in many other organisms such as *S. cerevisiae, Drosophila, Mus musculus* and *Homo sapiens*. There are 7 *mus musculus* proteins, which have been identified as containing a MSP domain (Figure 3.1).

These proteins include the VAP protein family, the motile sperm domain containing proteins 1-4 (MOSPD1, MOSPD2, MOSPD3, MOSPD4) and hydin. MOSPD3 is a protein with an MSP domain and two transmembrane domains and is very similar to

MOSDP1. Using a gene trap vector MOSPD3 has been found to play a role in right ventricle development in the heart (Pall et al., 2004). Hydin has been identified as causing hydrocephalus in mice when a frameshift mutation is introduced. Hydrocephalus is a net accumulation of cerebrospinal fluid in the ventricular system of the brain. As hydin is specifically expressed in the choroids plexus and ependymal cells lining the ventricles within the brain, dysfunction of these cells may play a role in the hydrocephalus seen (Davy et al., 2003). MOSPD2 contains a flavin-containing monooxygenase domain and can bind cellular retinaldehyde.

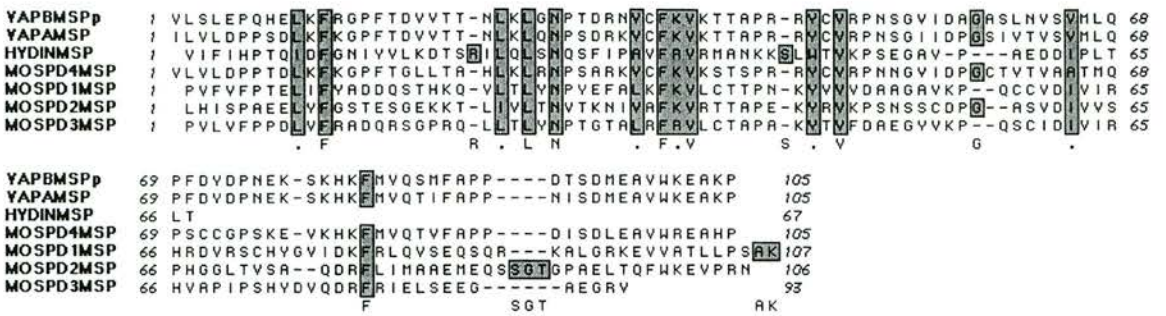

Figure 3.1. Major Sperm Protein (MSP) homology domain of MSP-containing proteins in the mouse.

In the VAP proteins the MSP domain is the location of the binding site for the FFAT (two phenylalanines in an acidic tract) motif of lipid binding proteins. Critical residues in *Mus musculus* VAPA for FFAT binding are lysine-46, threonine-48, lysine-86 and lysine-119. Modeled onto the known structure for *C. elegans* MSP the critical bases are in a core peripherally surrounded by the non-critical bases (Loewen et al., 2005). While VAPB and MOSPD4 share all the critical residues for FFAT motif binding in the mouse, the other MSP domain proteins have only one or none of these bases, suggesting that they do not bind proteins containing FFAT motifs (Table 3.1). Proteins containing FFAT motifs that are known to bind to the VAP proteins thus far are all involved in lipid synthesis.

PROTEIN	FFAT MOTIF
OSBP1	EFFDA
OSBPL2	EFFDA
OSBPL3	EFFDA
OSBPL4	EYFDA
OSBPL6	EFFDA
OSBPL9	EFYDA
NIR1	EFFDA
NIR2	EFFDA
NIR3	EFFDA
CERT	EFFDA
PITPNM1	EFFDA
CHOREIN	EFFDA
TESTIS SPERM APOPTOSIS RELATED GENE 6 PROTEIN	EFFDA
HOMOLOGUE OF DROSOPHILA RETINAL DEGENERATION B GENE	EFFDA
COG7	EFYDA

Table 3.1. Proteins containing a two phenylalanines in an acidic tract (FFAT) motif in mammals.

3.2 Yeast two-hybrid protein interaction screen using pGilda-MSP

To determine which proteins the MSP domain of the VAPA protein could bind to and interact with, a yeast two-hybrid screen using pGilda-MSP as the bait plasmid, and the mouse brain LexA JG4-5 library as a target, was carried out. $4x10^7$ colonies were screened in total and 115 potential positive transformants were found. Of these forty colonies were established as X-gal positive colonies (Figure 3.2). These colonies were then grown up and plasmid DNA was extracted. This plasmid DNA was then amplified in KC8 cells and was extracted via miniprep. The library plasmid DNA was then sequenced.

Of the forty colonies fifteen appeared after 48 hours and are presumed to be "strong interactors", while twenty-five appeared after 72 hours and are "weaker interactors", however the colonies that appear later may be slower to reach the nucleus and to activate transcription (Table 3.2). Of the strong interactors fourteen colonies contained sufficient target DNA for sequencing (Table 3.3). Of the weaker interactors nineteen colonies contained sufficient target DNA for sequencing (Table 3.3).

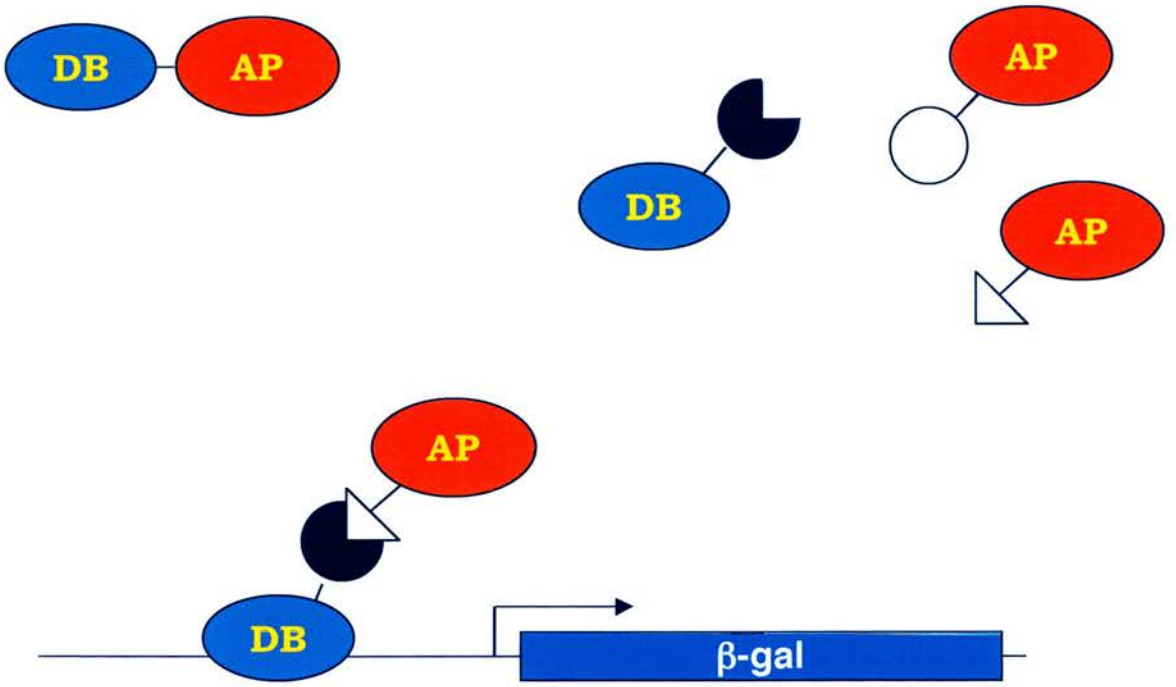

Figure 3.2. Yeast two-hybrid protein interaction screen. This is a Lex-A-based version of the yeast two-hybrid system originally developed by Fields and Song. In the Lex-A system the DNA binding protein (DB) is the *E. coli* Lex-A protein and the activation protein (AP) is the acid blob domain B42. The DNA binding protein and the activation protein cannot activate reporter expression on their own but when they are brought together via two interacting proteins they activate β-galactose reporter gene expression.

Table 3.2. Growth analysis of positive clones. The yeast clones 1-40 (Y1-40) were classified according to the time-point at which they appeared. "Strong interactors" with the bait VAPA MSP protein appeared after 48 hours, whereas "Weak interactors" appeared at 72 hours.

	GROWTH	
CLONE	48hrs	72hrs
Y1	*	
Y2	*	
Y3	*	
Y4	*	
Y5	*	
Y6	*	
Y7	*	
Y8	*	
Y9	*	
Y10	*	
Y11	*	
Y12	*	
Y13	*	
Y14	*	
Y15	*	
Y16		*
Y17		*
Y18		*
Y19		*
Y20		*
Y21		*
Y21		*
Y23		*
Y24		*
Y25		*
Y26		*
Y27		*
Y28		*
Y29		*
Y30		*
Y31		*
Y32		*
Y33		*
Y34		*
Y35		*
Y36		*
Y37		*
Y38		*
Y39		*
Y40		*

Table 3.3. Sequencing analysis of the potential positive yeast colonies identified in the yeast two-hybrid screen. A mixture of the bait and reporter plasmids along with the mouse brain cDNA library plasmid was rescued from the yeast colony. This library plasmid was then transformed into KC8 *E. coli* and selected for on ampicillin and – Tryptamine LB plates. Library plasmid DNA was then obtained via miniprep from the KC8 cells and sequenced on the ABI PRISM sequencer. A BLAST search was performed for each sequence obtained on the Ensembl website.

CLONE	CORRESPONDING cDNA	Length of clone DNA	Coding sequence of cDNA from Ensembl
Y1	TAF1	2953 -3876	1 - 3873
Y2	Good pasture antigen binding protein (GPBP or CERT	1294 - 2211	337 - 2211
Y3	OSBP1	1 - 990	169 - 2217
Y4	ZINC FINGER DHHC DOMAIN CONTAINING PROTEIN 7 (SERTOLI CELL GENE WITH A ZINC FINGER DOMAIN PROTEIN)	1 - 916	1 - 192
Y5	Rnf144	422 - 1300	422 - 1300
Y6	ATF6α	1135 - 1710	2 - 2038
Y7	Good pasture antigen binding protein (GPBP or CERT	1294 - 2211	337 - 2211
Y8	Rad17	293 - 2067	293 - 2359
Y9	TAF1	2953 -3876	1 - 3873
Y10	No sequence gained due to difficulties obtaining plasmid DNA		
Y11	COG7	198 - 1152	3 - 2117

Y12	ATF6α	1135 - 1710	2 - 2038
Y13	DnaJa1	112 - 918	112 - 1305
Y14	ORP9	269 - 1149	65 - 1929
Y15	GLUTAMATE DEHYDROGENASE, MITOCHONDRIAL PRECURSOR(GDH)	889 - 1824	1 - 1821
Y16	No sequence gained due to difficulties obtaining plasmid DNA		
Y17	No sequence gained due to difficulties obtaining plasmid DNA		
Y18	ENSMUST00000092805	1 - 195	1 - 195
Y19	Rnf144	422 - 1300	422 - 1300
Y20	ATP SYNTHASE DELTA CHAIN, MITOCHONDRIAL PRECURSOR	102 - 608	3 - 608
Y21	ENSMUST00000092805	1 - 195	1 - 195
Y22	Trappc4	248 - 907	248 - 907

Y23	GLUTAMATE DEHYDROGENASE, MITOCHONDRIAL PRECURSOR(GDH)	889 - 1824	1 - 1821
Y24	pcdhb13	1879 - 2454	1 - 2445
Y25	GLUTAMATE DEHYDROGENASE, MITOCHONDRIAL PRECURSOR(GDH)	889 - 1824	1 - 1821
Y26	Psd4	2380 - 3188	171 - 3188
Y27	No sequence gained due to difficulties obtaining plasmid DNA		
Y28	MOSPD2	1000 - 1669	113 - 1669
Y29	ENSMUSG00000031983	187 - 1155	187-1155
Y30	Q80TB9	1 - 759	1 - 3246
Y31	MOSPD4	1 - 576	1 - 576
Y32	MOSPD2	1000 - 1669	113 - 1669
Y33	Q80TB9	1 - 759	1 - 3246

Y34	MOSPD2	1000 - 1669	113 - 1669
Y35	MOSPD4	1 - 576	1 - 576
Y36	ZINC FINGER DHHC DOMAIN CONTAINING PROTEIN 7 (SERTOLI CELL GENE WITH A ZINC FINGER DOMAIN PROTEIN)	1 - 916	1 - 192
Y37	ENSMUSG00000031983	187 - 1155	187-1155
Y38	No sequence gained due to difficulties obtaining plasmid DNA		
Y39	No sequence gained due to difficulties obtaining plasmid DNA		
Y40	No sequence gained due to difficulties obtaining plasmid DNA		

3.3 Discussion

Of the sequences obtained from the yeast two-hybrid screen four of the proteins contain a FFAT motif and therefore are predicted to interact with the MSP domain of VAPA. These proteins include oxysterol binding protein 1 (OSBP1) and OSBP related protein 9 (ORP9), which are already known to interact with VAPA. Oxysterol binding protein (OSBP) can interact with VAPA on the ER membrane via its FFAT motif. Overexpression in CHO cells of a PH domain mutant of OSBP that constitutively interacted with VAPA formed unusual distensions of the ER that accumulated a fluorescent ceramide analogue, unfolded vesicular stomatitis virus G protein-GFP and ER chaperones such as PDI (Wyles et al., 2002). There are 12 members of the OSBP-related protein (ORP) family and these proteins have 2 conserved motifs, a C-terminal OSBP homology (OH) domain and an N-terminal PH domain. OSBP was originally identified as a high affinity 25-hydroxycholesterol receptor (Dawson et al., 1989). 25-hydroxycholesterol promotes rapid PH-domain-dependent translocation of OSBP to the Golgi apparatus. Cholesterol and sphingomyelin have similar effects on OSBP translocation suggesting that cellular lipid and cholesterol metabolism have an effect on the cellular location of OSBP.

Of the ORP family OSBP and ORPs 1, 2, 3, 4, 6, 7 and 9 have been shown to interact with VAPA. VAPA and VAPB have both been found to co-immunoprecipitate with ORP 9. Compared to non-induced cells ORP 9 overexpression caused dramatic reorganisation of ER and ERGIC compartments. VAPA was shifted from a reticular pattern to the edges of numerous large vesicular structures that appeared in the cytoplasm

after induction of ORP 9 for 48 hours. Calnexin also localised to the same large vesicles, as did ERGIC-53/p58, a marker for the ER-Golgi intermediate compartment. The dramatic effect of ORP 9 and the VAPA-binding mutant on the distribution of ERGIC53/p58 and Sec31 suggests that the COPII transport pathway may be affected (Wyles et al., 2004).

Good pasture antigen binding protein (GPBP or CERT) is involved in the transfer of ceramide between the ER and Golgi (Kuge et al., 1994) and conserved oligomeric Golgi 7 (COG7), a protein involved in Golgi associated membrane trafficking (Oka et al., 2005) and these proteins also contain FFAT domains. Ceramide is synthesised in the ER and then taken to the Golgi apparatus to be converted to sphingomyelin. Ceramide transfer protein, CERT, is a protein that contains a PI-binding pleckstrin homology (PH) domain, and a putative lipid-transfer-catalysing domain named SMART. The PH domain targets CERT to the Golgi by recognising PtdIns(4)P (Levine et al, 2004). CERT can specifically extract ceramide from the ER via its START domain and is known to catalyse the transfer of ceramide to donor membranes in vitro (Kuge et al., 1994).

There are other proteins with an FFAT domain that have been previously identified as interacting with the MSP domain of VAPA. The reasons that they have not been detected in this screen may be that not enough colonies were screened to pick up every interaction of the VAPA MSP domain or that these proteins were of low abundance in the mouse brain library used. Of the VAPA MSP domain interacting proteins not detected in the screen the Nir protein family is of interest. Nir1, Nir2 and Nir3 are proteins expressed in

the Golgi apparatus. Nir2 and Nir3 contain an N-terminal PI transfer domain, followed by a short acidic region, 6 hydrophobic stretches and a highly conserved C-terminal domain. The PI transfer domain has the ability to transfer PI and phosphatidylcholine between membrane bilayers in vitro. Nir1, Nir2 and Nir3 all interact with VAPB. Overexpression of wild-type Nir2 with VAPB caused production of large heterologous granular structures that were dispersed around the nucleus throughout the cytosol. VAPB expressed alone is a dimer but its interaction with Nir2 creates complexes of various sizes that may represent different oligomerisation forms. Coexpression of Nir1 and VAPB had no apparent effect on either of their localisations. Coexpression of VAPB and Nir3 dramatically modified the organisation of microtubules. The microtubules were unusually thick and not organised and the microtubule organisation centre was not visible. The microtubule staining also aligned with the VAPB and Nir3 immunostaining. It also reorganised the ER into a tubular structure (Amarilio et al., 2005). This is particularly interesting as mouse VAPA is known to be involved in interactions with microtubules (Skehel et al., 2000).

Three proteins containing a MSP domain were obtained in the screen MOSPD2, MOSPD4 and Q80TB9 may interact with the VAPA MSP domain via their MSP domain. Other proteins of note include activating transcription factor 6 (ATF6), one of the effector proteins of the ER stress response (Ye et al., 2000) and deoxyribonucleic acid replication factor with a J motif (DnaJ), a heat shock protein (Raabe et al., 1991). SCS2 is the yeast homologue of VAPA and it has been found to be involved in the yeast ER stress response (Kagiwada et al., 1998). ATF6 is a type II membrane protein and is cleaved by the site

proteases S1P and S2P (Ye et al., 2000) in response to accumulation of unfolded proteins. When cleaved in response to ER stress the bZIP containing N terminal half becomes a soluble transcription factor and is translocated into the nucleus where it induces XBP-1 transcription (Yoshida et al., 2001). The cDNA clone found in the yeast two-hybrid assay was only a partial clone containing the transmembrane domain of the protein and parts of the luminal N terminal domain and the C terminal extra-luminal domain. As the N terminus MSP domain of VAPA is extra-luminal, it is presumed that it would interact with the C terminal portion of ATF6.

4. The MSP domain and the ER stress response

4.1 Background

The VAP proteins are predominantly localized at the endoplasmic reticulum in Mus musculus and Homo sapiens (Skehel et al., 2000). SCS2, the yeast homologue of VAPA, is also a type II ER membrane protein. Yeast strains where the Scs2 gene has been disrupted do not grow as well as wild-type strains in inositol-free medium and display inositol auxotrophy (Kagiwada et al., 1998). SCS2 has been found to interact with OPI1 via its FFAT motif. OPI1 is a transcription factor, which regulates inositol transcription (Loewen et al., 2003). This interaction binds OPI1 so that it cannot interact with INO1. This releases Ino2 and Ino4 to activate inositol. The activation of HAC1 via the unfolded protein response acts to release OPI1 from chromatin. This leaves INO1 free to be recruited to the nuclear membrane (Brickner et al., 2004). OPI1 can also bind to an inhibitor, phosphatidic acid (PA), on the ER. Therefore, it can translocate to the nucleus in response to consumption of PA by inositol (Loewen et al., 2004). As HAC1 is important for the unfolded protein response (UPR) and INO1 is important for ER membrane biogenesis SCS2 plays a role in both of these pathways (Figure 4.1).

In the mammalian ER stress response three signalling cascades have been identified as being important (Figure 4.2). These pathways are regulated by the activation of the kinases IRE1 and PERK and also by the transcription factor ATF6 (Kaufman et al., 2002). An increase in the amount of unfolded proteins in the ER causes activation of

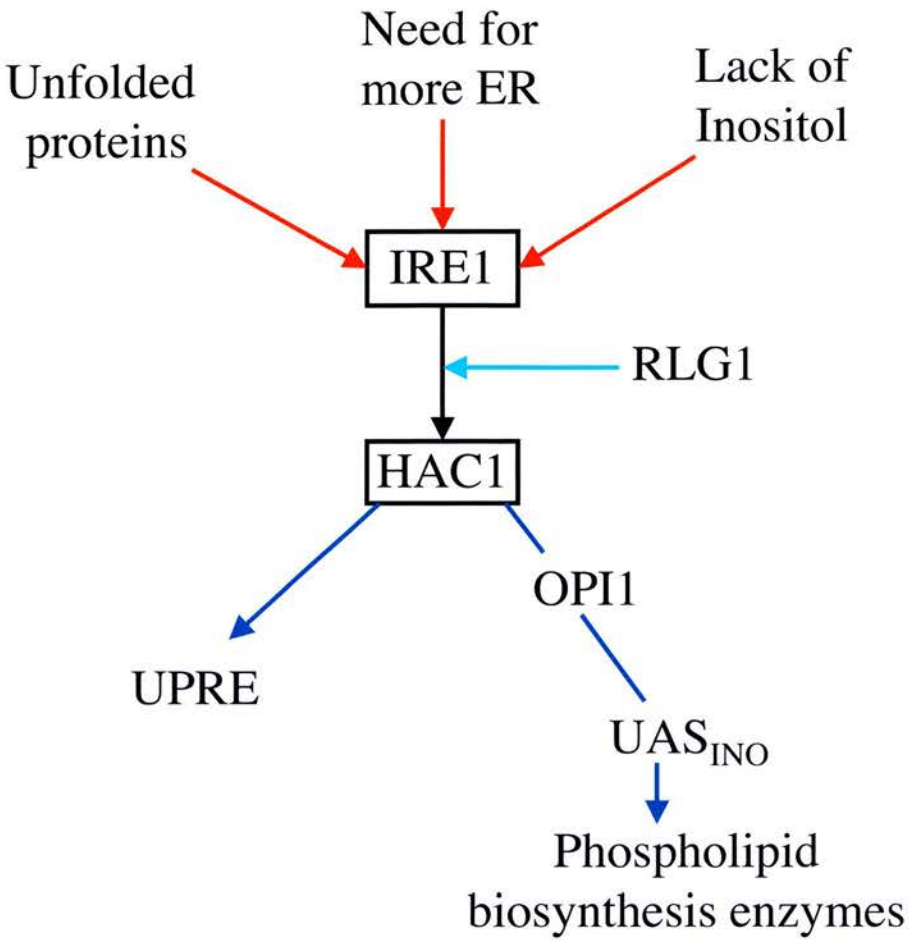

Figure 4.1 The Unfolded Protein Response (UPR) and phospholipid biosynthesis are linked in yeast. The main components of the UPR in yeast are IRE1 and HAC1. As increased biosynthesis of the ER would increase its capacity to handle unfolded proteins it is unsurprising to find that these proteins can activate phospholipid biosynthesis via OPI1.

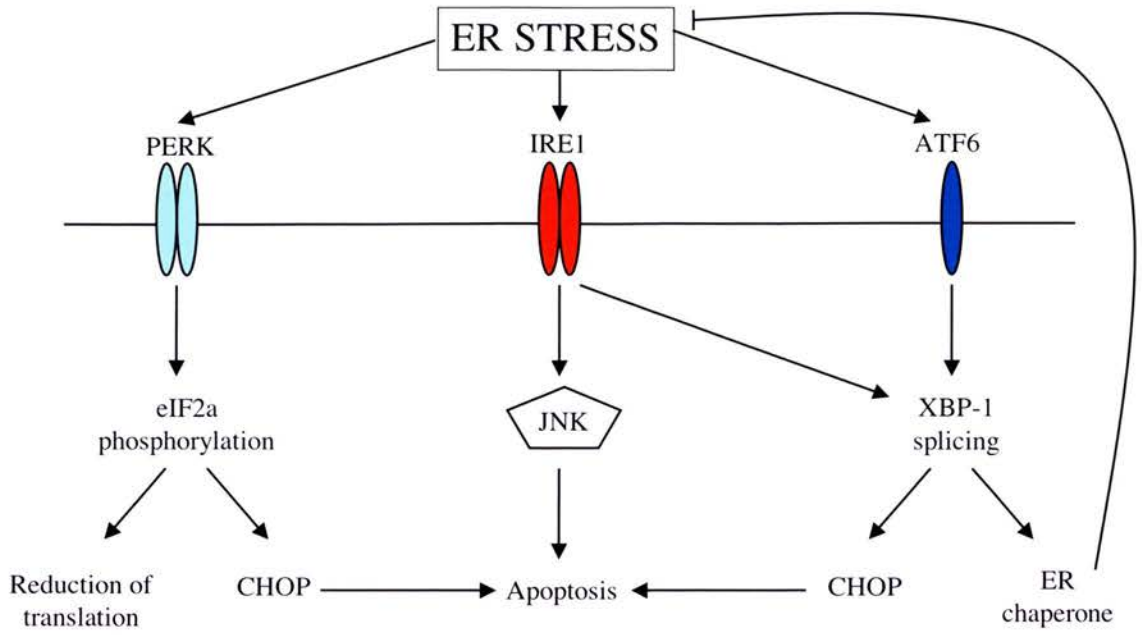

Figure 4.2 The mammalian ER stress response has three main effector pathways. In mammalian cells three proteins mediate the ER stress response, PERK, IRE1 and ATF6. Both PERK and IRE1 are activated by dimerisation and autophosphorylation, while being proteolysed activates ATF6. The activation of these proteins due to increased ER stress leads to a reduction in general protein translation coupled by increased translation of chaperone proteins via XBP-1 splicing to assist with protein folding. Inappropriate or sustained activation of these ER stress effector proteins leads to apoptosis via CHOP activation.

IRE1 or PERK via dimerisation and autophosphorylation (Shamu et al., 1996). BiP, an ER chaperone protein, is thought to regulate the activation of IRE1/PERK through binding to these proteins when there are few unfolded proteins and preventing their dimerisation (Kimata et al., 2003). IRE1 is a kinase/endonuclease, and is a type I ER membrane protein (Tirasophon et al., 1998). IRE1 splices a small 26 nucleotide intron from XBP-1 mRNA thus activating it. ATF6 is a bZIP protein, which is expressed as a type II membrane protein in the ER and is activated by proteolysis by the site proteases S1P and S2P (Ye et al., 2000). When cleaved in response to ER stress the bZIP containing N terminal half becomes a soluble transcription factor and is translocated into the nucleus where it induces XBP-1 transcription (Yoshida et al., 2001). As levels of XBP-1 protein rise in the cell, genes, which have a UPR element (UPRE) or ER stress response element (ERSE) in their promoters are induced. This leads to an increase in chaperone proteins to assist in folding. Activation of PERK leads to translational attenuation via phosphorylation of the eukaryotic initiation factor eIF2α (Okada et al., 2002).

However, if the ER is still overloaded, the ER stress response can lead to apoptosis of the cell mediated via a transcription factor or a caspase mediated pathway. IRE1 can upregulate the transcription factor GADD153/CHOP and alter the balance between Bcl-2 and Bax (Wang et al., 1998, Ghribi et al., 2001) thus promoting apoptosis. In the second pathway procaspase 12 could interact with IRE1 through the c-Jun-N terminal kinase (JNK) pathway and the adaptor molecule TRAF2. Upon ER stress procaspase 12 is released from TRAF2, homodimerises and undergoes auto-processing. Caspase 12

translocates from the ER to the cytosol where it directly cleaves procaspase 9. Caspase 9 then activates the apoptosis effector caspase 3 (Yoneda et al., 2001).

XBP-1, the mammalian homologue of HAC1, has also been reported to be involved in the biogenesis of the ER in NIH-3T3 fibroblasts (Sriburi et al., 2004). Mammalian VAPA is known to interact with several oxysterol binding protein (OSBP) homologues (Wyles et al., 2004) and with CERT, which is involved in ceramide transport (Hanada et al., 2003). Therefore, the mammalian VAP proteins may be involved in ER membrane biogenesis and the ER stress response. In this chapter we determine whether the major sperm protein (MSP) domain of the VAP proteins can activate the mammalian ER stress response.

4.2 Overexpression of the VAP MSP domain fused to GFP causes protein aggregation and neuronal cell death

The MSP domain of VAPA fused to GFP was transfected into primary hippocampal cultured neurons from E19 rats as it had been noted previously that these cells appeared to undergo cell death when transfected with this construct. MSP-GFP transfected neurons had large aggregates of the GFP tagged protein as compared to GFP-alone transfected controls. When VAPA was co-transfected into the hippocampal neurons with DS.Red the red staining, which was throughout the cell, showed that the neuron was not a typical shape with clear axons, but was a shrunken cell body with punctate axons like those seen in dying neurons. This experiment was repeated with the VAPB MSP fused to GFP, and again, large GFP protein aggregates were seen and DS.Red co-transfection revealed atypical neuron morphology consistent with neuronal cell death (Figure 4.3A).

Terminal deoxynucleotidyl transferase-mediated dUTP-biotin nick end labelling (TUNEL) of DNA fragments was carried out on the primary hippocampal neurons transfected with MSP-GFP or GFP alone (Loo et al., 1998). Neurons containing MSP-GFP showed increased TUNEL staining as compared with GFP alone controls. This indicates that MSP-GFP hippocampal neurons have increased DNA fragmentation due to the chromosomal degradation seen in dying cells (Figure 4.3B).

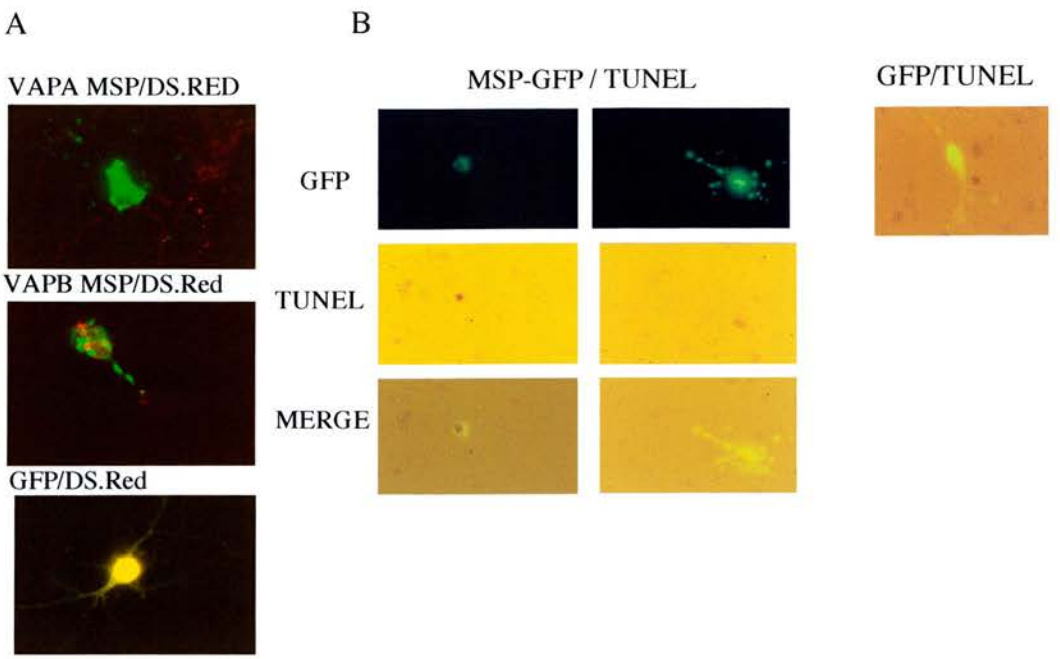

Figure 4.3. Increased TUNEL staining in primary hippocampal neurons expressing MSP-GFP. A. The MSP domain of VAPA or VAPB fused to GFP or GFP alone was co-transfected into E19 primary cultured hippocampal neurons along with a general cell marker DS.Red. After 48 hours the neurons were imaged. The neurons expressing the MSP constructs had large protein aggregates and did not appear to be healthy whereas those transfected with GFP alone had diffuse staining and more normal morphology. B. Terminal deoxynucleotidyl transferase-mediated dUTP-biotin nick end labelling (TUNEL) of DNA fragments was carried out on the primary hippocampal neurons expressing MSP-GFP or GFP alone (n=3). As the representative figure shows neurons containing MSP-GFP showed increased TUNEL staining as compared with GFP alone controls.

4.3 HEK293 cells expressing MSP-GFP also have large protein aggregates and increased TUNEL staining

HEK293 cells expressing VAPA MSP-GFP were imaged 24 hours after transfection. Large protein aggregates were seen of the GFP tagged MSP in these cells. TUNEL staining also indicates that the transfected HEK293 cells showed increased TUNEL staining as compared with non-transfected cells (Figure 4.4).

4.4 Overexpression of the MSP domain fused to GFP does not change gross ER structure

VAPA fused to GFP and overexpressed in HEK293 cells colocalises with a DS.Red-ER marker, which contains a calreticulin signal sequence and a KDEL sequence to localise it to the ER compartment. The MSP domain of VAPA fused to GFP does not colocalise with the DS.Red-ER marker so it is not localised to the ER. Overexpression of MSP-GFP does not cause any gross changes in the ER compartment. This is true for MSP-GFP overexpression in primary hippocampal neurons as well, where gross ER structure is unchanged (Figure 4.5). This suggests that it is unlikely the cell death due to overexpression of MSP-GFP is due to gross structural abnormalities in the ER compartment.

MSP-GFP

TUNEL staining

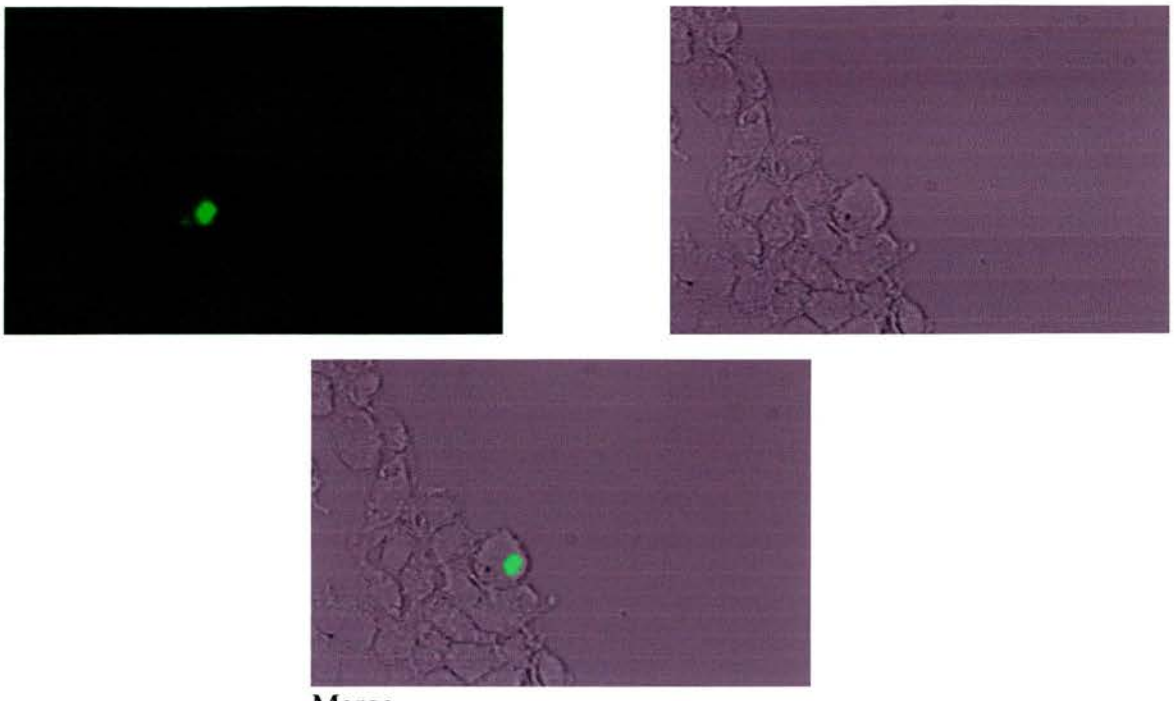

Merge

Figure 4.4 Increased TUNEL staining in HEK293 cells expressing VAPA MSP-GFP. Terminal deoxynucleotidyl transferase-mediated dUTP-biotin nick end labelling (TUNEL) of DNA fragments was carried out on HEK cells transfected with MSP-GFP. HEK293 cells containing MSP-GFP showed increased TUNEL staining as compared with non-transfected controls (n=3).

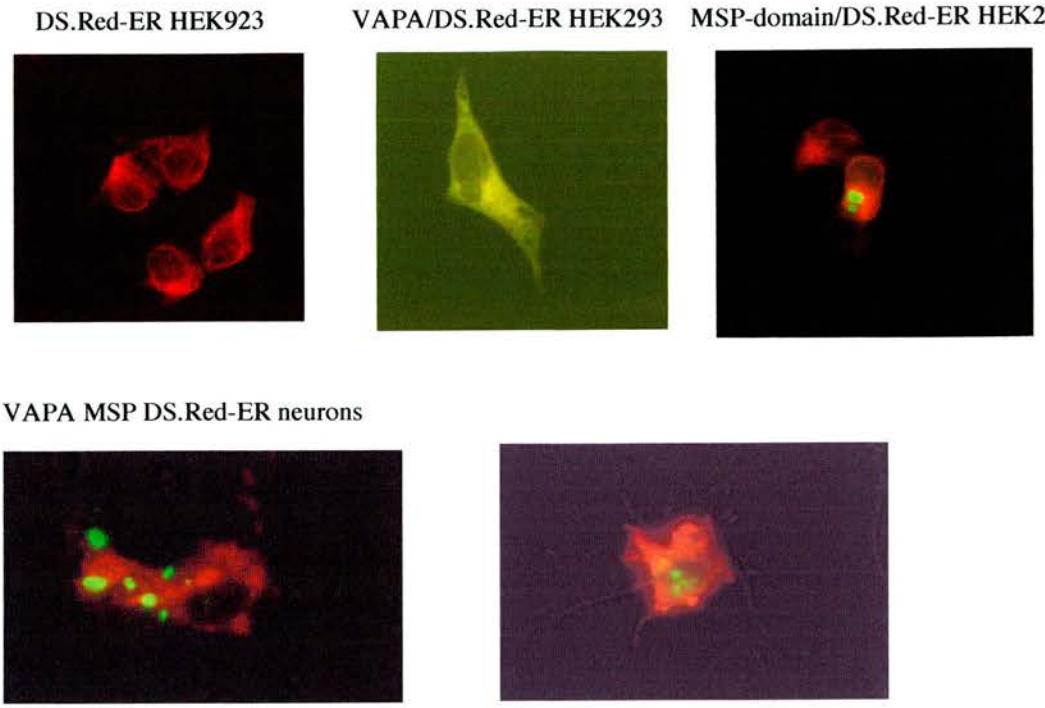

Figure 4.5 No gross ER disruption in cells expressing MSP-GFP. HEK cells or E19 primary cultured hippocampal neurons were transfected with VAPA-GFP and DS.Red-ER, VAPA MSP-GFP and DS.Red-ER or DS.Red-ER alone. No gross changes in ER structure were seen in any of these cells (n=6).

4.5 Production of tetracycline inducible MSP-GFP and GFP stable cell lines

As biochemical assays on the primary hippocampal neurons would have been difficult due to a less than 5% transfection rate of MSP-GFP with calcium phosphate and a less than 20% transfection rate with lipofectamine, and the short time course of MSP-GFP transfected cell death, it was decided to make an inducible stable cell line on which to perform these studies. VAPA MSP-GFP and GFP were cloned into pcDNA4/TO, an expression vector under the transcriptional control of tetracycline. HEK293 cells that stably express the tetracycline repressor pcDNA6/TR (Trex cells), were transfected with MSP-GFP/TO and GFP/TO. 48 hours after transfection, zeocin was added to the cells at a concentration of 50μg/ml. 1 week after this point stable colonies were found on the plate. These colonies were picked and grown for a further week. Of 4 colonies, which grew well and contained the repressor, 4 were found to express reasonable levels of MSP-GFP and all further studies were carried out on clone 2 (Figure 4.6A). The GFP stable cell line was generated in the same manner (Figure 4.7A). Protein aggregates were seen in the tetracycline-induced (1μg/ml) MSP-GFP cells after 48 hours of induction, no aggregates were observed in the GFP cells after the same amount of time. Western blots were carried out on both cell lines to confirm expression of proteins of the correct size (Figures 4.6B and 4.7B).

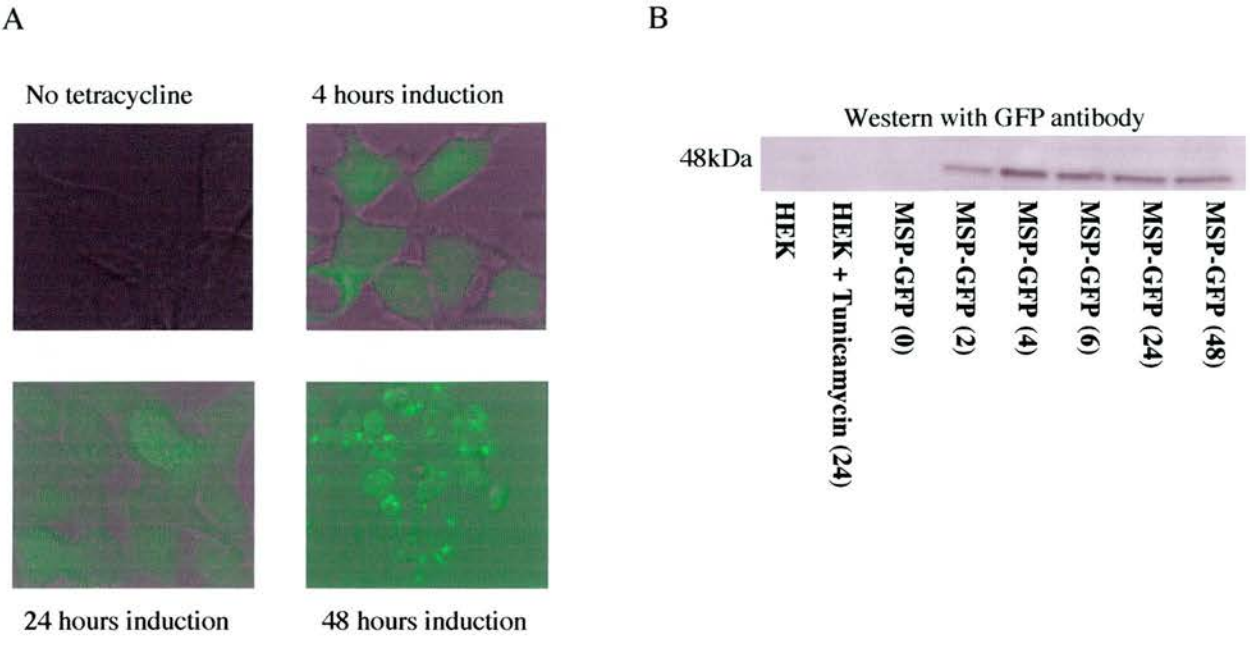

Figure 4.6. HEK293 tetracycline inducible cell line expressing MSP-GFP gives large protein aggregates. A. A stable tetracycline-inducible HEK cell line expressing VAPA MSP-GFP was made. These cells contained large protein aggregates at 48 hours when imaged on a fluorescent microscope. B. Protein extracts were taken of these cells at 0, 2, 4, 6, 24, and 48 hours after tetracycline addition. Western blotting of these extracts showed maximal induction of MSP-GFP protein at 4 hours after tetracycline induction of protein transcription.

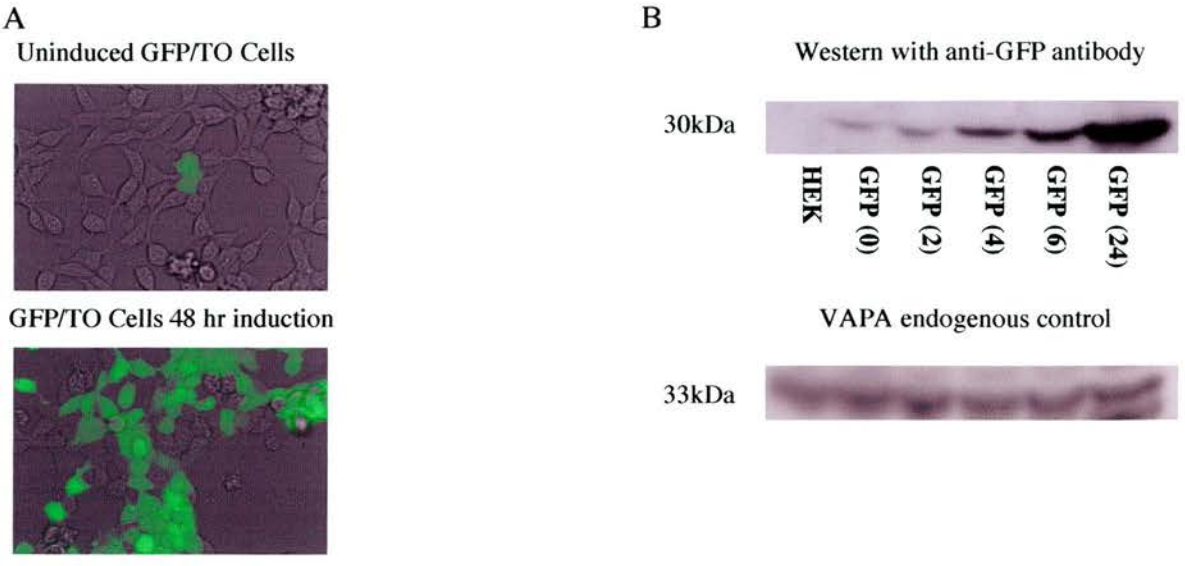

Figure 4.7. HEK293 tetracycline inducible cell line expressing GFP. A. A stable tetracycline-inducible HEK cell line expressing GFP was made. These cells had strong diffuse GFP expression at 48 hours when imaged on a fluorescent microscope. B. Protein extracts were taken of these cells at 0, 2, 4, 6, and 24 hours after tetracycline addition. Western blotting of these extracts showed maximal induction of GFP protein at 24 hours after tetracycline induction of protein transcription.

4.6 MSP-GFP cells show no growth after induction of protein expression

A growth assay was carried out upon MSP-GFP uninduced cells, MSP-GFP cells induced with 1μg/ml tetracycline, and Trex cells only containing pcDNA6/TR treated with 1μg/ml tetracycline. Cells in 4 defined boxes in each well were counted. This was repeated for 3 wells of each of induced MSP-GFP, uninduced MSP-GFP and tetracycline treated Trex cells at the point of tetracycline addition (day 1), and then at 24 (day 2), 48 (day 3) and 72 (day 4) hours. The results for each well were averaged and the percentage of cell growth was calculated along with the standard deviation. Both the uninduced MSP-GFP cells and the tetracycline treated Trex cells grew normally. However the induced MSP-GFP cells did not grow at all and there were less cells sticking to the cell plate, i.e. those that were healthy, after 72 hours of induction than there were to begin with (Figure 4.8). This experiment was repeated with the inducible GFP cell line and it was observed that both induced and uninduced GFP cells grew at the same rate (Figure 4.9). This data shows that induction of the expression of the MSP-GFP protein inhibits cell growth in HEK293 cells and may induce cell death.

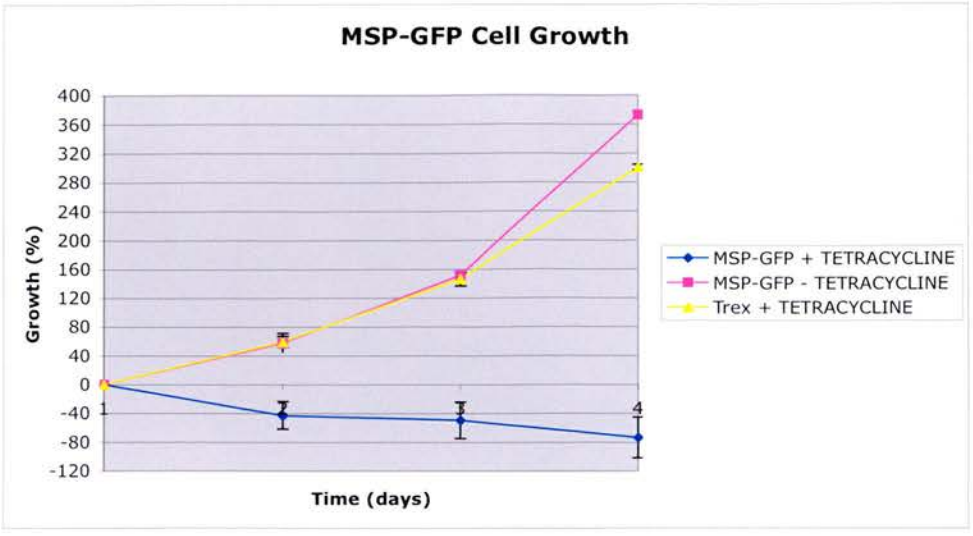

Figure 4.8 HEK293 tetracycline inducible cell line expressing MSP-GFP shows no cell growth. Stable MSP-GFP cells and Trex (HEK cells expressing pcDNA6/TR) cells were seeded at a low density into 6 well plates. Half of the MSP-GFP cells and the Trex cells were treated with 1μg/ml tetracycline. At 0, 24, 48 and 72 hours after tetracycline treatment the number of cells in a boxed area of the each well was counted with 4 marked boxes counted in each well at each timepoint. The number of cells in each well and between the wells with the same cells and treatment were averaged for each timepoint. While uninduced MSP-GFP cells and tetracycline treated Trex cells grew normally, induced MSP-GFP cells did not grow at all and may even be undergoing cell death (n=3).

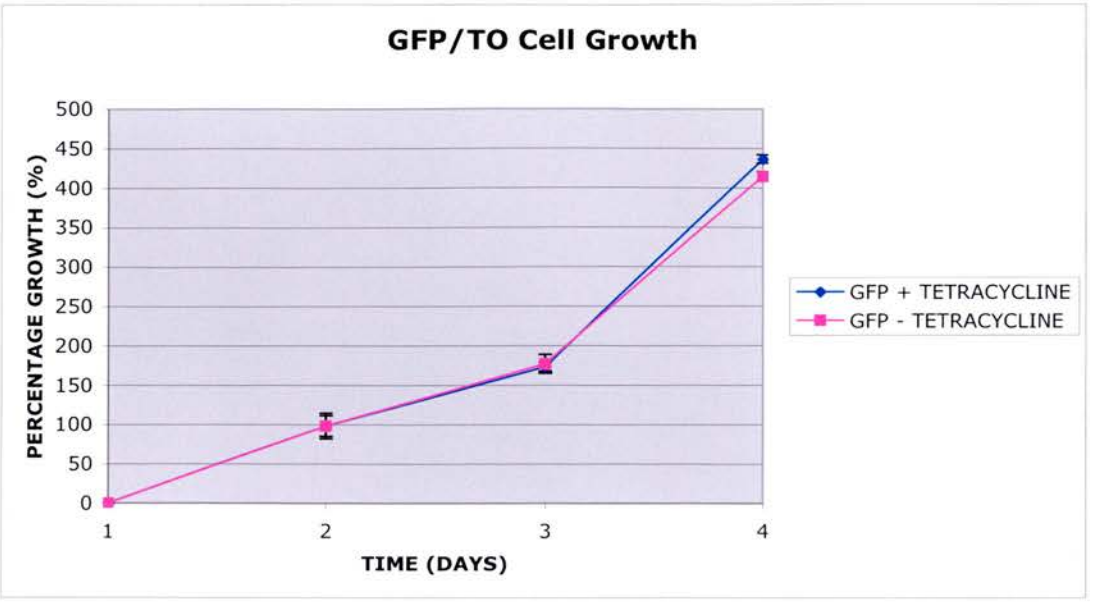

Figure 4.9 HEK293 tetracycline inducible cell line expressing GFP shows normal cell growth. Stable GFP cells were seeded at a low density into 6 well plates. Half of the GFP cells were treated with 1μg/ml tetracycline. At 0, 24, 48 and 72 hours after tetracycline treatment the number of cells in a boxed area of the each well was counted with 4 marked boxes counted in each well at each timepoint. The number of cells in each well and between the wells with the same cells and treatment were averaged for each timepoint. Both induced and uninduced GFP cells grew at the same rate (n=3).

4.7 Induced MSP-GFP cells have increased propidium iodide staining compared to control cells

To confirm that the induced MSP-GFP cells were undergoing cell death a vital dye, propidium iodide was used. When cells are dying their cell membrane becomes more permeable and there is increased up-take of small molecules such as propidium iodide. As before induced MSP-GFP, uninduced MSP-GFP, and tetracycline treated Trex cells were counted. 1μg/ml of tetracycline was added to the cells and 24 hours later they were treated with 5μl/ml propidium iodide for 20 minutes and imaged and counted immediately (day 1). The propidium iodide staining was repeated on a different set of cells at 48 hours after tetracycline addition (day 2). The results for each well were averaged and the percentage of propidium iodide containing cells was calculated along with the standard deviation in the sample. The uninduced MSP-GFP cells and the tetracycline treated Trex cells had an extremely small percentage of propidium iodide stained cells at 24 and 48 hours. However, the induced MSP-GFP cells showed significantly higher levels of propidium iodide staining at 24 hours (42.1 ± 18.3%) and at 48 hours (75.9 ± 27.2%) (Figure 4.10). This indicates that induction of MSP-GFP protein expression in HEK cells causes cell death.

Figure 4.10 HEK293 tetracycline inducible cell line expressing MSP-GFP undergoes cell death. Stable MSP-GFP cells and Trex (HEK cells expressing pcDNA6/TR) cells were seeded at a low density into 6 well plates. Half of the MSP-GFP cells and the Trex cells were treated with 1μg/ml tetracycline. All of the cells were treated with 5μg/ml propidium iodide. At 24 and 48 hours after tetracycline treatment the number of red or propidium iodide containing cells in a boxed area of the each well was counted with 4 marked boxes counted in each well at each timepoint and divided by the total number of cells in each boxed area to determine the percentage of red cells. The number of cells in each well and between the wells with the same cells and treatment were averaged for each timepoint. While the Trex plus tetracycline and uninduced MSP-GFP cells contained very few propidium iodide stained and therefore dying cells, the induced MSP-GFP cells showed a high percentage of dying cells at 24 hours and almost all of them were dead at 48 hours (n=3).

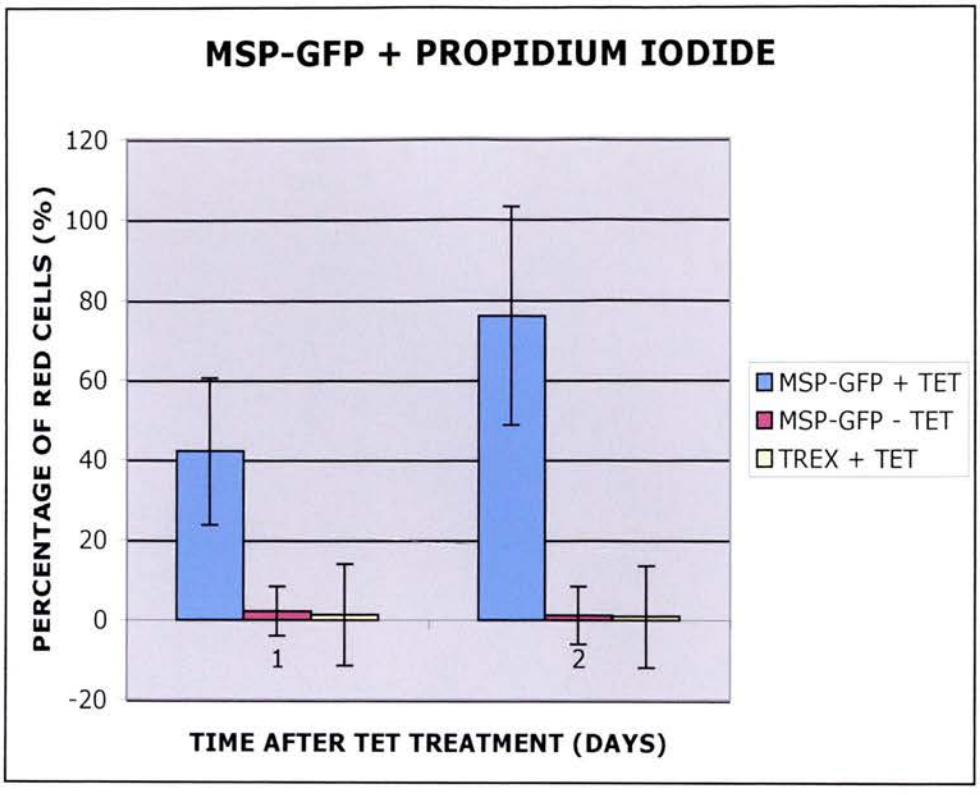
MSP-GFP + PROPIDIUM IODIDE
PERCENTAGE OF RED CELLS (%)
120
100
80
60
40
20
0
-20
1
2
TIME AFTER TET TREATMENT (DAYS)
MSP-GFP + TET
MSP-GFP - TET
TREX + TET

4.8 DNA laddering in induced MSP-GFP HEK cells indicates apoptotic cell death

In order to determine whether the cell death seen in the induced MSP-GFP cells was apoptotic or necrotic a DNA laddering experiment was carried out. Dithiothreitol (DTT) reduces formation of disulphide bonds and causes retention of proteins in the ER and ER stress (Jamsa et al., 1994), and if the ER is under stress for long enough the cell will undergo apoptosis. Therefore, addition of 10mM DTT for 48 hours was the positive control for DNA laddering due to apoptosis. Trex cells treated with tetracycline and uninduced MSP-GFP cells showed no DNA laddering when run on a 2% agarose gel. However, the MSP-GFP cells, which had been induced for 48 hours, showed significant DNA laddering comparable to that seen with the Trex cells treated with DTT (Figure 4.11). This indicates that the cell death seen in the stable MSP-GFP cell line is apoptotic in nature.

4.9 HEK cells transiently transfected with MSP-GFP and VAPA have upregulated levels of BiP mRNA

To determine whether MSP-GFP protein expression in HEK293 cells activates apoptotic pathways, via the ER stress response, a northern blot was carried out on transiently transfected HEK293 cells. Tissue plasminogen activator (t-PA) is a serine protease and its expression in *A. niger* leads to transcriptional up-regulation of genes encoding the ER chaperones and foldases BIPA, CYPB and PDIA (Wiebe et al., 2001).

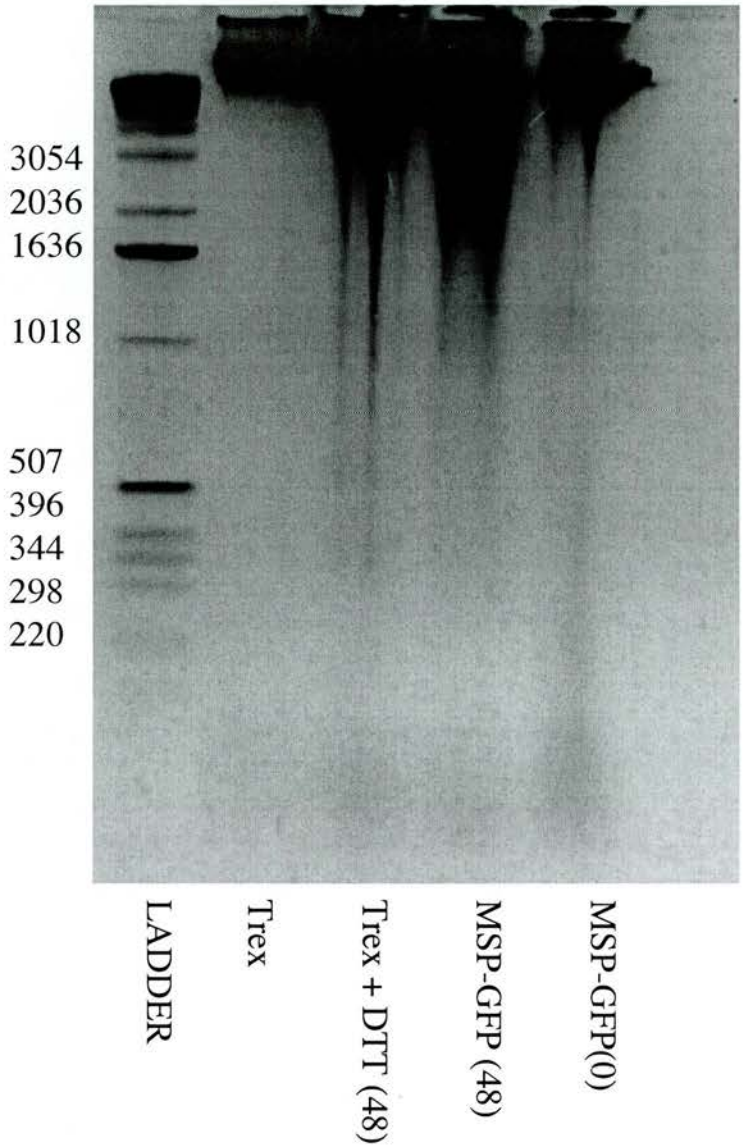

Figure 4.11 HEK293 tetracycline inducible cell line expressing MSP-GFP undergoes DNA laddering, indicative of apoptosis. DNA extracts of MSP-GFP cells induced for 0 and 48 hours with 1 μg/ml tetracycline, Trex cells and Trex cells treated with 10mM Dithiothreitol (DTT) for 48 hours were taken and run on a high percentage agarose gel. The Trex cells and the uninduced MSP-GFP cells showed no DNA laddering whereas the Trex cells treated with DTT and the induced MSP-GFP cells both showed DNA laddering indicative of apoptotic cell death (n=2).

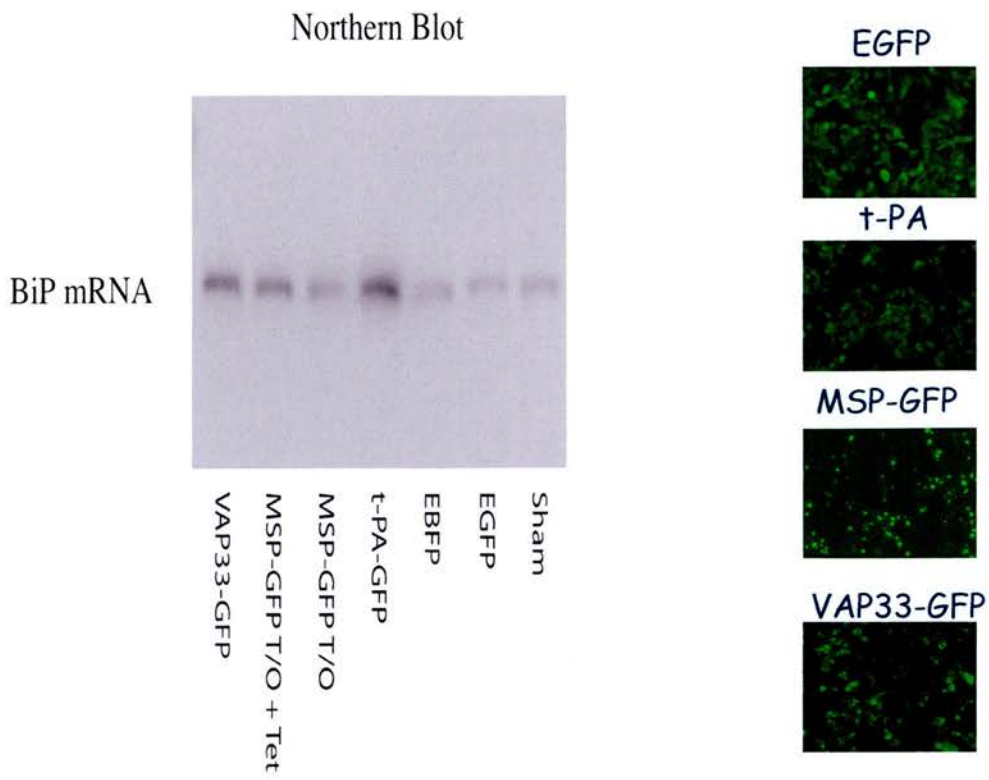

Figure 4.12 (contributed by Paul Skehel). HEK293 tetracycline inducible cell line expressing MSP-GFP has increased BiP mRNA production. HEK293 cells were transiently transfected with VAPA-GFP, tPA-GFP, GFP, inducible MSP-GFP, BFP and a no-DNA control. RNA extracts were prepared and the Northern blot shows that tPA-GFP, MSP-GFP and VAPA-GFP transfected cells have higher levels of BiP mRNA compared with controls.

In HEK293 cells t-PA also increases BiP mRNA levels, hence it was used as a positive control. GFP, BFP, sham (calcium phosphate treated) and MSP-GFP/TO uninduced HEK cells showed no increase in the levels of BiP mRNA. MSP-GFP and full-length VAPA transfected cells showed increases in the levels of BiP mRNA (Figure 4.12). As previously mentioned, full length VAPA is a type II membrane protein, which resides in the ER, facing out of the ER lumen into the cytoplasm. The overexpression of various ER proteins facing into the lumen have been found to increase ER stress, hence the overexpression of VAPA may also shift ER dynamics and increase ER stress as it resides in the ER. However, MSP-GFP does not reside in the ER, as it has no transmembrane domain so it may affect ER stress pathways via protein interactions or a signaling function.

4.10 Phospho-PERK and caspase 3 levels are increased in induced MSP-GFP cells

To confirm the involvement of ER stress pathways in the MSP-GFP induced apoptosis other effector proteins in this pathway were studied by western blot. PERK is a key effector protein in this pathway and there is a clear increase in PERK phosphorylation at Thr980 after 2 hours of MSP-GFP protein expression, which lasts until 24 hours (Figure 4.13). This is similar to the levels seen with treatment with 1μg/μl tunicamycin, which inhibits N-linked glycosylation of proteins and so increases ER stress (Welihinda et al., 1999). However, no phosphorylated PERK is seen in the induced GFP cells even after 24 hours of induction (Figure 4.14). Caspase 3 is also involved in the end stages of ER stress induced apoptosis and at 6 hours activated caspase 3 is found in the induced MSP-GFP cells (Figure 4.13). The activation of these ER stress proteins in the induced MSP-

GFP cells demonstrates that the ER stress response is activated by the induction of MSP domain protein expression and is responsible for the activation of apoptotic proteins.

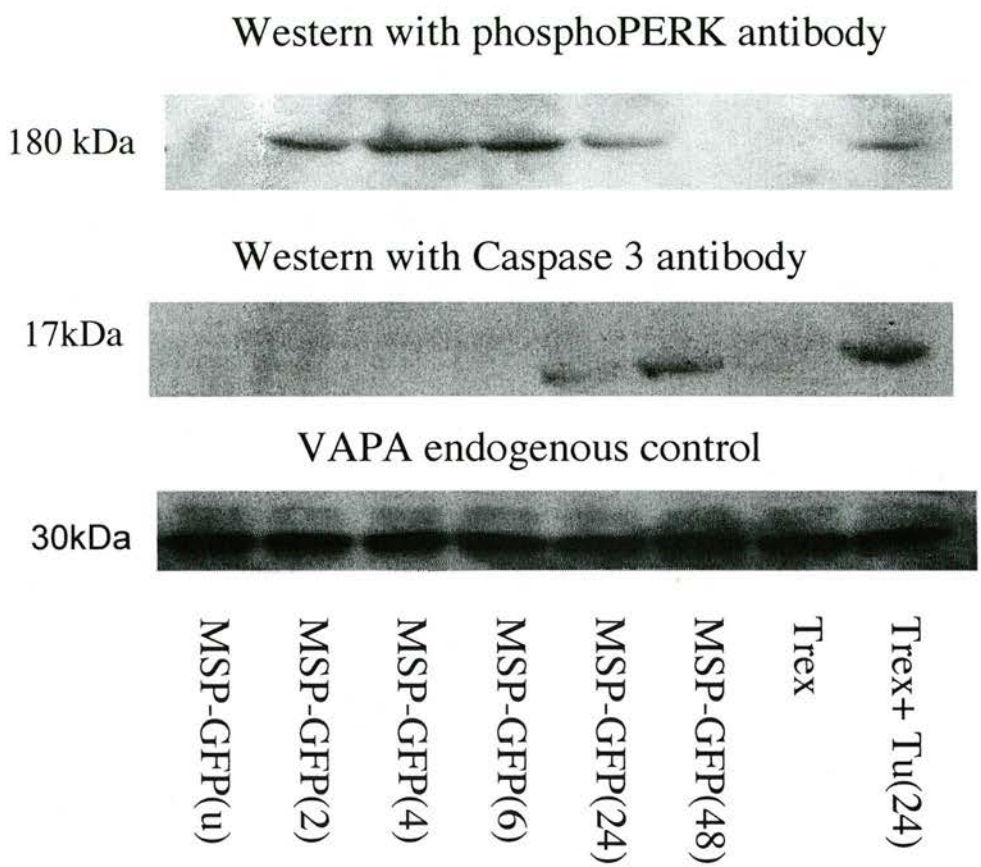

Figure 4.13 HEK293 tetracycline inducible cell line expressing MSP-GFP has increased phospho-PERK and caspase 3 production. Protein extracts were taken of the MSP-GFP cells at 0, 2, 4, 6, 24 and 48 hours after 1 μg/ml tetracycline addition and of Trex cells and Trex cells treated with tunicamycin for 24 hours. Western blotting of 20μg of these extracts showed that PERK was maximally phosphorylated after 2-4 hours of MSP-GFP expression while caspase 3 was activated after 24-48 hours of MSP-GFP expression (n=5).

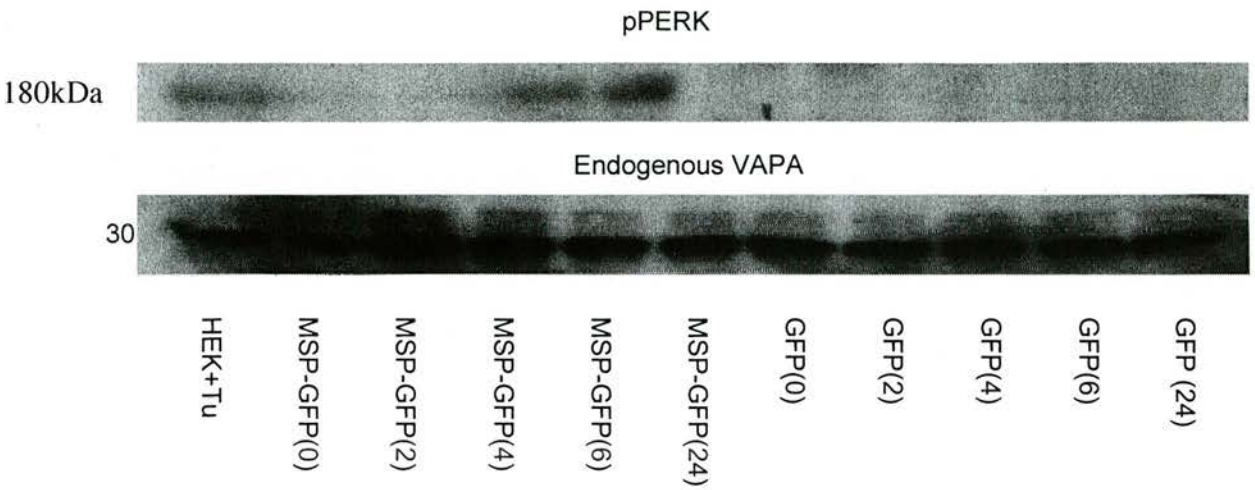

Figure 4.14 Confirmation that HEK293 tetracycline inducible cell line expressing MSP-GFP has increased phospho-PERK production. Protein extracts were taken of the MSP-GFP and GFP cells at 0, 2, 4, 6 and 24 hours after 1 μg/ml tetracycline addition and Trex cells treated with tunicamycin for 24 hours. Western blotting of these extracts showed that PERK was maximally phosphorylated after 4-6 hours of MSP-GFP expression whereas no phosphorylation of PERK is seen in the induced GFP cells at any timepoint (n=2).

4.11 Discussion

VAPA and VAPB are known to reside on the ER (Skehel et al., 2000), which is the organelle responsible for protein translation, protein folding and post-translational protein modifications. We have discovered that when the MSP domain of VAPA is expressed without the coiled-coil or tail domains in both HEK293 cells and primary cultured hippocampal neurons, these cells undergo apoptotic cell death due to inappropriate activation of the ER stress response.

The MSP domain tagged with GFP expressed in either HEK293 cells, or primary hippocampal neurons, formed large intracellular protein aggregates. The MSP domain was toxic to these cell types and transfected HEK cells died within 48 hours. In a stably induced MSP domain cell line large protein aggregates formed within 24 hours but were not present before this time point. However, phosphoPERK induction was evident at 2 hours after induction when there was MSP protein present but no large aggregates had formed. The induction of BiP mRNA transcription and PERK phosphorylation are indicative of ER stress response activation, as is the induction of caspase-3 leading to apoptotic cell death. It is likely that the MSP domain disrupts ER stress signalling in some manner.

The MSP domain of the VAP proteins folds into an Ig-like domain, which is structurally related to PaPD, a bacterial chaperone. This domain is predicted to be involved in

protein-protein interactions. VAPA can dimerise and is thought to interact via both its coiled-coil and tail regions but does not dimerise via its MSP domain (Kaiser et al., 2005). Therefore it is unlikely that the MSP domain is interacting with the endogenous VAPA or VAPB but may be influencing ER stress signalling via other protein interactions.

The yeast homologue of VAPA, SCS2, is known to be involved in the yeast ER stress response (Loewen et al., 2003) and in yeast ER membrane biogenesis. VAPA and VAPB may play a similar role in humans.

VAPA AND VAPB

5.1 Background

Mouse VAPA is known to be an ER protein, which is integral to the ER membrane and in a type II orientation (Skehel et al., 1995). Mouse VAPB had not yet been cloned at the beginning of these studies. In order to determine whether VAPA and VAPB were identical in structure and function, VAPB was cloned, and various cDNA truncation constructs were generated and expressed in HEK293 cells so that protein localisation and function could be studied.

5.2 Cloning and gross cellular localisation of VAPB

The proteins VAPA and VAPB show a high degree of homology in the MSP domain but show a much lower degree of homology in the coiled-coil and tail regions (Figure 5.1). To determine whether VAPB had a similar localisation pattern as VAPA it was cloned from a mouse cDNA library and ligated into EGFP-C1. This construct was transfected into HEK293 cells and primary cultured rat (E19) hippocampal neurons on its own and co-transfected with DS.Red-ER, which is targeted to the ER membrane. VAPB has a similar gross distribution to VAPA and colocalises with the DS.Red-ER marker (Figure 5.2). This data demonstrates that VAPB is localised on the ER in both HEK cells and in hippocampal neurons.

5.3 VAPA and VAPB antibody staining colocalises on the ER

To examine the localisation patterns in more detail specific VAPA and VAPB antibodies were used to stain HEK293 cells. HEK293 cells were plated onto coverslips, fixed and stained with a specific VAPA antibody, followed by a specific VAPB antibody. The two marker show a high degree of colocalisation on the ER as shown by the yellow staining of the merged signals (Figure 5.3).

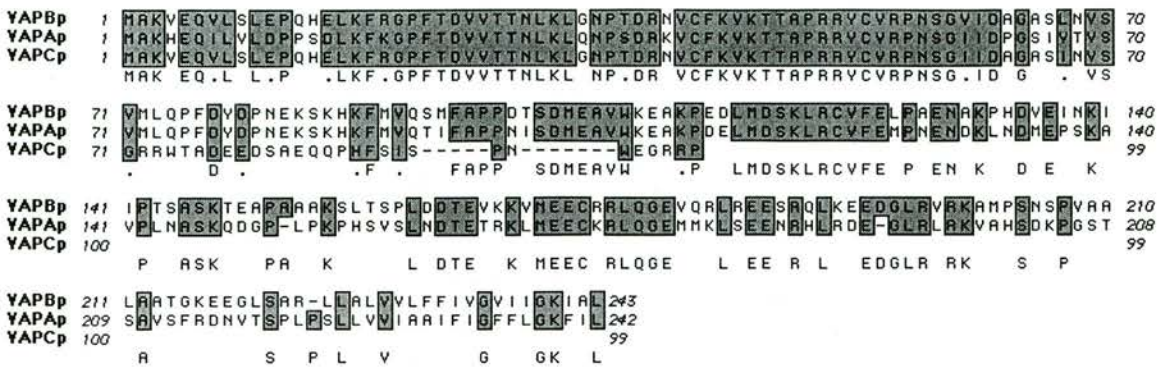

Figure 5.1 VAP family homology. VAPA and VAPB have very similar MSP domains. Their coiled-coil domains and hydrophobic tails show a much smaller degree of homology. Both VAPA and VAPB contain conserved residues responsible for FFAT motif binding. VAPC, a splice variant of VAPB, does not contain all of these residues so may not bind FFAT-containing proteins.

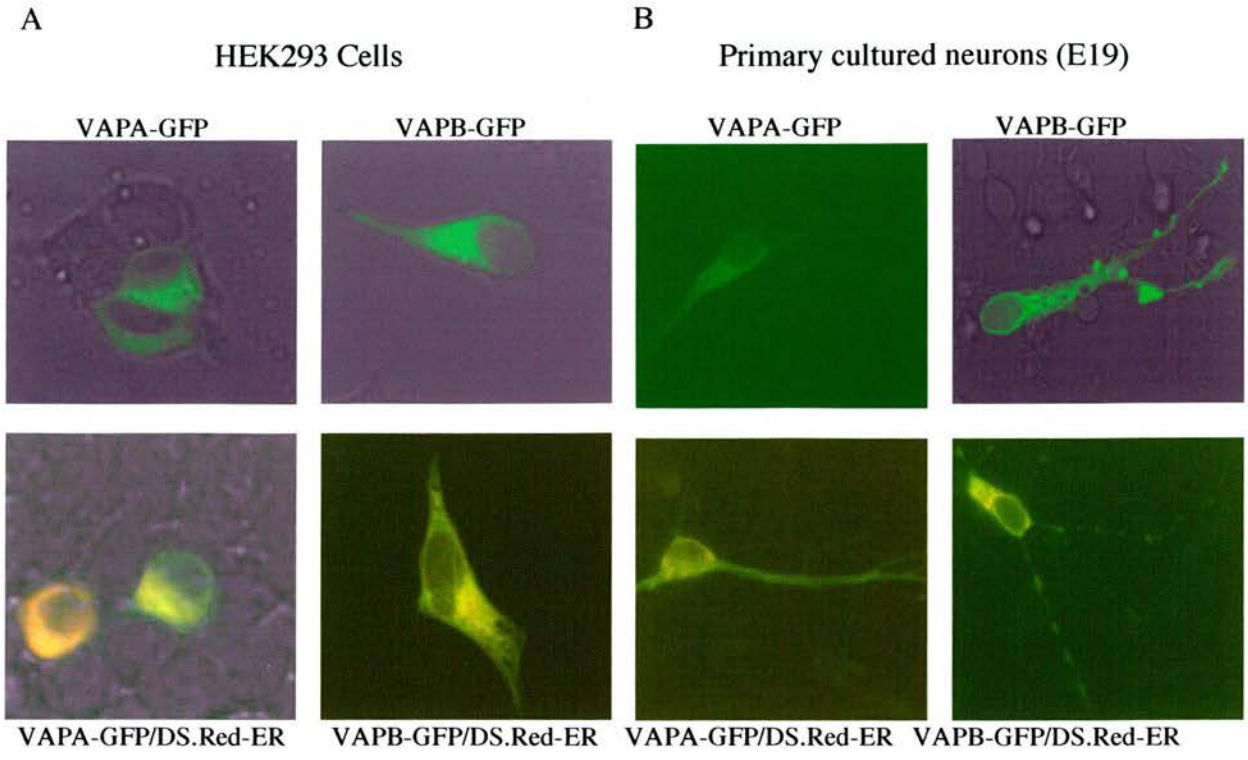

Figure 5.2 VAPA and VAPB colocalise predominantly with ER markers in primary hippocampal neurons and HEK293 cells. HEK293 cells and E19 primary hippocampal cultured neurons were transfected with VAPA-GFP or VAPB-GFP with or without DS.Red-ER. Both VAPA and VAPB predominantly colocalise with the DS.Red-ER marker (n=6).

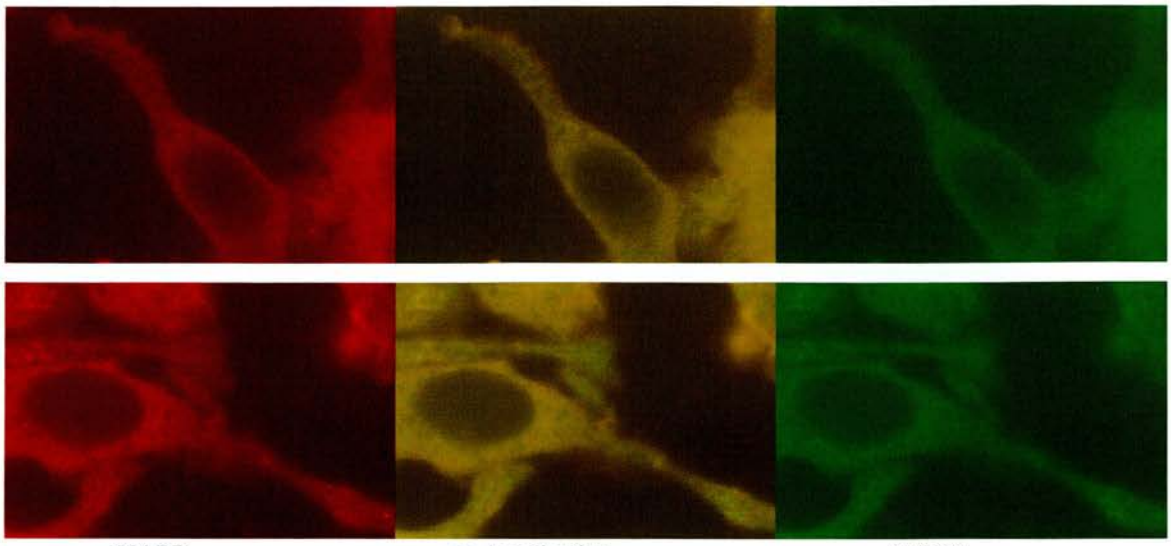

Figure 5.3 Colocalisation of VAPA and VAPB. HEK cells were plated on glass coverslips coated with poly-D-lysine and then fixed. The coverslips were treated with specific VAPA and VAPB antibodies. The VAPA and VAPB staining shows that there is a significant amount of co-localisation (yellow) (n=6).

5.4 Fractionation and Triton X114 extraction of VAPA and VAPB demonstrates differences in membrane association

To elucidate whether VAPA and VAPB were in biochemically distinct areas of the ER Triton X114 extractions were carried out. P1, P2, S2, P3 and S3 fractions were prepared from HEK293 cells as described in the materials and methods. Using this method VAPB was identified as being essentially soluble in contrast to VAPA, as most of VAPA was pelleted at P2 whereas VAPB was not completely pelleted at P3 (Figure 5.4A). When the P2 layer of the HEK293 cells was detergent extracted with Triton X114 (Bordier et al., 1981) VAPA was extracted into the detergent indicating that it is lipophilic. However, VAPB was not extracted into the detergent and remained in the aqueous layer indicating that VAPB hydrophilic (Figure 5.4B). It also highlights differences in the hydrophobicity of VAPA and VAPB, which may be important in their interactions with lipids and lipid binding proteins.

5.5 VAPA and VAPB MSP constructs Triton X114 extract differently

Various truncation constructs of VAPA and VAPB were then generated to determine which domains were responsible for their differing localisations. The VAPA and VAPB MSP constructs (Figure 5.5) were transiently transfected into HEK293 cells and P1, P2, and S2 layers prepared as described in the materials and methods.

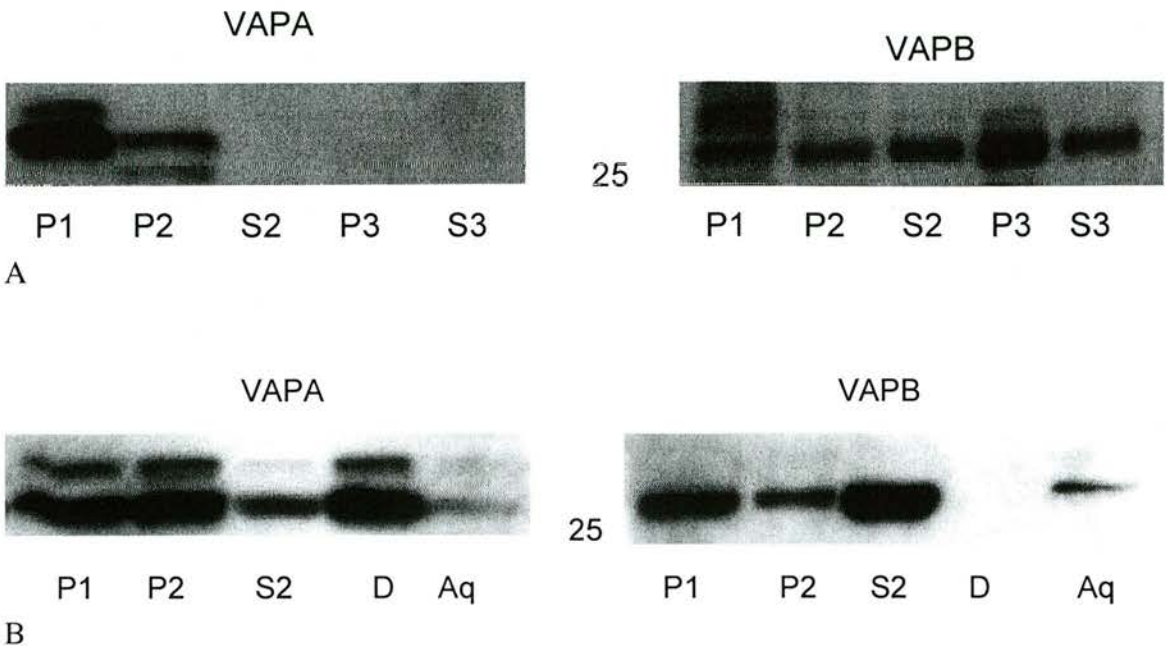

Figure 5.4 Fractionation and Triton X114 extraction of endogenous VAPA and VAPB in HEK293 cells. A. HEK cells were lysed and P1, P2, S2, P3 and S3 layers were prepared. 10mg of P1, P2 and S2 were run on the gel and 20mg of P3 and S3 were run. Specific VAPA and VAPB antibodies were used to probe the extracts on a western blot. This revealed that VAPA was present predominantly in the heavier fractions P1 and P2, while VAPB was also present in the lighter fractions P3 and S3. B. The P2 layer of the HEK cells was detergent extracted using Triton X114. This reveals that VAPA is mainly detergent extracted while VAPB is found in the aqueous layer (n=3).

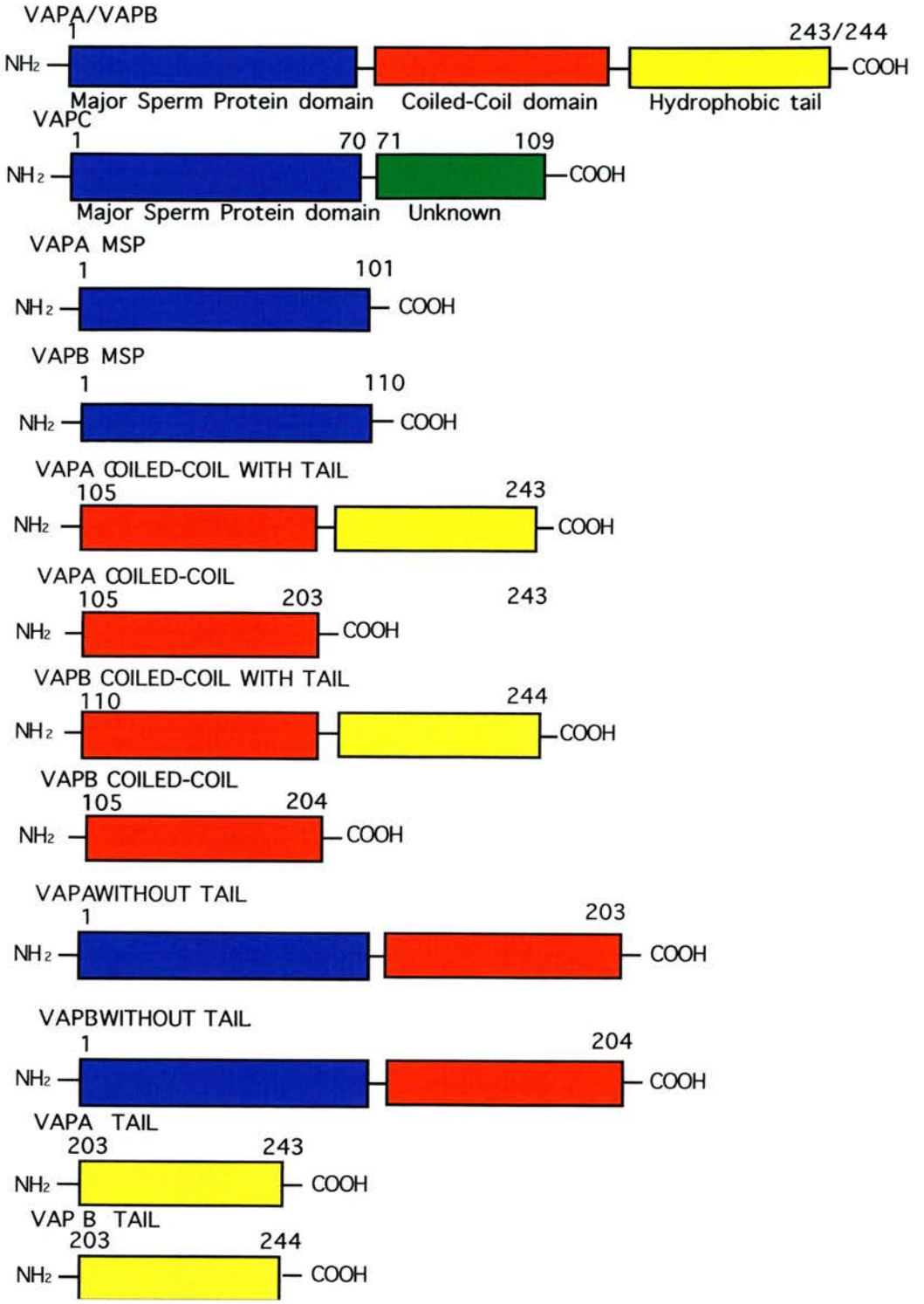

Figure 5.5 Truncation constructs of VAPA and VAPB.

The P2 layer was detergent extracted (Bordier et al., 1981) with Triton X114 and the samples were analysed by western blots probed with GFP antibody. As described in the previous chapter both the VAPA and VAPB MSP-GFP construct form large protein aggregates in HEK293 cells at this timepoint and these aggregates do not co-localise with the DS.Red-ER marker (Figure 5.6A and 5.7A). The VAPA MSP domain was mostly found in the soluble fraction and in the aqueous layer when Triton X114 extracted which is consistent with it being in the cytoplasm (Figure 5.6B). The VAPB MSP domain was mostly found in the P2 layer and was roughly 50% detergent extracted (Figure 5.7B). This could be due to strong interactions with an ER protein.

5.6 VAPA and VAPB coiled-coil domains are cytoplasmic

The VAPA and VAPB coiled-coil constructs fused to GFP have a diffuse distribution in HEK cells similar to that of GFP expressed alone. Consistent with a diffuse cytoplasmic distribution they are found almost exclusively in the S2 fraction (Figure 5.8 and 5.9).

5.7 Triton X114 extraction reveals that the tail region of both VAPA and VAPB are sufficient to target the protein to the correct ER subdomain

The VAPA and VAPB tails expressed on their own gave the same subcellular distribution as the endogenous VAPA and VAPB (Figure 5.10 and 5.11). However these tail domains contain a GxxxG domain predicted to be involved in transmembrane helix-helix association (Russ et al., 2000).

A

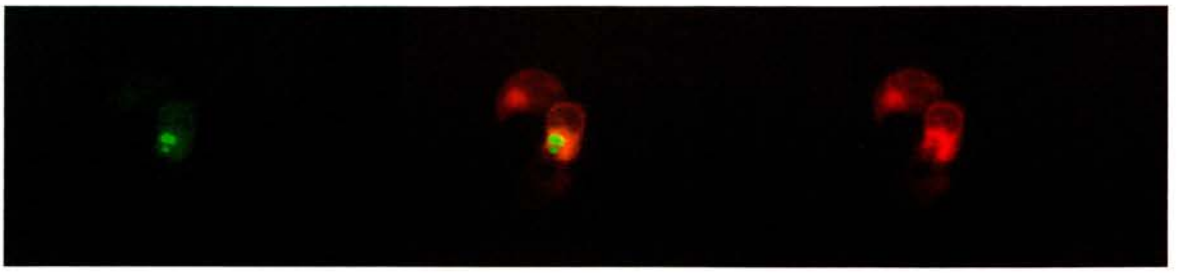

VAPAMSP-GFP Merge DS.Red-ER

B

P1 P2 S2

Figure 5.6 Triton X114 extraction of HEK293 cells, expressing VAPA MSP-GFP. A. VAPA MSP-GFP was transiently transfected into HEK cells along with DS.Red-ER and the cells were imaged after 48 hours. The VAPA MSP-GFP does not co-localise with the DS.Red-ER marker. B. HEK cells were lysed and P1, P2, and S2 layers were prepared. The P2 layer of the HEK cells was detergent extracted using Triton X114. VAPA MSP-GFP is found mainly in the S2 layer (n=3).

A

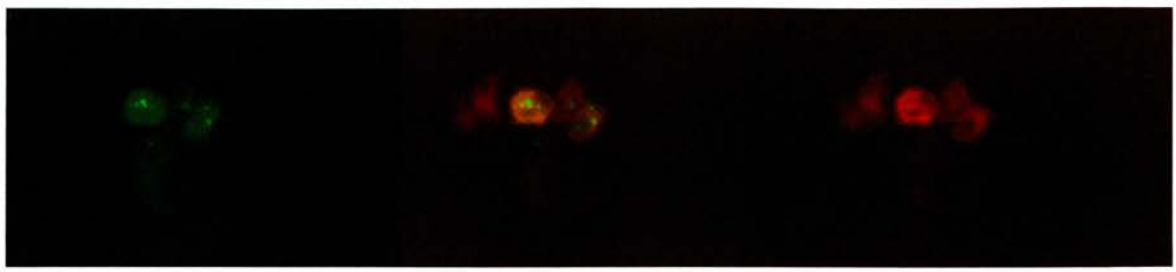

VAPB MSP-GFP Merge DS.Red-ER

B

Figure 5.7 Triton X114 extraction of HEK293 cells, expressing VAPB MSP-GFP. A. VAPB MSP-GFP was transiently transfected into HEK cells along with DS.Red-ER and the cells were imaged after 48 hours. At this timescale all of the VAPB MSP-GFP cells were dying so it was not possible to determine its cellular localisation. B. HEK cells were lysed and P1, P2, and S2 layers were prepared. The P2 layer of the HEK cells was detergent extracted using Triton X114. VAPB MSP-GFP is found predominantly in the P2 layer and is partially detergent extracted in Triton X114 (n=3).

A

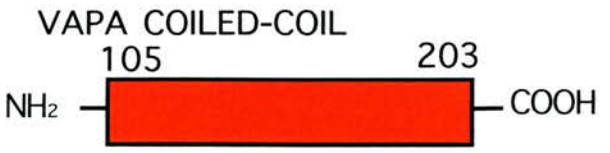

VAPA coiled-coil-GFP Merge DS.Red-ER

B

Figure 5.8 Triton X114 extraction of HEK293 cells, expressing VAPA coiled-coil-GFP. A. VAPA coiled-coil-GFP was transiently transfected into HEK cells along with DS.Red-ER and the cells were imaged after 48 hours. VAPA coiled-coil-GFP partially co-localises with the DS.Red-ER marker but in general its distribution is much more diffuse. B. HEK cells were lysed and P1, P2, and S2 layers were prepared. The P2 layer of the HEK cells was detergent extracted using Triton X114. VAPA coiled-coil-GFP is found mainly in the S2 layer (n=3).

A

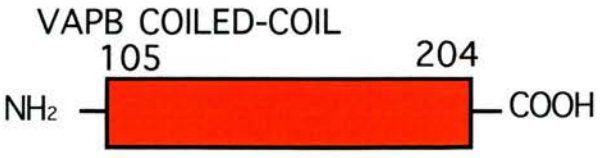

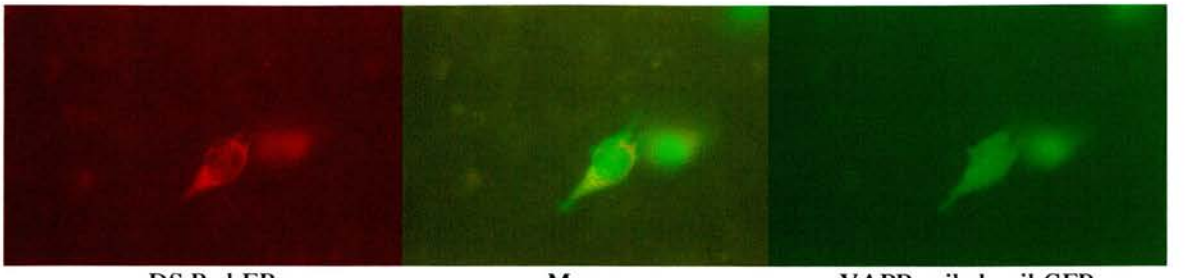

DS.Red-ER Merge VAPB coiled-coil-GFP

B

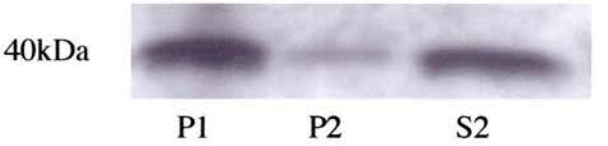

Figure 5.9 Triton X114 extraction of HEK293 cells, expressing VAPB coiled-coil-GFP. A. VAPB coiled-coil-GFP was transiently transfected into HEK cells along with DS.Red-ER and the cells were imaged after 48 hours. VAPB coiled-coil-GFP did not co-localise with the DS.Red-ER marker. B. HEK cells were lysed and P1, P2, and S2 layers were prepared. The P2 layer of the HEK cells was detergent extracted using Triton X114. VAPB coiled-coil-GFP is found predominantly in the S2 layer (n=3).

A

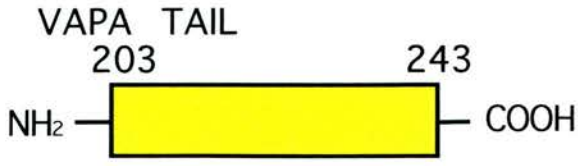

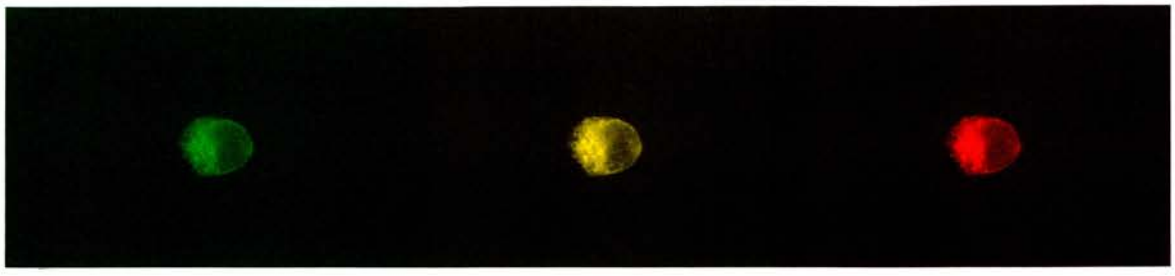

VAPA Tail-GFP Merge DS.Red-ER

B

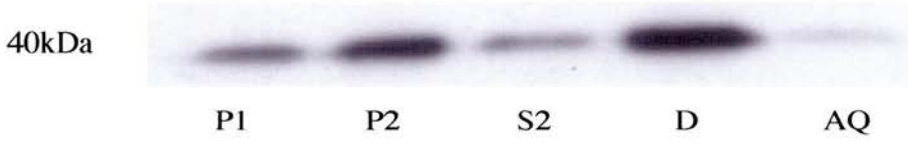

Figure 5.10 Triton X114 extraction of HEK293 cells, expressing VAPA Tail-GFP. A. VAPA Tail-GFP was transiently transfected into HEK cells along with DS.Red-ER and the cells were imaged after 48 hours. VAPA Tail-GFP completely co-localises with the DS.Red-ER marker. B. HEK cells were lysed and P1, P2, and S2 layers were prepared. The P2 layer of the HEK cells was detergent extracted using Triton X114. VAPA Tail-GFP is found mainly in the P2 layer and is detergent extracted in Triton X114 (n=3).

A

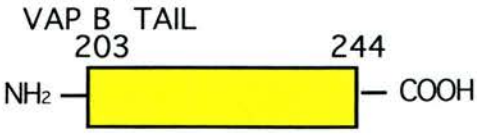

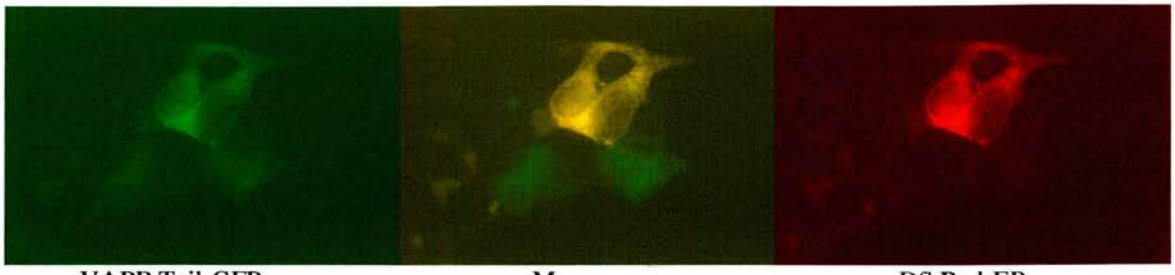

B

Figure 5.11 Triton X114 extraction of HEK293 cells, expressing VAPB Tail-GFP. A. VAPB Tail-GFP was transiently transfected into HEK cells along with DS.Red-ER and the cells were imaged after 48 hours. VAPB Tail-GFP completely co-localised with the DS.Red ER marker. B. HEK cells were lysed and P1, P2, and S2 layers were prepared. The P2 layer of the HEK cells was detergent extracted using Triton X114. VAPB Tail-GFP is found predominantly in the S2 layer (n=3).

Therefore the tail domains may be targeted to the correct ER subdomain via specific interactions with endogenous VAPA or VAPB. When VAPA Tail-GFP and DS.Red-VAPB Tail are co-expressed in HEK cells, a similar distribution is seen to that of endogenous VAPA and VAPB (Figure 5.12).

5.8 VAPA and VAPB expressed without the tail domain have different cellular localisations

The VAPA and VAPB constructs without the tail domains appear to have different cellular localisations. VAPA without the tail has a diffuse distribution similar to that of the coiled-coil domain expressed alone. VAPB without the tail, however, largely co-localises with the DS.Red-ER marker although this co-localisation is not as great as that of full-length VAPB. This construct is definitively excluded from the nucleus however, whereas VAPA without the tail is not. The constructs do not have the tail domain to insert them into the ER membrane and this is confirmed by neither of them being detergent extracted in Triton X114 (Figure 5.13 and 5.14). The differences in localisation seen may be due to differing protein interactions.

A

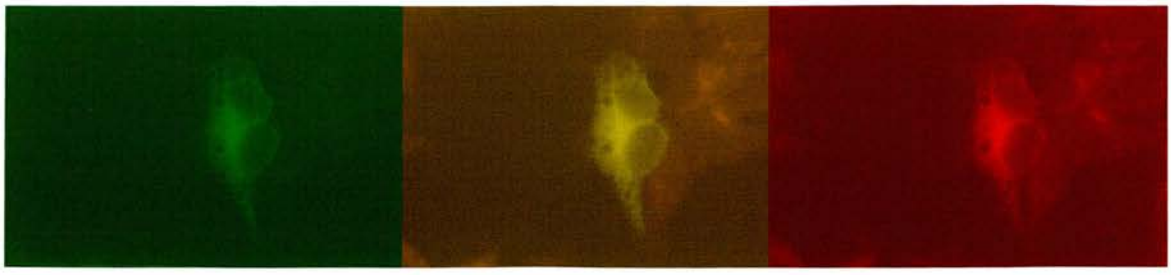

VAPA Tail-GFP Merge DS.Red-VAPB Tail

B

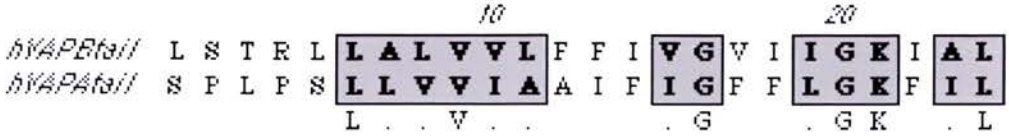

Figure 5.12 VAPA and VAPB tail comparison. A. VAPA Tail-GFP was transiently transfected into HEK cells along with DS.Red-VAPB Tail and the cells were imaged after 48 hours. VAPA Tail-GFP and DS.Red-VAPB-Tail partially co-localise in HEK cells. B. VAPA and VAPB Tail homology (n=6).

A

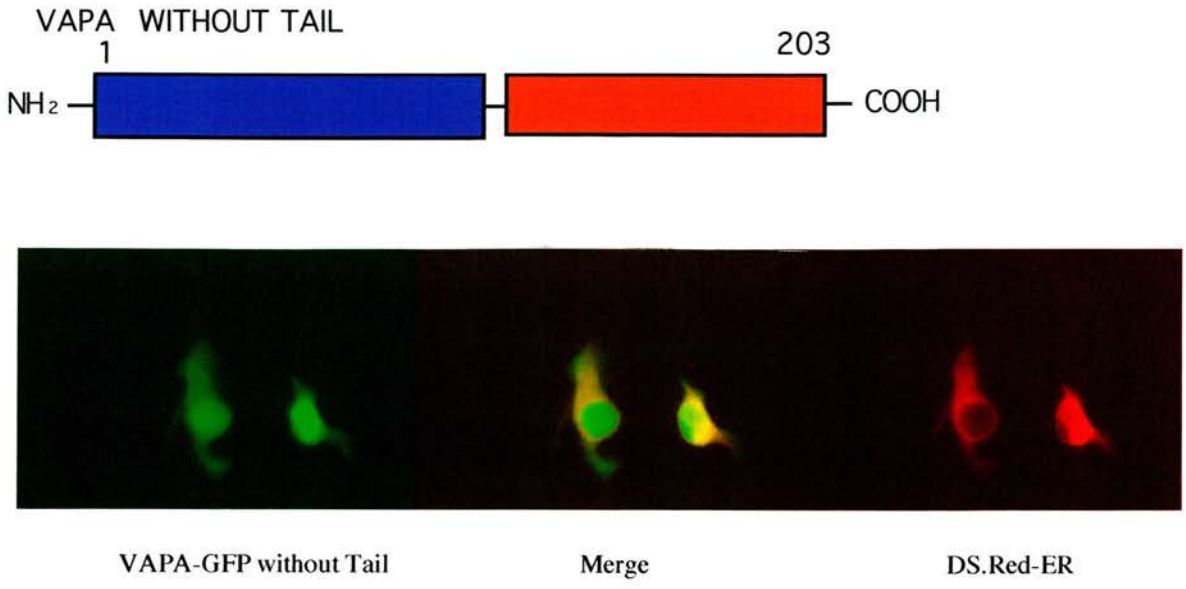

B

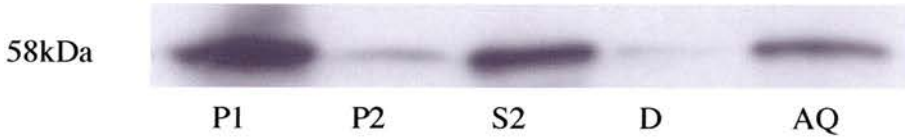

Figure 5.13 Triton X114 extraction of HEK293 cells, expressing VAPA-GFP without Tail. A. VAPA-GFP without Tail was transiently transfected into HEK cells along with DS.Red-ER and the cells were imaged after 48 hours. VAPA-GFP without Tail does not co-localise with the DS.Red-ER marker. B. HEK cells were lysed and P1, P2, and S2 layers were prepared. The P2 layer of the HEK cells was detergent extracted using Triton X114. VAPA-GFP without Tail is found mainly in the S2 layer and is not detergent extracted in Triton X114 (n=3).

A

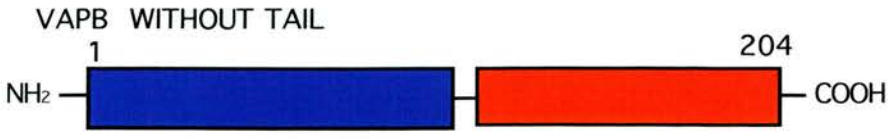

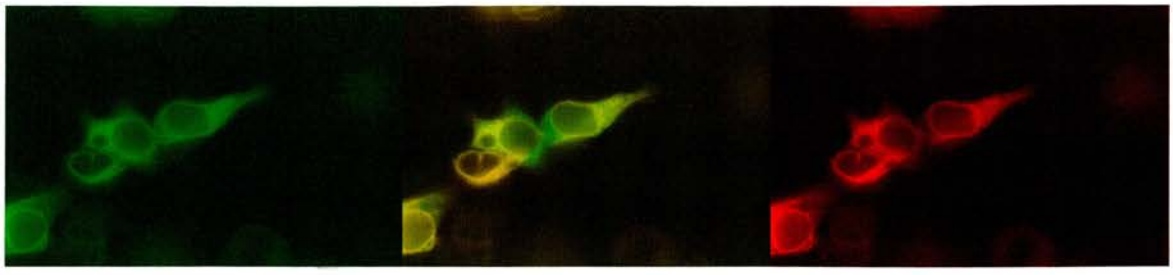

VAPB-GFP without Tail Merge DS.Red-ER

B

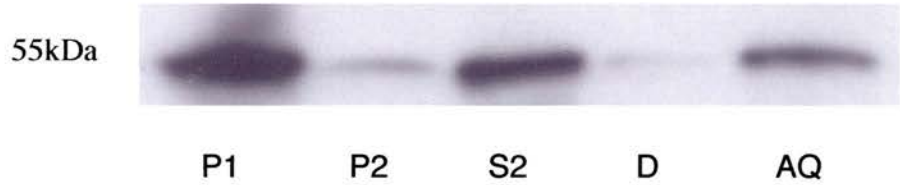

Figure 5.14 Triton X114 extraction of HEK293 cells, expressing VAPB-GFP without Tail. A. VAPB-GFP without Tail was transiently transfected into HEK cells along with DS.Red-ER and the cells were imaged after 48 hours. VAPB-GFP without Tail partially co-localised with DS.Red-ER marker. B. HEK cells were lysed and P1, P2, and S2 layers were prepared. The P2 layer of the HEK cells was detergent extracted using Triton X114. VAPB-GFP without Tail is found predominantly in the S2 layer (n=3).

5.9 VAPA and VAPB expressed without the MSP domains co-localise with DS.Red-ER and are in similar fractions

Both VAPA and VAPB expressed without their MSP domain co-localise with the DS.Red-ER marker. When fractions of these constructs are made they are found in both the P2 and S2 layers at a similar volume. The protein found in the S2 layer appears in two bands of slightly different sizes. This may indicate proteolysis of these constructs, presumably at the c-terminal end of the protein as they are N-terminally tagged with GFP and the smaller fragment would not be picked up if it were N-terminally cleaved (Figure 5.15 and 5.16).

5.10 VAPA with the tail replaced with the VAPB tail localises to the same ER subdomain as endogenous VAPB

The VAPB tail construct was removed from the GFP vector by restriction digest and inserted into the VAPA without a tail construct, to give VAPA with the VAPB tail. This construct had a gross ER distribution when imaged as it colocalised with the DS.Red-ER marker. When fractionated and extracted with Triton X114 it shared the same subdomain localisation as endogenous VAPB (Figure 5.17). Therefore no other part of the protein appears to affect subdomain localisation, which is determined by the tail alone.

A

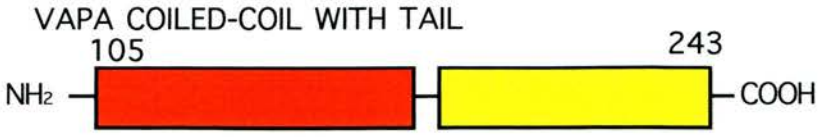

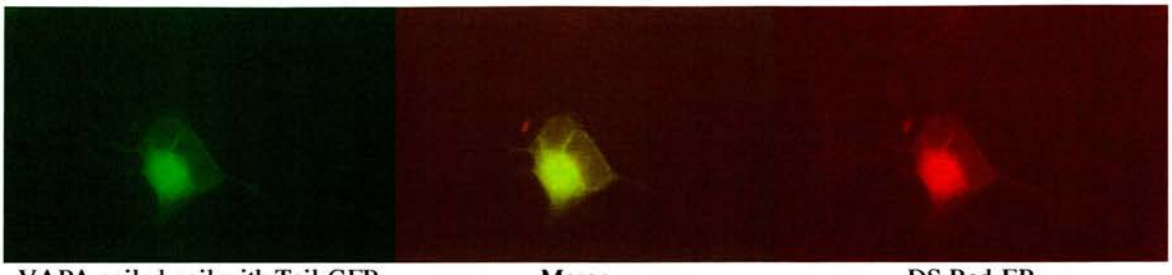

VAPA coiled-coil with Tail-GFP Merge DS.Red-ER

B

Figure 5.15 Triton X114 extraction of HEK293 cells, expressing VAPA coiled-coil with Tail-GFP. A. VAPA coiled-coil with Tail-GFP was transiently transfected into HEK cells along with DS.Red-ER and the cells were imaged after 48 hours. VAPA coiled-coil with Tail-GFP completely co-localised with the DS.Red-ER marker. B. HEK cells were lysed and P1, P2, and S2 layers were prepared. The P2 layer of the HEK cells was detergent extracted using Triton X114. VAPA coiled-coil with Tail-GFP is found in the P2 and S2 layers and is detergent extracted in Triton X114.

A

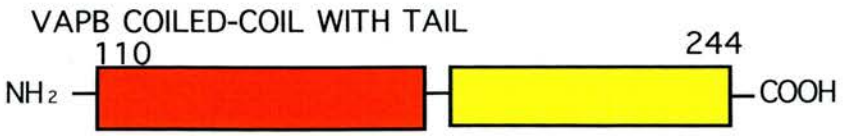

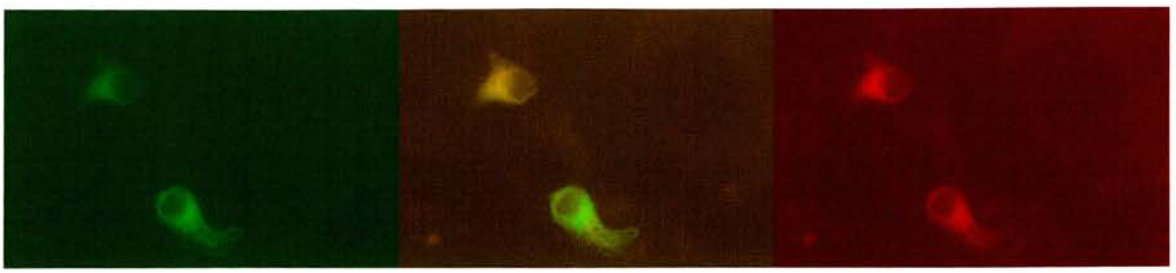

VAPB coiled-coil with Tail-GFP Merge DS.Red-ER

B

Figure 5.16 Triton X114 extraction of HEK293 cells, expressing VAPB coiled-coil with Tail-GFP. A. VAPB without MSP-GFP was transiently transfected into HEK cells along with DS.Red-ER and the cells were imaged after 48 hours. VAPB coiled-coil with Tail-GFP completely co-localised with DS.Red-ER marker. B. HEK cells were lysed and P1, P2, and S2 layers were prepared. The P2 layer of the HEK cells was detergent extracted using Triton X114. VAPB coiled-coil with Tail-GFP is found in the P2 and S2 layers.

A

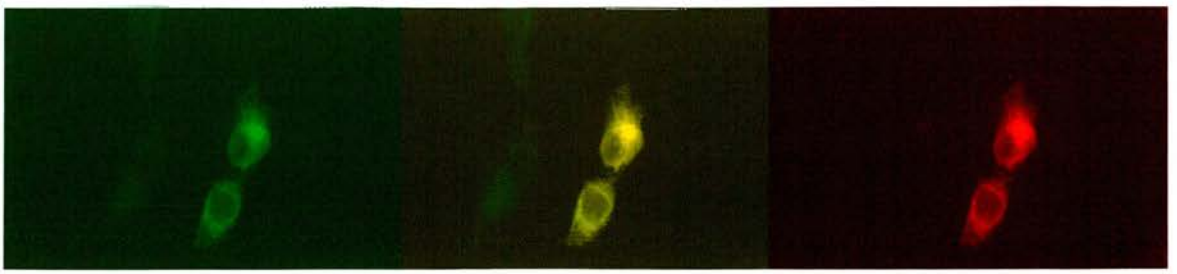

VAPAwithBTail-GFP Merge DS.Red-ER

B

Figure 5.17 Triton X114 extraction of HEK293 cells, expressing VAPA with B Tail-GFP. A. VAPA with B Tail-GFP was transiently transfected into HEK cells along with DS.Red-ER and the cells were imaged after 48 hours. VAPA with B Tail-GFP completely co-localises with the DS.Red-ER marker. B. HEK cells were lysed and P1, P2, and S2 layers were prepared. The P2 layer of the HEK cells was detergent extracted using Triton X114. VAPA with B Tail-GFP is found predominantly in the S2 layer (n=3).

5.11 Variant of VAPB found in humans, VAPC may also be present in mice.

VAPC is a splice variant of VAPB, which has been previously identified in humans by northern blot (Nishimura et al., 1999). VAPC contains exons 1, 2 and 6 of VAPB therefore it contains almost the entire MSP domain and a short sequence of C terminal which is not homologous to either VAPA or VAPB. Using specific PCR primers a 300 base pair PCR product was made form a mouse brain cDNA library along with a band corresponding to full length VAPB (Figure 5.18). However this band has yet to be cloned and sequenced. Therefore the mouse may also contain the splice variant of VAPB named VAPC.

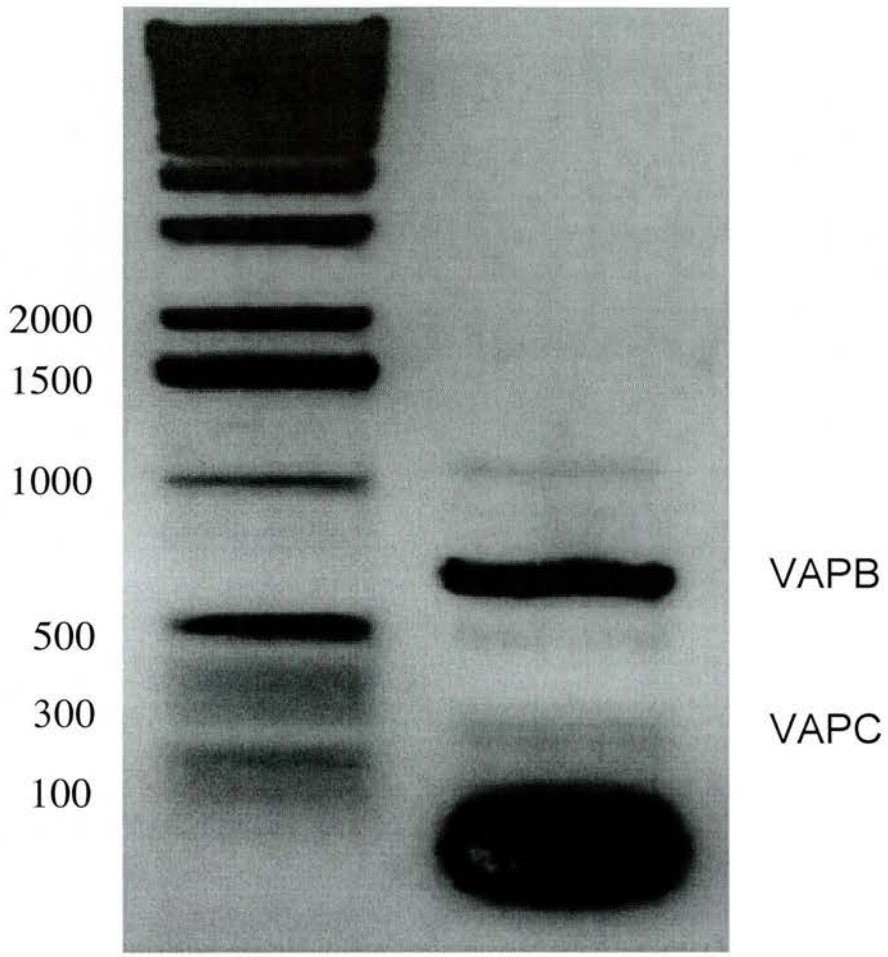

Figure 5.18 PCR band of correct size for VAPC in the mouse.

VAP mutant	Cell localisation	Fraction present in				
		P1	P2	S2	D	AQ
ENDOGENOUS VAPA	endoplasmic reticulum	Y	80%	20%	90%	10%
ENDOGENOUS VAPB	endoplasmic reticulum	Y	20%	80%		100%
VAPA MSP	cytosolic aggregates	Y	30%	70%		
VAPB MSP	cytosolic aggregates	Y	90%	10%	50%	50%
VAPA COILED COIL	diffuse cytosolic	Y		100%		
VAPB COILED COIL	diffuse cytosolic	Y	5%	95%		
VAPA TAIL	endoplasmic reticulum	Y	80%	20%	95%	5%
VAB TAIL	endoplasmic reticulum	Y	20%	80%	50%	50%
VAPA WITHOUT TAIL	diffuse cytosolic	Y	10%	90%	5%	95%
VAPB WITHOUT TAIL	endoplasmic reticulum	Y	10%	90%	5%	95%
VAPA COILED COIL WITH TAIL	endoplasmic reticulum	Y	60%	40%	100%	
VAPB COILED COIL WITH TAIL	endoplasmic reticulum	Y	50%	50%		
VAPA WITH VAPB TAIL	endoplasmic reticulum	Y	5%	95%		

Table 5.1 Differences in localisation of VAP truncation constructs.

5.13 Discussion

The VAP family of proteins appears to play a major role in the localisation of oxysterol and other lipid binding proteins to the ER, as well as in sensing ER stress. We have identified differences in the subcellular localisation of VAPA and VAPB on the ER membrane.

VAPA localises like an integral ER protein and pellets mostly in the P2 layer, and is in the detergent phase in Triton X114. VAPB, however, does not pellet as well into the P2 layer, suggesting that it is in lighter membrane fractions and is in the aqueous phase in Triton X114 suggesting that it is not an integral membrane protein. These differences are surprising as VAPA and VAPB share a high degree of homology.

To determine which domains were responsible for the differences in VAPA and VAPB localisation we made a variety of truncations of the VAP proteins. This revealed that the tail region of VAPA was sufficient to insert it into the ER membrane. The tail region of VAPB however localises in a similar manner to the full-length protein.

The VAPB tail was then substituted into VAPA in place of the native tail. This construct localised in a similar fashion to VAPB. Again this could be due to the exogenous VAPB tail interacting with the endogenous VAPB protein.

Also interesting is the fact that the VAPB MSP domain pellets mostly into the P2 layer and partially detergent extracts into Triton X114, whereas the VAPA MSP construct is

mostly cytoplasmic and does not detergent extract. The VAPA MSP construct behaves as expected, as it has not been found to dimerise (Kaiser et al., 2005) so will not bind to endogenous VAPA. The VAPB MSP domain may act in a different fashion and dimerise or may be interacting with another ER protein, leading to its unexpected extraction. This may also effect the localisation of VAPC, now identified in humans and mice, as it contains almost the entire VAPB MSP domain.

Therefore, the minor differences in VAPA and VAPB homology in each domain appear to lead to differences in localisation and possibly in protein interactions (Table 5.1). These differences may reveal important differences in their roles in the ER.

6. The VAP family and motor neuron degeneration

6.1 Background

VAPB has recently been identified as being linked to ALS via a mutation of a proline residue at position 56 of the protein to a serine (Nishimura et al., 2004). This mutation leads to three different phenotypes of the disease. One phenotype is atypical ALS8 where the patients have late-onset motor neuron death; fasiculations and disease progression is 10-20 years. Some patients have late onset spinal muscular atrophy with slowly progressing late on-set degeneration of cells in the anterior horn. The final set of patients display, typical ALS and have a life expectancy of 2-3 years. The reason for this wide range of phenotypes is not yet clear. However, there are so-called modifying factors for ALS, which are not directly linked to the disease but may modify its progress. These factors include ciliary neurotrophic factor (CNTF), a survival factor in spinal motor neurons, which is decreased in the frontal cortex of ALS patients (Ono et al, 1999). CNTF knockout mice also have slowly progressing motor neuron disease (Masu et al., 1993). Apurinergic apyrimidic endonuclease (APEX), a DNA repair factor, is also decreased in the frontal cortex of ALS patients (Kisby et al., 1997). It may play a role in the Guamanian ALS-dementia-Parkinsonism complex as a metabolite of cycasin, methylazoxymethanol (MAM), decreases APEX levels and activity in neurons (Esclaire et al., 1999). Neurofilament aggregation in motor neurons is seen in both familial and sporadic ALS (Cote et al., 1993). Recently 2 peripherin, a neuronal intermediate filament, variants were found only in patients with ALS. One of these caused a premature stop codon in the protein and disrupted neurofilament light chain assembly

into the intermediate filament assembly. These peripherin variants may play a role in some ALS cases (Gros-Louis et al., 2004).

There is also evidence that excess lipid accumulation can cause apoptosis and motor neuron cell death. In some ALS patients, and in Cu/Zn SOD mutant mice, increased oxidative stress in conjunction with accumulation of sphingomyelin, ceramides and cholesterol esters. The inhibition of this lipid accumulation by pharmacological means protects motor neurons from apoptotic cell death induced by oxidative stress (Cutler et al., 2002). Exogenous ceramide can also cause apoptotic cell death. The mechanism by which this occurs is unknown. However, there is evidence that ceramide can reduce the phosphorylation of BAD, allowing it to heterodimerise with Bcl-2 and act as a pro-apoptotic agent (Zundel et al., 1998). The liver X receptors (LXRα and LXRβ) are ligand activated nuclear receptors that play a role in the regulation of cholesterol and sterol trafficking between tissues. Their endogenous ligands are oxysterols (Andersson et al., 2005). LXRα knockout animals accumulate cholesterol in their livers, which is where the proteins get their name (Peet et al., 1998). However, the LXRβ receptor is broadly expressed in the developing and adult rodent brain (Kainu et al., 1996). In adult mammals 95% of the cholesterol in the brain is synthesised in situ but synthesis exceeds the brain's requirement so the cholesterol must be excreted. The major pathway for this excretion is via cholesterol 24 hydroxylase. In the spinal cord there is 5-fold more cholesterol synthesised than in the cerebellum or cerebrum but the concentration of cholesterol is only 2-fold higher (Quan et al., 2003). The spinal cord must have a high capacity for cholesterol secretion, but cholesterol 24 hydroxylase is not highly expressed

there (Lund et al., 1999) so there must be some other means of excretion. The absence of LXRβ in male mice causes a selective vulnerability of large motor neurons. At 7 months these mice exhibit impaired performance on the rota-rod and this impairment is associated with lipid accumulation and loss of motor neurons in the spinal cord, together with axonal atrophy and astrogliosis. The onset of this impairment is between 3 and 7 months, as 3 month-old mice do not appear to be impaired (Andersson et al., 2005). The motor neuron selective cell death and late onset appear to be very similar to the effects seen in ALS. Lipid accumulation in the spinal cord may be an important factor in human cases of ALS.

6.2 VAPB and VAPBP56S have different subcellular distributions

Recently our colleagues in Brazil (Nishimura et al., 2004) discovered that a mutation in the VAPB gene was linked to an atypical form of ALS. This mutation leads to the proline residue at position 56 of the protein being replaced with a serine residue (P56S). Computational analysis of the change in residues predicts that the proline to serine mutation will change the tertiary structure of the protein such that a kink in the structure will become straight (Figure 6.1). This is predicted to alter the MSP-MSP protein interactions of VAPB as proline 56 is a conserved residue thought to be key in these interactions (Baker et al., 2002). This is not a key residue for FFAT protein binding so these interactions should be unaffected (Loewen et al., 2005).

We made VAPB with the proline to serine mutation (VAPBP56S) fused to GFP and expressed the protein in HEK293 cells and in primary hippocampal neurons. The distribution of VAPBP56S in both HEK cells and neurons is altered with the mutant version forming protein aggregates (Figure 6.2)

6.3 VAPA and VAPB without the MSP domain fused to GFP form cisternae in the ER membrane but VAPB without the MSP domain fused to HA does not

Low affinity interactions of ER membrane proteins is known to induce ER cisternae, or stacked smooth ER biogenesis, when these proteins are fused to GFP (Snapp et al., 2003).

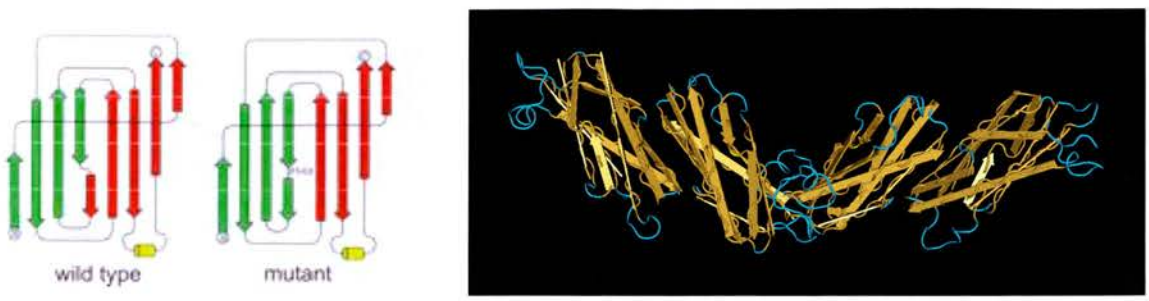

Figure 6.1 The P56S mutation is predicted to affect the tertiary structure of the MSP domain. The figure shows two MSP domains side by side and the arrows represent β sheets. In a comparison between the wild-type and mutant VAPB MSP domains computational analysis of the change in residues predicts that the proline to serine mutation will change the tertiary structure of the protein such that a kink in the structure will become straight.

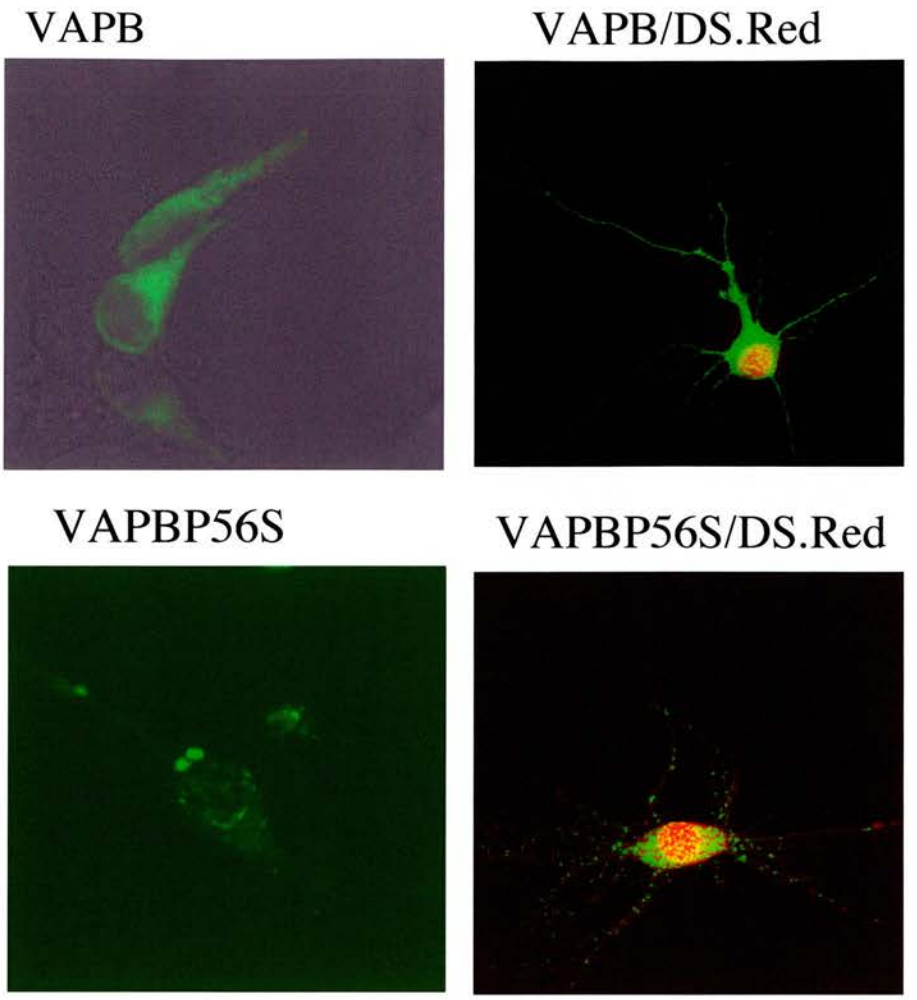

Figure 6.2 VAPB and VAPB P56S have different subcellular distributions. HEK293 cells were transfected with VAPB/VAPBP56S and E19 primary cultured hippocampal neurons were co-transfected with VAPB/VAPBP56S and DS.Red. VAPB has a diffuse, perinuclear distribution whereas VAPBP56S has a punctate distribution, which suggests that it forms protein aggregates (n=6).

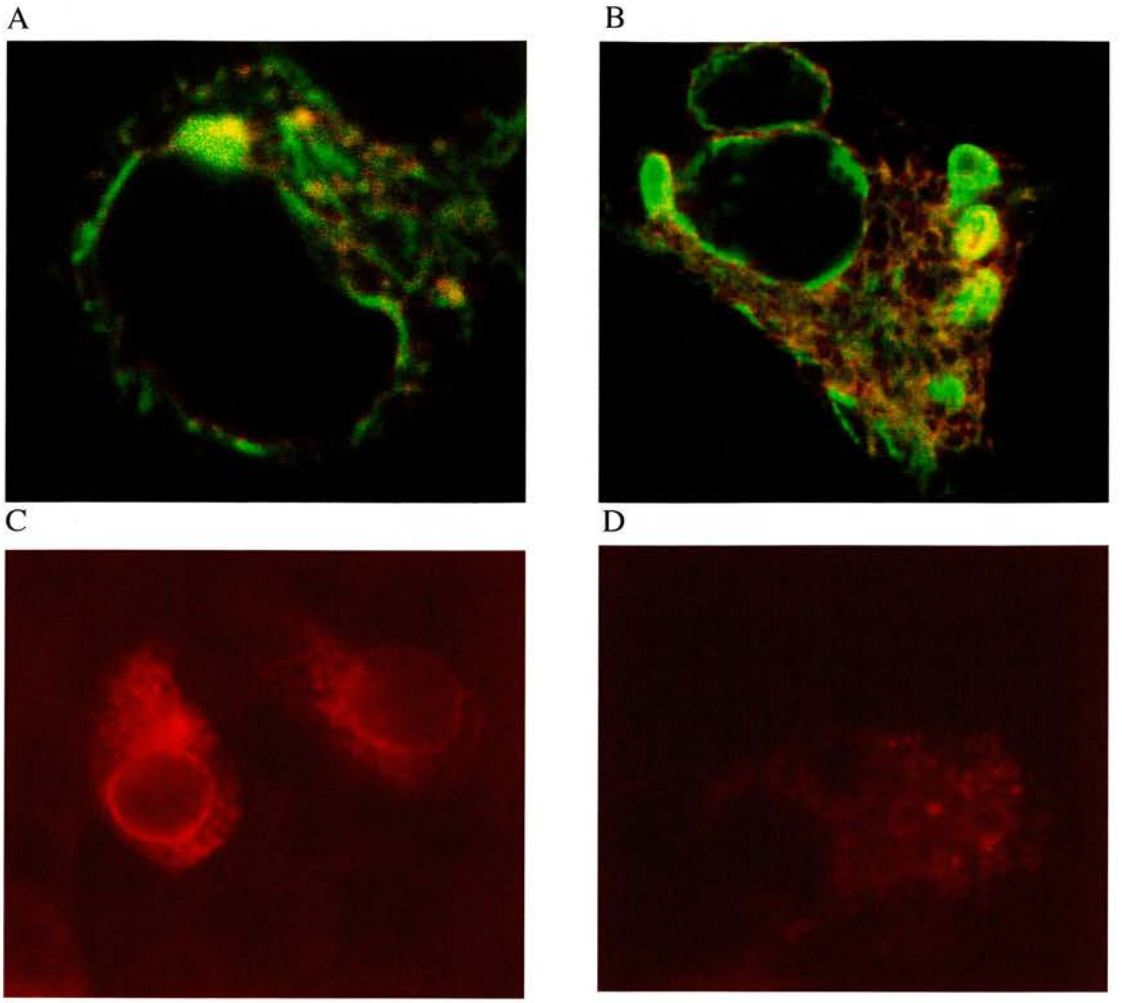

Figure 6.3 VAPA and VAPB without the MSP domain fused to GFP form cisternae in the ER membrane but VAPB without the MSP domain fused to HA does not. A. HEK293 cells expressing VAPA without the MSP domain fused to GFP and DS.Red-ER. B. HEK293 cells expressing VAPB without the MSP domain fused to GFP and DS-Red-ER. C. HEK293 cells expressing VAPB without the MSP domain fused to HA and HA antibody stained. D. HEK293 cells expressing VAPBP56S fused to HA and HA antibody stained (n=3).

This also happens with the most highly overexpressing cells transfected with VAPA-GFP or VAPB-GFP. However the more predominant, lower overexpressing cells do not give cisternae but smooth reticular fluorescence. However, VAPA and VAPB without the MSP domain fused to GFP overexpressing cells predominantly give cisternae (Figure 6.3A and B). This does not occur when these proteins are expressed with a non-dimerising HA tag (Figure 6.3C). These cisternae are, therefore artificially induced by the GFP fusion tag. However VAPBP56S fused to HA still has the characteristic protein aggregates so these are not cisternae nor are they GFP induced.

6.4 VAPBP56S aggregates are associated with the ER membrane but are not enriched in the Golgi apparatus

The gross cellular localisation of VAPB has previously been determined and it has been found to associate with the ER and Golgi apparatus (Soussan et al., 1999). To find out whether VAPBP56S shared this localisation it was co-transfected into HEK293 cells with either DS.Red-ER or Cyan-Golgi. VAPBP56S aggregates partially co-localise with the DS.Red-ER marker (Figure 6.4), so are associated with the ER membrane. However, VAPBP56S aggregates do not colocalise with the Cyan-Golgi marker, therefore they are not enriched in the Golgi apparatus (Figure 6.5).

6.5 VAPAP56S forms similar aggregates to VAPBP56S and shares the same intracellular distribution

To determine whether the P56S mutation in VAPA would have similar effects to the VAPB mutant we made the P56S form of VAPA fused to GFP. This construct was expressed in HEK293 cells along with either the DS.Red-ER or Cyan-Golgi markers. VAPAP56S was found to form protein aggregates and to colocalise with DS.Red-ER (Figure 6.6). Both VAPA and VAPB respond in a similar manner to the P56S mutation on a gross level.

6.6 MSPP56S forms similar protein aggregates to MSP

To reveal whether the P56S mutation would have any effect upon the MSP aggregates seen when the MSP domain is expressed alone the P56S version of VAPA MSP was made. VAPA MSP-GFP and VAPA MSPP56S-GFP were expressed in HEK293 cells. On a gross level both of these constructs form large protein aggregates within the cell (Figure 6.7).

Figure 6.4 VAPB and VAPBP56S and the ER. VAPB/VAPBP56S and DS.Red-ER were co-transfected into E19 primary cultured hippocampal neurons and HEK293 cells. In both cell types VAPB co-localised with the DS.Red-ER marker, as did the VAPBP56S aggregates suggesting that the mutated protein is still found on the ER.

HEK293 cells

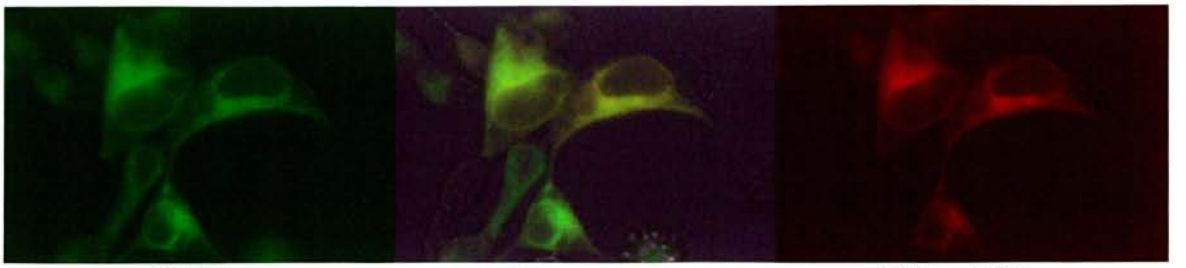

VAPB Merge DS.Red-ER

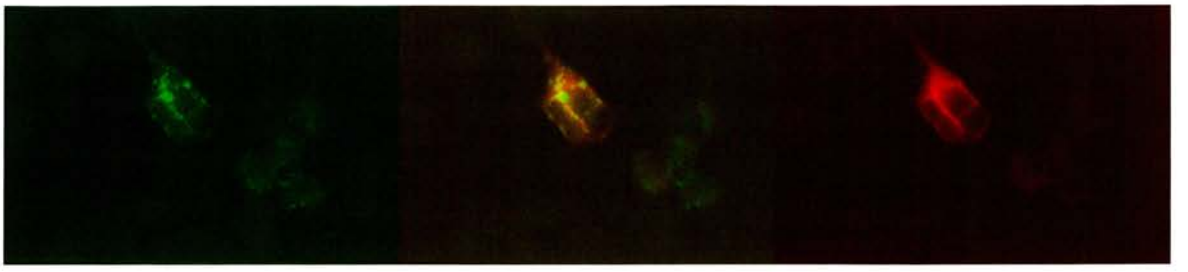

VAPBP56S Merge DS.Red-ER

Hippocampal neurons

VAPB Merge DS.Red-ER

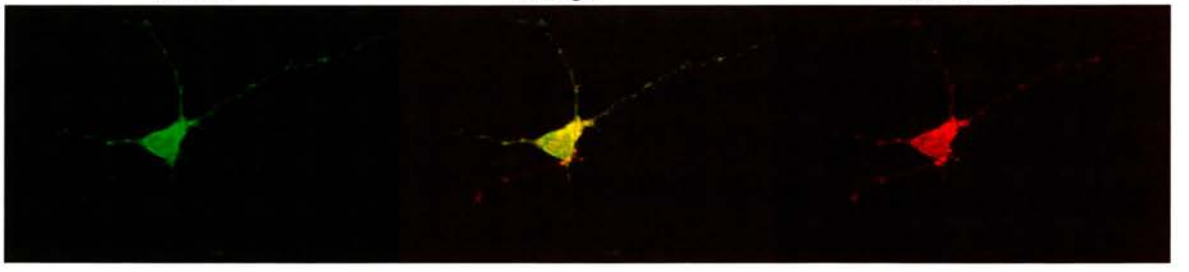

VAPB mutant Merge DS.Red-ER

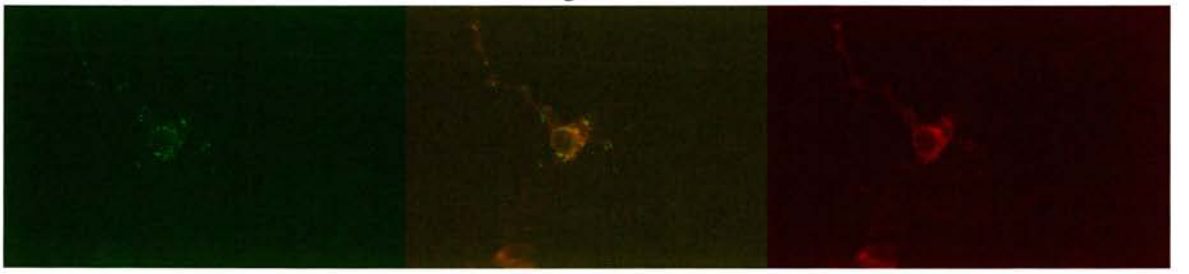

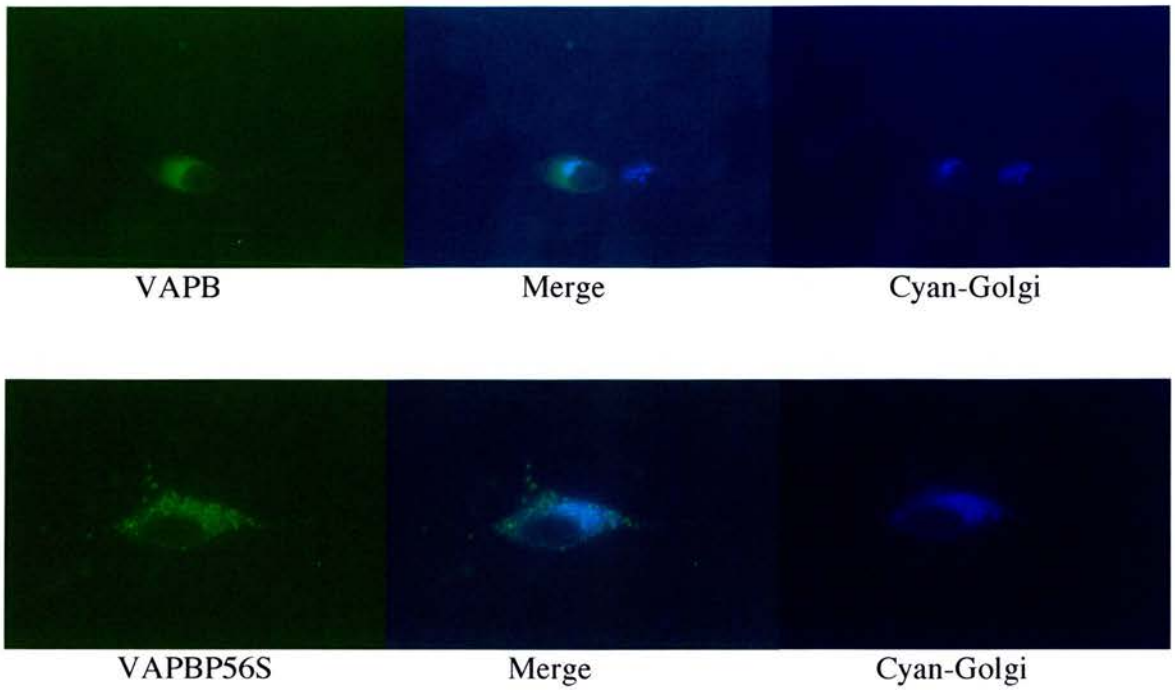

Figure 6.5 VAPB and VAPBP56S and cyan Golgi in HEK293 cells. VAPB/VAPBP56S were co-transfected into HEK293 cells with a cyan-golgi marker. VAPB expression does overlap with that of the cyan-golgi marker, therefore it is expressed in the Golgi. However, VAPBP56S aggregates do not appear to overlap in expression with the cyan-golgi marker (n=6).

Figure 6.6 VAPA and VAPAP56S and ER or Golgi markers in HEK293 cells. VAPA and VAPAP56S was co-transfected into HEK293 cells along with DS.Red-ER/Cyan-golgi. VAPA and VAPAP56S colocalise with the DS.Red-ER marker. VAPA also partially colocalises with the cyan-golgi marker but the VAPA aggregates do not appear to co-localise with the Cyan-golgi marker (n=6).

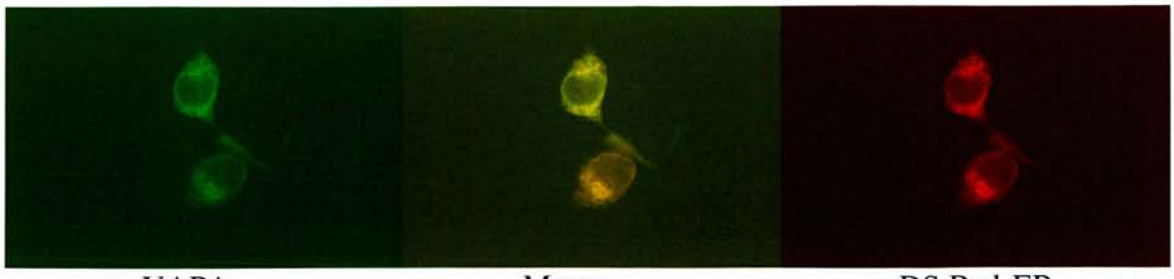

VAPA Merge DS.Red-ER

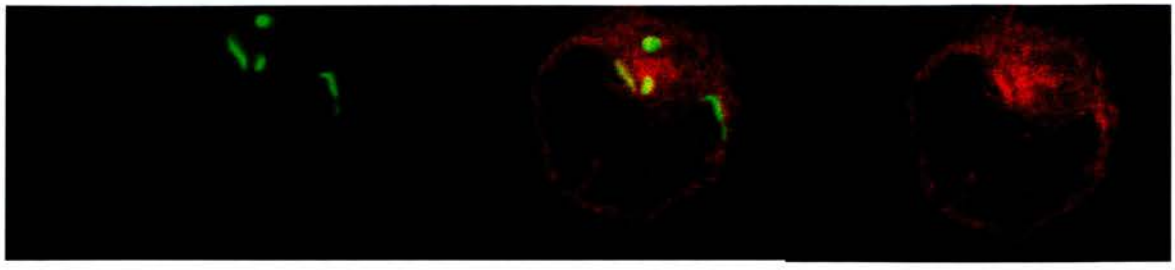

VAPAP56S Merge DS.Red-ER

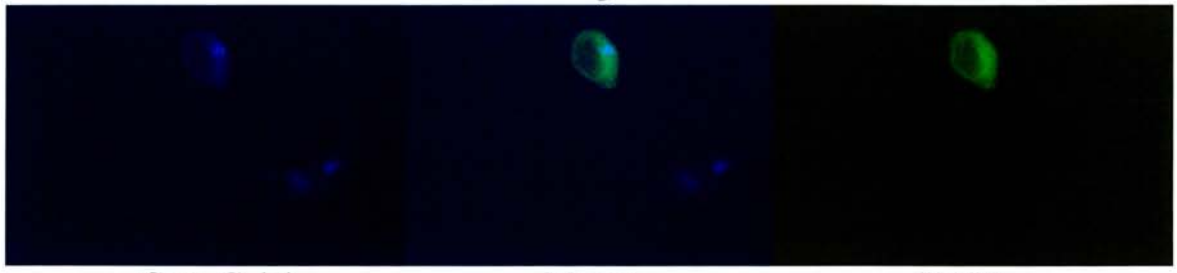

Cyan-Golgi Merge VAPA

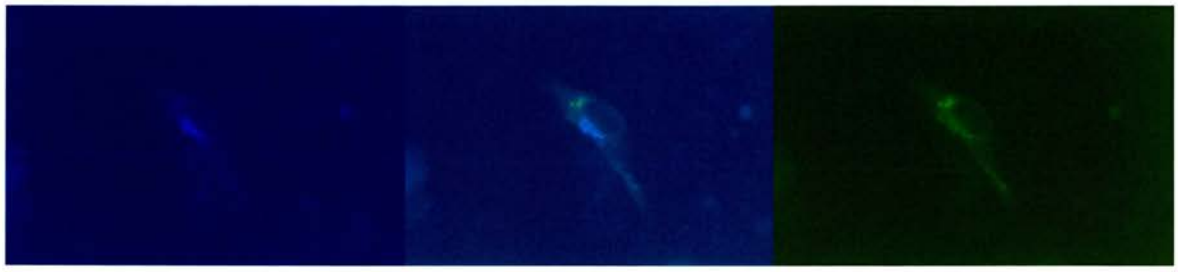

Cyan-Golgi Merge VAPAP56S

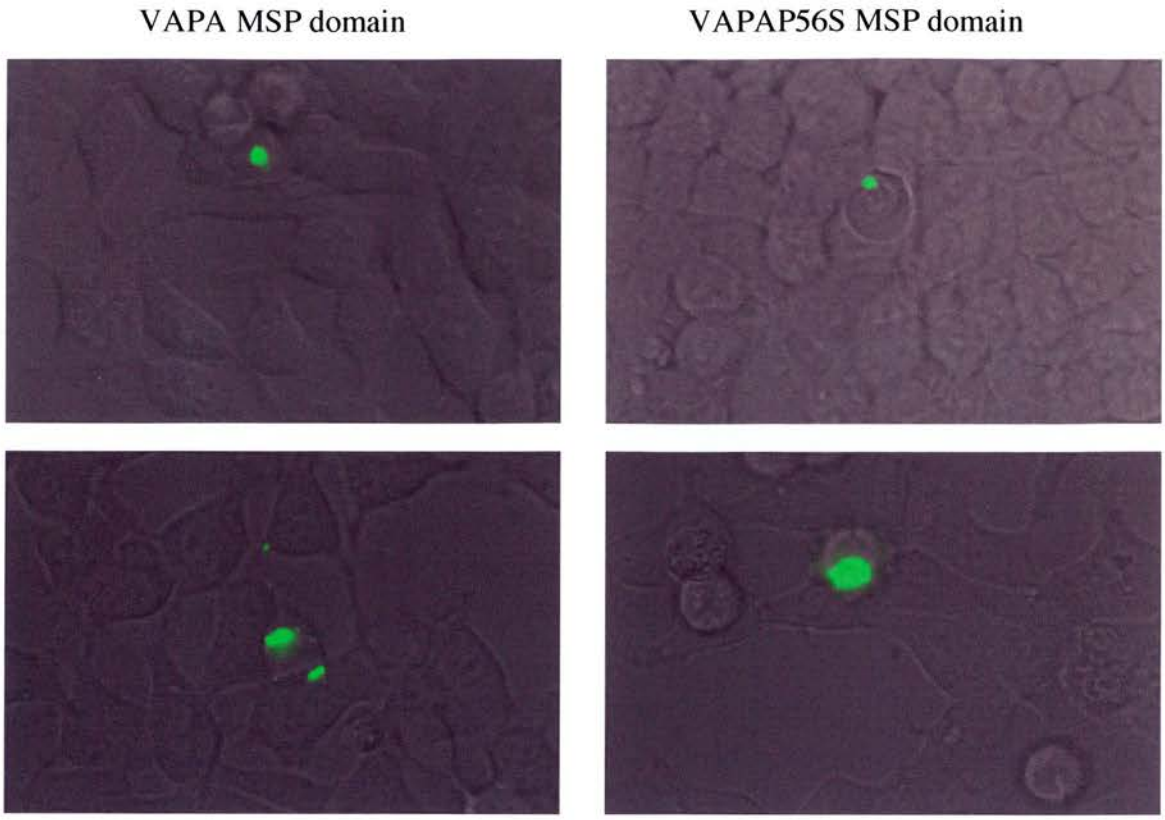

Figure 6.7 The VAPA MSP domain and VAPAP56S MSP domain were expressed in HEK293 cells. Both form large intracellular protein aggregates (n=6).

6.7 Triton X114 extraction of VAPBP56S demonstrates differences in subcellular distribution to VAPB

To examine the subcellular localisation of VAPBP56S compared to that of VAPB the VAPB-GFP and VAPBP56S-GFP constructs were expressed in HEK293 cells and P1, P2, and S2 layers prepared as described in the materials and methods. The P2 layer was detergent extracted (Bordier et al., 1981) with Triton X114 and the samples were analysed by western blots probed with GFP antibody. VAPB is found at higher levels in the S2 layer and is not in the detergent phase (Figure 6.8). However VAPBP56S pellets in the P2 layer and is completely in the detergent phase in TX114 (Figure 6.9). This suggests that VAPBP56S acts more like VAPA than VAPB, and that the subcellular localisation of VAPB is in some way dependent on the MSP domain or level of multimersation of the protein.

6.8 P56S constructs without tails show that aggregation is not dependent on membrane integration

To determine whether the aggregation of the P56S constructs was due to membrane association VAPAP56S and VAPBP56S without their tail domains were constructed and fused to GFP. These constructs were expressed in HEK293 cells and imaged. While VAPA and VAPB without their tail domains show a cytoplasmic distribution the P56S constructs form large protein aggregates (Figure 6.10 and 6.11).

A

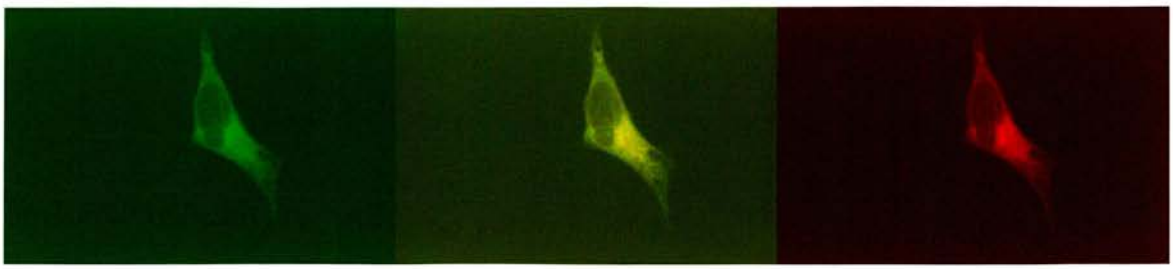

B

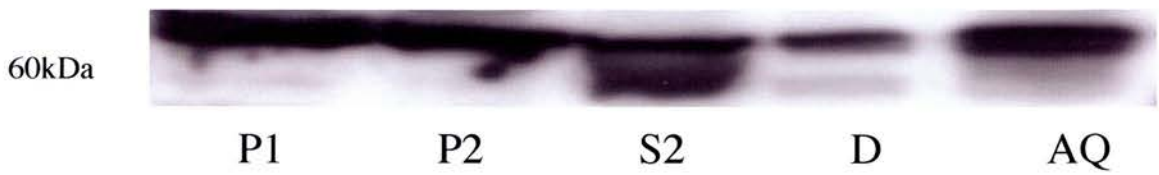

Figure 6.8 Triton X114 partitioning of HEK293 cells, expressing VAPB-GFP. A. VAPB-GFP was transiently transfected into HEK cells along with DS.Red-ER and the cells were imaged after 48 hours. The VAPB-GFP partially co-localises with the DS.Red-ER marker. B. HEK cells were lysed and P1, P2, and S2 layers were prepared. The P2 layer of the HEK cells was detergent partitioned using Triton X114. VAPB-GFP is found at a greater level in the S2 layer than the P2 layer and is mostly in the detergent phase in Triton X114 (n=3).

A

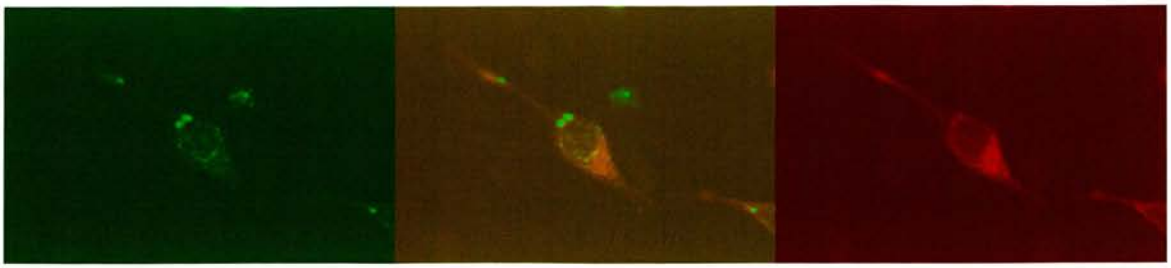

B

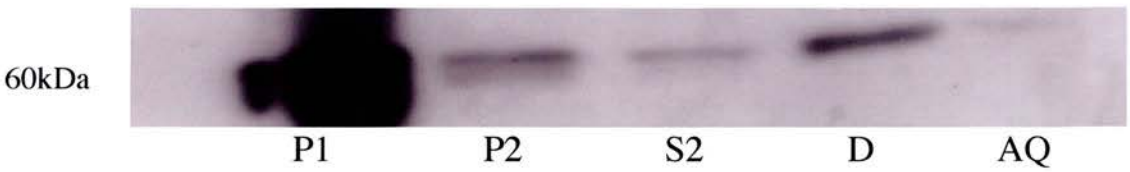

Figure 6.9 Triton X114 partitioning of HEK293 cells, expressing VAPBP56S-GFP. A. VAPBP56S-GFP was transiently transfected into HEK cells along with DS.Red-ER and the cells were imaged after 48 hours. The VAPBP56S-GFP partially co-localises with the DS.Red-ER marker. B. HEK cells were lysed and P1, P2, and S2 layers were prepared. The P2 layer of the HEK cells was detergent extracted using Triton X114. VAPBP56S-GFP is found at a greater level in the P2 layer than in the S2 layer and is mostly in the detergent phase in Triton X114 (n=3).

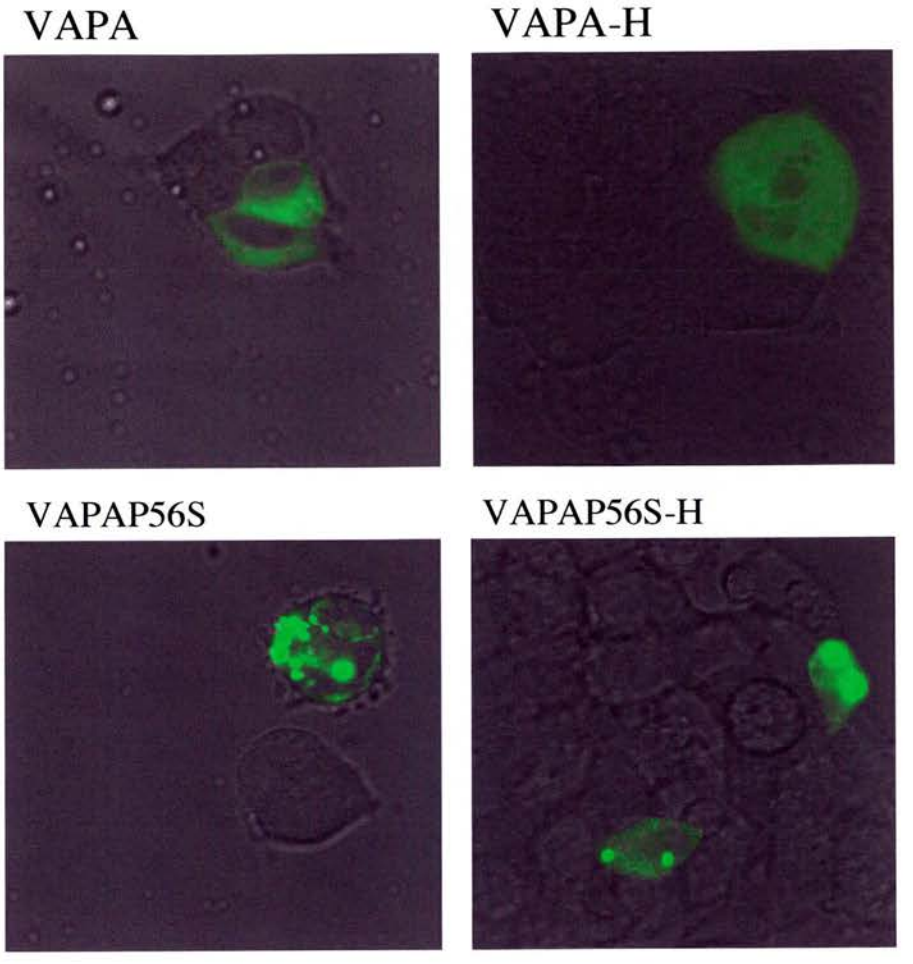

Figure 6.10 VAPA, VAPAP56S, VAPA without Tail and VAPAP56S without Tail were transfected into HEK293 cells. This revealed that the aggregates seen in the VAPAP56S mutant did not depend upon the tail region of the protein (n=3).

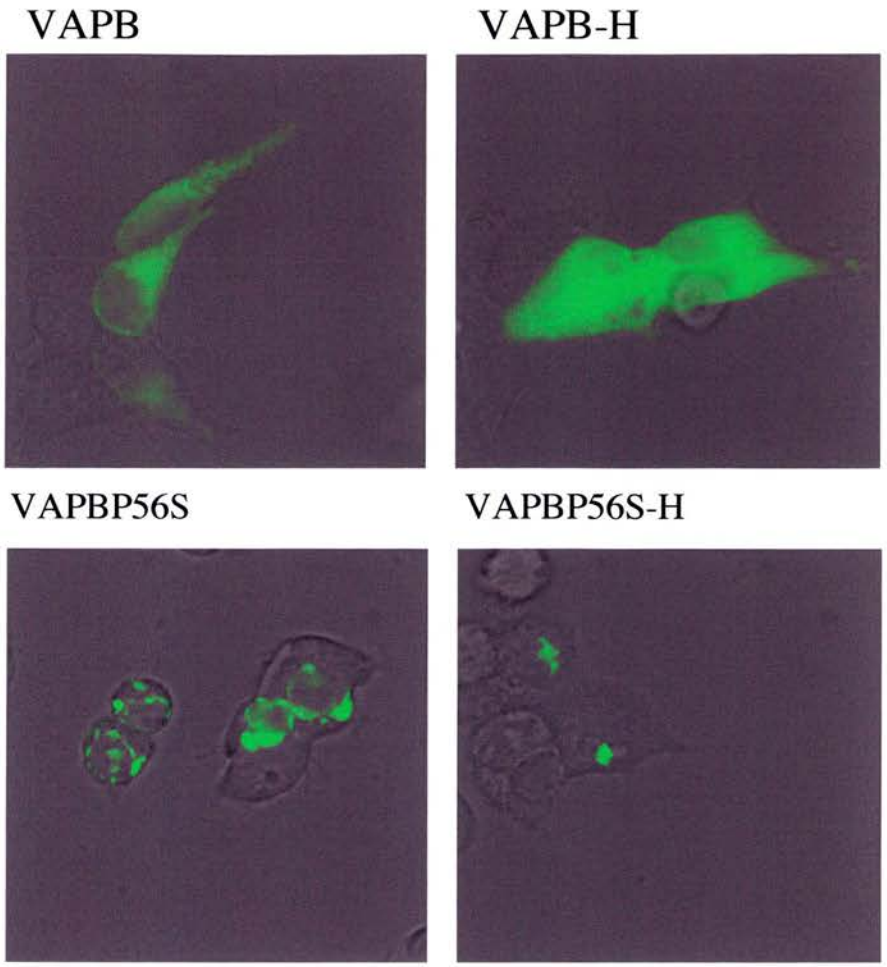

Figure 6.11 VAPB, VAPBP56S, VAPB without Tail and VAPBP56S without Tail were transfected into HEK293 cells. This revealed that the aggregates seen in the VAPBP56S mutant did not depend upon the tail region of the protein (n=3).

This proves that integration into the membrane is not required for aggregation as a Triton X114 extraction of VAPBP56S without the tail shows that it is in the aqueous layer (Figure 6.12).

6.9 Cross-linking experiments show that VAPBP56S forms higher order structures than VAPB

Cross-linking studies reveal the size of multimers formed by a specific protein. VAPB and VAPBP56S were expressed in HEK293 cells, left for 24 hours, treated with disuccinimidyl suberate (DSS) for 10 minutes, the protein was extracted, run on an SDS gel, transferred to a membrane and probed with VAPB antibody. VAPB is predominantly found in lower order bands on the gel with a small amount in higher order bands, whereas, VAPBP56S appears to be pushed towards forming larger order bands with most of the protein expressed in these bands (Figure 6.13). The P56S mutation appears to increase the likelihood of VAPB forming higher order structures, which the wild-type protein can form, but rarely does.

6.10 VAPBP56S aggregates do not appear to include VAPA or VAPB

To determine whether the VAPBP56S multimers included wild type VAPA or VAPB VAPBP56S fused to GFP was expressed in HEK293 cells, they were left for 48 hours and then subjected to paraformaldehyde fixation. The slides were then treated with VAPA antibody. The VAPA antibody staining did not colocalise with the VAPBP56S aggregates.

A

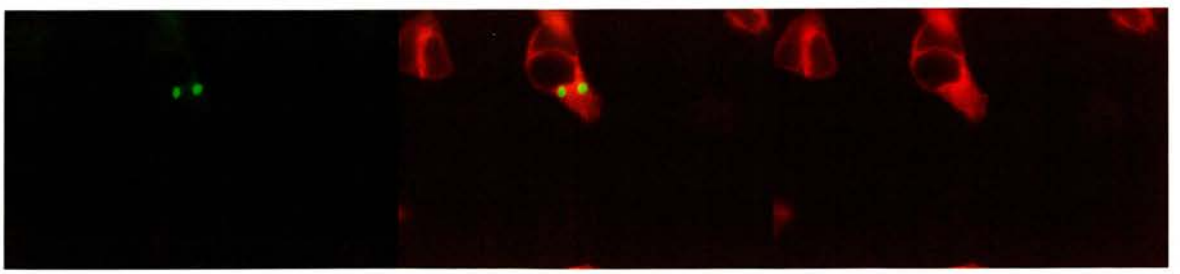

58kDa

B

P1 P2 S2

Figure 6.12 Triton X114 extraction of HEK293 cells, expressing VAPBP56S without Tail-GFP. A. VAPBP56S without Tail-GFP was transiently transfected into HEK cells along with DS.Red-ER and the cells were imaged after 48 hours. The VAPBP56S without Tail-GFP partially co-localises with the DS.Red-ER marker. B. HEK cells were lysed and P1, P2, and S2 layers were prepared. The P2 layer of the HEK cells was detergent extracted using Triton X114. VAPBP56S without Tail-GFP is found in the S2 layer (n=3).

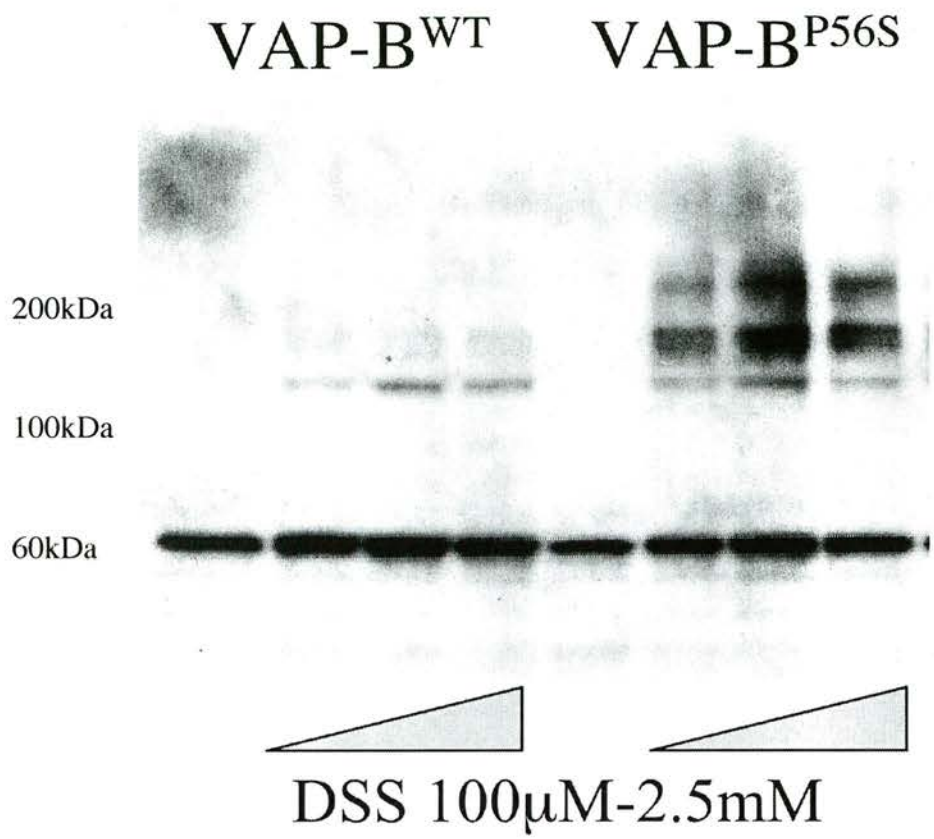

Figure 6.13 (Contributed by Paul Skehel) Cross-linking of VAPB-GFP and VAPBP56S-GFP. Protein extracts were made from HEK293 cells transiently expressing VAPB or VAPBP56S and these samples were cross-linked with increasing concentrations of disuccinimidyl suberate (DSS). VAPBP56S forms higher order multimers than VAPB.

VAPB-DS.Red and VAPBP56S-GFP or VAPB-GFP were expressed HEK293 cells and then imaged. The VAPB-GFP colocalised completely with VAPB-DS.Red but the VAPBP56S-GFP aggregates did not colocalise with the VAPB (Figure 6.14). Therefore VAPBP56S aggregates do not appear to include wild type VAPA or VAPB.

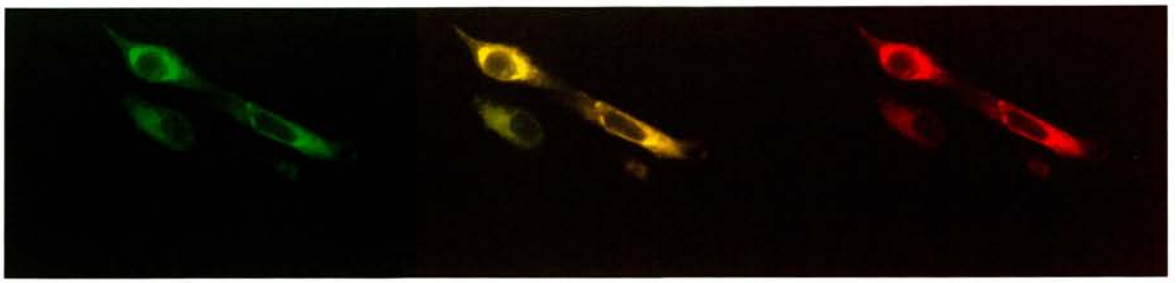

VAPB-GFP Merge DS.Red-VAPB

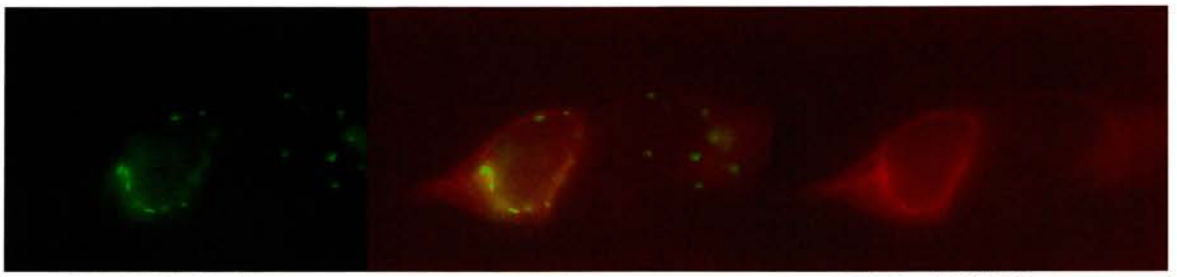

VAPBP56S-GFP Merge DS.Red-VAPB

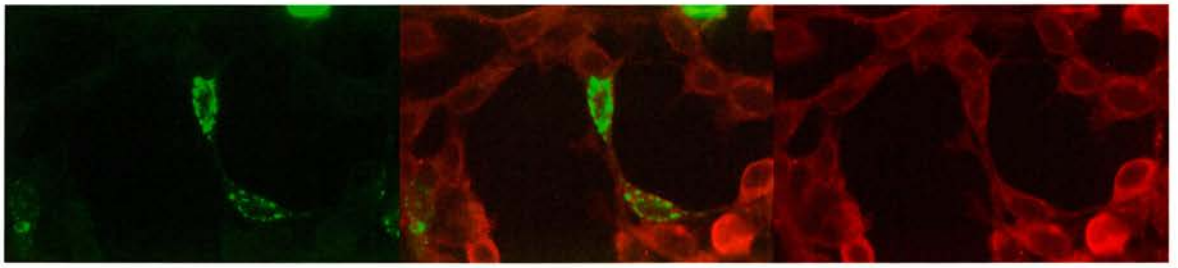

VAPBP56S-GFP Merge VAPA antibody

Figure 6.14 VAPBP56S aggregates do not appear to contain wild-type VAPA or VAPB. VAPB-GFP or VAPBP56S-GFP were co-transfected with DS.Red-VAPB into HEK293 cells. Although both of the wild-type VAPB constructs fully co-localised the aggregates of VAPBP56S did not contain any wild-type VAPB when they were co-expressed. VAPBP56S was also transfected into HEK cells, which were fixed and stained with VAPA antibody. Again the VAPBP56S aggregates did not appear to contain wild-type VAPA (n=6).

6.11 Discussion

The locus 20q13 was recently linked with ALS (Nishimura et al., 2004a) and hereditary and autonomic neuronopathy 1 (Marques et al., 2004). Our colleagues then identified the protein involved, VAPB, which has a proline to serine mutation at position 56 in the affected individuals (Nishimura et al., 2004b).

We introduced this mutation into the VAPB protein and expressed it with a GFP tag in primary cultured hippocampal neurons and HEK293 cells. VAPBP56S forms integral ER membrane aggregates with a different subcellular localisation to endogenous VAPB. These aggregates do not depend upon membrane integration, and crosslinking experiments show that VAPBP56S forms higher order multimers more frequently than endogenous VAPB. Also, these aggregates do not appear to contain wild type VAPA or VAPB. The differences in subcellular localisation of VAPBP56S may therefore be due to a blocked protein interaction rather than increased interactions with wild type VAPA. Proline 56 is not involved in VAPB's interactions with FFAT proteins (Kaiser et al., 2005), however, the changes in tertiary structure induced by this mutation may change the position of crucial residues and therefore the binding site. This may lead to deficits in oxysterol or ceramide binding or synthesis, which could have detrimental effects on motor neurons. As it is the MSP domain that is affected, and this domain can affect components of the ER stress response, it may be that this mutation decreases motor neurons ability to sense ER stress. Previously, there have been reports that motor neurons have reduced ability to sense ER stress and to induce production of heat shock proteins (Batulan et al., 2003). The additional factor of the P56S mutation in VAPB may

decrease the motor neurons ability to sense ER stress to a critical level, thus inducing apoptosis.

The discovery that P56S mutation may cause differences in subcellular localisation of the VAPB, in ER stress responsiveness, and possibly, in protein interactions may, shed some light on the molecular mechanisms involved in ALS.

7. General Discussion

This study has concentrated upon the MSP domain of the VAP family of proteins. This domain appears to have an important function in the VAP proteins as, when it is expressed independently from the rest of the protein, large protein aggregates are formed. Both primary hippocampal cultured neurons and HEK293 cells expressing this construct undergo apoptotic cell death. In many neurodegenerative diseases, such as Alzheimer's, Parkinson's or Huntintons disease, protein aggregates are found in the brains of patients. There is much debate as to whether these protein aggregates are detrimental or beneficial. Some investigators have shown that aggregation or inclusion body formation in Huntington disease reduces neuronal cell death. It has been discovered that the more diffuse forms of the protein Huntingtin are the ones more likely to cause apoptosis (Arrasate et al., 2004). In the stably induced MSP domain cell line large protein aggregates formed within 24 hours but were not present before this time point. However, phosphoPERK induction was evident at 2 hours after induction when there was MSP protein present but no large aggregates had formed. This suggests that the MSP domain was producing toxic effects upon the cell before the large protein aggregates had formed.

ALS patients also have protein aggregates in the spinal cords of patients and our colleagues in Brazil (Nishimura et al., 2004) identified a proline to serine mutation at position 56 of the VAPB protein. When the VAPBP56S protein was expressed in primary hippocampal neurons or HEK293 cells, it was discovered to have an ER localisation like the endogenous VAPB. However, instead of a diffuse reticular pattern of fluorescence,

the P56S mutation gives an aggregated pattern of distribution on the ER membrane. This aggregation is not due to the proteins membrane localisation, as when the tail region is removed the VAPBP56S protein still precociously aggregates. Cross-linking also shows that the P56S mutation causes VAPB to preferentially form higher molecular weight multimers. While endogenous VAPB can form these multimers, the P56S mutation seems to increase the likelihood of aggregation. Perhaps surprisingly the VAPBP56S aggregates do not sequester endogenous VAPA or VAPB.

Computational analysis of the change in residues predicts that the proline to serine mutation will change the tertiary structure of the protein such that a kink in the structure will become straight (Nishimura et al., 2004b). This may affect the VAPB protein's ability to fold correctly. This has been investigated in the SOD1 mutants linked to ALS where a correlation in protein stability and survival time for the patient carrying the mutations was observed. Thus far, the mutations studied, which are linked to ALS, have been identified as being gain of function mutations. Neither the SOD1 (Reaume et al., 1996) nor the Alsin (Cai et al., 2005) knockout mice have shown an ALS phenotype. It is thought, therefore, that these proteins have a toxic gain of function, possibly via inappropriate protein interactions.

In a yeast two hybrid protein interaction screen the MSP domain of VAPA was found to interact with OSBP and ORP9, proteins involved in lipid synthesis, as previously determined in other studies (Wyles et al., 2004). Also found in the screen was a member of the conserved oligomeric Golgi complex (COG7), which has been implicated in Golgi

and COPI transport (Oka et al., 2004). These proteins all share a FFAT domain, which is predicted to interact with lysine-46, threonine-48, lysine-86 and lysine-119 of VAPA (Loewen et al., 2005).

Although proline 56 is not involved in VAPB's interactions with FFAT proteins (Kaiser et al., 2005) the P56S mutation may decrease the VAPB protein's ability to interact with other proteins, thus leading to motor neuron vulnerability with the onset of age. It is known that in some ALS patients, and in Cu/Zn SOD mutant mice, increased oxidative stress was discovered in conjunction with accumulation of sphingomyelin, ceramides and cholesterol esters (Cutler et al., 2002). LXRβ receptor knockout male mice also show selective vulnerability of large motor neurons (Andersson et al., 2005). Therefore, it may be that the interaction of VAPB with the oxysterol binding proteins and CERT is disrupted in some way, leading to motor neuron death.

Autosomal recessive ALS has been linked to mutations in the Alsin gene. When the truncated form of Alsin was expressed in monkey Cos-7 cells it resulted in enlargement and accumulation of early endosomes, impairment of mitochondria trafficking and fragmentation of the Golgi apparatus. As such, it is postulated that the Alsin protein is involved in trafficking in neurons (Hadano et al., 2001). Rat VAPB antibodies were found to inhibit retrograde intra Golgi transport and to result in the accumulation of COPI vesicles (Soussan et al., 1999). COG7 is also involved in COPI transport (Oka et al., 2004). Therefore, it is plausible that the mutation in VAPB also disrupts retrograde Golgi trafficking in motor neurons.

ATF6 was also identified as a possible binding partner for the MSP domain of VAP proteins in the yeast two-hybrid screen. The yeast protein Scs2p, a homologue of mammalian VAPA, has previously been identified as being involved in the yeast ER stress response and in inositol auxotrophy (Kagiwada et al., 1998, Loewen et al., 2004) via interactions with Opi1p, an inositol transcription factor (Loewen et al., 2003). ATF6 is a bZIP protein, which is expressed as a type II membrane protein in the ER and is activated by proteolysis in the mammalian ER stress response. When the MSP domain of VAPA is expressed alone as a GFP fusion protein in HEK293 cells or primary hippocampal cultured neurons, it forms large protein aggregates and these cells undergo apoptotic cell death. When the apoptotic process was investigated in more detail it was discovered that there was an increase in BiP mRNA in these cells as compared to controls, there was an increase in PERK phosphorylation and caspase 3 production was increased. These responses are all indicators of an increase in the ER stress response in these cells, as compared with controls, and that this response triggers apoptotic cell death. Full length VAPA also gave an increase in BiP mRNA production and it is postulated that the mammalian VAP proteins are also involved in the ER stress response and that this may be via the MSP domain interacting with ATF6.

Previously, there have been reports that motor neurons have reduced ability to sense ER stress and to induce production of heat shock proteins (Batulan et al., 2003). The SOD1 mutations linked to ALS have been studied the most extensively and motor neuron death has been linked to the ER stress response in SOD1 mutant mice (Tobisawa et al., 2003,

Wootz et al., 2004). VAP proteins may perform a chaperoning function for specific proteins so that they do not inappropriately interact. Therefore, the P56S mutation in the VAPB protein may disrupt its ability to sense ER stress or its chaperoning ability, thus leading to motor neuron cell death.

During our investigation of the differences between VAPA and VAPB we discovered that, while VAPA behaves as an integral ER membrane protein and is in the detergent phase of Triton X114. VAPB is in lighter membrane fractions and is in the aqueous phase of Triton X114. This difference in ER membrane localization and interaction appears to be in part mediated by the different tails of the proteins. However, when VAPBP56S protein was studied it was found to behave as an integral ER membrane protein and partially detergent extracts in Triton X114 in a similar manner to VAPA. It may be a joint interaction between the tail and MSP domains that is responsible for VAPB's unusual localization. This difference in VAPBP56S localization may contribute to motor neuron degeneration.

There are a range of clinical phenotypes associated with VAPBP56S induced ALS. These include atypical ALS8 where the patients have late-onset motor neuron death; fasiculations and disease progression is 10-20 years. Some patients have late onset spinal muscular atrophy with slowly progressing late on-set degeneration of cells in the anterior horn. The final set of patients display, typical ALS and have a life expectancy of 2-3 years. The reason for this wide range of phenotypes is not yet clear. However a number of modifying factors for ALS disease progression have been found. These include

CNTF, which is a spinal motor neuron survival factor (Ono et al, 1999), APEX, a DNA repair factor (Kisby et al., 1997), and 2 peripherin, an intermediate filament in neurons (Gros-Louis et al., 2004).

The GFP induced cisternae formation seen with the VAP proteins may be physiologically relevant as they are similar to those seen in early onset torsion dystonia (Hewett et al., 2000) and at the axonal-myelin sheath interface in spinal motor neurons (Li et al., 2005). VAPA is also induced to form these cisternae when ORP-9 is overexpressed (Wyles et al., 2004). These structures may be linked to new membrane formation as seen with the yeast VAP homologue, SCS2, and the INO1 pathway in yeast (Loewen et al., 2004). However, some investigators postulate that these structures are purely artifactual (Snapp et al., 2003).

The discovery that the splice variant of VAPB, VAPC, may exist in mice as well as in humans may be significant. VAPC has no hydrophobic membrane-spanning domain, therefore, it is unlikely to share the ER localisation of VAPA and VAPB. It does contain proline 56 and an MSP domain and may form toxic protein aggregates. Further study of this member of the VAP family is essential to elucidating the role of these proteins in ALS.

This study has used a variety of approaches to determine VAP protein function. The yeast-two hybrid assay with the MSP domain of VAPA has revealed many potentially positive interactions, which remain to be validated by co-immunoprecipitation or pull-

down assay. Studies to determine whether the VAPB MSP domain shares the same protein interactions, which is highly likely as the MSP domain is highly conserved, and whether the P56S mutation affects the protein interactions would also be illuminating. The increase in phospho-PERK induction and caspase 3 activation due to the expression of the VAPA MSP domain, is interesting as this may mean that the VAP proteins may be effectors of the ER stress response under physiological or pathological conditions. However, further studies will have to be carried out to determine whether this effect is purely artifactual and whether it has any relevance in the pathology of ALS8. The discovery that ALS8 is linked to the P56S mutation in VAPB has led to a new avenue of research into the function of the VAP proteins. Our studies have concentrated on the localization of the VAPB and VAPBP56S proteins thus far. Future research will probably focus on the generation of mice expressing the VAPBP56S protein and this should yield many interesting results.

In summary it has been discovered that the MSP domain of the VAP proteins is involved in many potentially interesting interactions including those linked to lipid synthesis, COPI transport and the ER stress response. This domain when expressed alone gives large protein aggregates and initiates increased BiP mRNA production, PERK phosphorylation and caspase 3 production. This leads us to postulate that the VAP proteins are involved in the mammalian ER stress response possibly via interactions of their MSP domains with ATF6. The P56S mutation of VAPB linked to ALS causes aggregation and mislocalisation of the protein. This may lead to decreased ability to interact with other proteins and motor neuron vulnerability.

8. References

Amarilio R, Ramachandran S, Sabanay H, Lev S (2005) Differential regulation of endoplasmic reticulum structure through VAP-Nir protein interaction. J Biol Chem 280:5934-5944.

Andersson S, Gustafsson N, Warner M, Gustafsson JA (2005) Inactivation of liver X receptor beta leads to adult-onset motor neuron degeneration in male mice. Proc Natl Acad Sci U S A 102:3857-3862.

Arrasate M, Mitra S, Schweitzer ES, Segal MR, Finkbeiner S (2004) Inclusion body formation reduces levels of mutant huntingtin and the risk of neuronal death. Nature 431:805-810.

Baker AM, Roberts TM, Stewart M (2002) 2.6 A resolution crystal structure of helices of the motile major sperm protein (MSP) of Caenorhabditis elegans. J Mol Biol 319:491-499.

Barlowe C, Orci L, Yeung T, Hosobuchi M, Hamamoto S, Salama N, Rexach MF, Ravazzola M, Amherdt M, Schekman R (1994) COPII: a membrane coat formed by Sec proteins that drive vesicle budding from the endoplasmic reticulum. Cell 77:895-907.

Batulan Z, Shinder GA, Minotti S, He BP, Doroudchi MM, Nalbantoglu J, Strong MJ, Durham HD (2003) High threshold for induction of the stress response in motor neurons is associated with failure to activate HSF1. J Neurosci 23:5789-5798.

Becker T, Volchuk A, Rothman JE (2005) Differential use of endoplasmic reticulum membrane for phagocytosis in J774 macrophages. Proc Natl Acad Sci U S A 102:4022-4026.

Bordier C (1981) Phase separation of integral membrane proteins in Triton X-114 solution. J Biol Chem 256:1604-1607.

Bragg DC, Kaufman CA, Kock N, Breakefield XO (2004) Inhibition of N-linked glycosylation prevents inclusion formation by the dystonia-related mutant form of torsinA. Mol Cell Neurosci 27:417-426.

Brickner JH, Walter P (2004) Gene recruitment of the activated INO1 locus to the nuclear membrane. PLoS Biol 2:e342.

Broadwell RD, Cataldo AM (1983) The neuronal endoplasmic reticulum: its cytochemistry and contribution to the endomembrane system. I. Cell bodies and dendrites. J Histochem Cytochem 31:1077-1088.

Brooks BR (1994) El Escorial World Federation of Neurology criteria for the diagnosis of amyotrophic lateral sclerosis. Subcommittee on Motor Neuron Diseases/Amyotrophic Lateral Sclerosis of the World Federation of Neurology Research Group on Neuromuscular Diseases and the El Escorial "Clinical limits of amyotrophic lateral sclerosis" workshop contributors. J Neurol Sci 124 Suppl:96-107.

Burri L, Varlamov O, Doege CA, Hofmann K, Beilharz T, Rothman JE, Sollner TH, Lithgow T (2003) A SNARE required for retrograde transport to the endoplasmic reticulum. Proc Natl Acad Sci U S A 100:9873-9877.

Buttery SM, Ekman GC, Seavy M, Stewart M, Roberts TM (2003) Dissection of the Ascaris sperm motility machinery identifies key proteins involved in major sperm protein-based amoeboid locomotion. Mol Biol Cell 14:5082-5088.

Cai H, Lin X, Laird FM, Lai C, Wen H, Chiang HC, Shim H, Farah MH, Hoke A, Price DL, Wong PC (2005) Loss of ALS2 function is insufficient to trigger motor neuron degeneration in knockout mice but predisposes neurons to oxidative stress. Neurosci 25:7567-7574.

Chen YZ, Bennett CL, Huynh HM, Blair IP, Puls I, Irobi J, Dierick I, Abel A, Kennerson ML, Rabin BA, Nicholson GA, Auer-Grumbach M, Wagner K, De Jonghe P, Griffin JW, Fischbeck KH, Timmerman V, Cornblath DR, Chance PF (2004) DNA/RNA helicase gene mutations in a form of juvenile amyotrophic lateral sclerosis (ALS4). Am J Hum Genet 74:1128-1135.

Chevet E, Cameron PH, Pelletier MF, Thomas DY, Bergeron JJ (2001) The endoplasmic reticulum: integration of protein folding, quality control, signaling and degradation. Curr Opin Struct Biol 11:120-124.

Choo QL, Richman KH, Han JH, Berger K, Lee C, Dong C, Gallegos C, Coit D, Medina-Selby R, Barr PJ, et al. (1991) Genetic organization and diversity of the hepatitis C virus. Proc Natl Acad Sci U S A 88:2451-2455.

Chung YL, Sheu ML, Yen SH (2003) Hepatitis C virus NS5A as a potential viral Bcl-2 homologue interacts with Bax and inhibits apoptosis in hepatocellular carcinoma. Int J Cancer 107:65-73.

Cote F, Collard JF, Julien JP (1993) Progressive neuronopathy in transgenic mice expressing the human neurofilament heavy gene: a mouse model of amyotrophic lateral sclerosis. Cell 73:35-46.

Csordas G, Madesh M, Antonsson B, Hajnoczky G (2002) tcBid promotes Ca(2+) signal propagation to the mitochondria: control of Ca(2+) permeation through the outer mitochondrial membrane. Embo J 21:2198-2206.

Cudkowicz ME, McKenna-Yasek D, Sapp PE, Chin W, Geller B, Hayden DL, Schoenfeld DA, Hosler BA, Horvitz HR, Brown RH (1997) Epidemiology of mutations in superoxide dismutase in amyotrophic lateral sclerosis. Ann Neurol 41:210-221.

Cutler RG, Pedersen WA, Camandola S, Rothstein JD, Mattson MP (2002) Evidence that accumulation of ceramides and cholesterol esters mediates oxidative stress-induced death of motor neurons in amyotrophic lateral sclerosis. Ann Neurol 52:448-457.

Davy BE, Robinson ML (2003) Congenital hydrocephalus in hy3 mice is caused by a frameshift mutation in Hydin, a large novel gene. Hum Mol Genet 12:1163-1170.

Dawson PA, Ridgway ND, Slaughter CA, Brown MS, Goldstein JL (1989) cDNA cloning and expression of oxysterol-binding protein, an oligomer with a potential leucine zipper. J Biol Chem 264:16798-16803.

Delepine M, Nicolino M, Barrett T, Golamaully M, Lathrop GM, Julier C (2000) EIF2AK3, encoding translation initiation factor 2-alpha kinase 3, is mutated in patients with Wolcott-Rallison syndrome. Nat Genet 25:406-409.

Demaurex N, Distelhorst C (2003) Cell biology. Apoptosis - the calcium connection. Science 300: 65-67

Desagher S, Martinou JC (2000) Mitochondria as the central control point of apoptosis. Trends Cell Biol 10:369-377.

Distel B, Erdmann R, Gould SJ, Blobel G, Crane DI, Cregg JM, Dodt G, Fujiki Y, Goodman JM, Just WW, Kiel JA, Kunau WH, Lazarow PB, Mannaerts GP, Moser HW, Osumi T, Rachubinski RA, Roscher A, Subramani S, Tabak HF, Tsukamoto T, Valle D, van der Klei I, van Veldhoven PP, Veenhuis M (1996) A unified nomenclature for peroxisome biogenesis factors. J Cell Biol 135:1-3.

Dreier L, Rapoport TA (2000) In vitro formation of the endoplasmic reticulum occurs independently of microtubules by a controlled fusion reaction. J Cell Biol 148:883-898.

Du C, Fang M, Li Y, Li L, Wang X (2000) Smac, a mitochondrial protein that promotes cytochrome c-dependent caspase activation by eliminating IAP inhibition. Cell 102:33-42.

Erin N, Bronson SK, Billingsley ML (2003) Calcium-dependent interaction of calcineurin with Bcl-2 in neuronal tissue. Neuroscience 117:541-555.

Esclaire F, Kisby G, Spencer P, Milne J, Lesort M, Hugon J (1999) The Guam cycad toxin methylazoxymethanol damages neuronal DNA and modulates tau mRNA expression and excitotoxicity. Exp Neurol 155:11-21.

Evans MJ, Rice CM, Goff SP (2004) Phosphorylation of hepatitis C virus nonstructural protein 5A modulates its protein interactions and viral RNA replication. Proc Natl Acad Sci U S A 101:13038-13043.

Filippin L, Magalhaes PJ, Di Benedetto G, Colella M, Pozzan T (2003) Stable interactions between mitochondria and endoplasmic reticulum allow rapid accumulation of calcium in a subpopulation of mitochondria. J Biol Chem 278:39224-39234.

Foster LJ, Weir ML, Lim DY, Liu Z, Trimble WS, Klip A (2000) A functional role for VAP-33 in insulin-stimulated GLUT4 traffic. Traffic 1:512-521.

Gale MJ, Jr., Korth MJ, Tang NM, Tan SL, Hopkins DA, Dever TE, Polyak SJ, Gretch DR, Katze MG (1997) Evidence that hepatitis C virus resistance to interferon is mediated through repression of the PKR protein kinase by the nonstructural 5A protein. Virology 230:217-227.

Galteau MM, Antoine B, Reggio H (1985) Epoxide hydrolase is a marker for the smooth endoplasmic reticulum in rat liver. Embo J 4:2793-2800.

Gao L, Aizaki H, He JW, Lai MM (2004) Interactions between viral nonstructural proteins and host protein hVAP-33 mediate the formation of hepatitis C virus RNA replication complex on lipid raft. J Virol 78:3480-3488.

Geuze HJ, Murk JL, Stroobants AK, Griffith JM, Kleijmeer MJ, Koster AJ, Verkleij AJ, Distel B, Tabak HF (2003) Involvement of the endoplasmic reticulum in peroxisome formation. Mol Biol Cell 14:2900-2907.

Ghribi O, Herman MM, DeWitt DA, Forbes MS, Savory J (2001) Abeta(1-42) and aluminum induce stress in the endoplasmic reticulum in rabbit hippocampus, involving nuclear translocation of gadd 153 and NF-kappaB. Brain Res Mol Brain Res 96:30-38.

Gong G, Waris G, Tanveer R, Siddiqui A (2001) Human hepatitis C virus NS5A protein alters intracellular calcium levels, induces oxidative stress, and activates STAT-3 and NF-kappa B. Proc Natl Acad Sci U S A 98:9599-9604.

Gotz J, Chen F, van Dorpe J, Nitsch RM (2001) Formation of neurofibrillary tangles in P301l tau transgenic mice induced by Abeta 42 fibrils. Science 293:1491-1495.

Griffiths G, Simons K (1986) The trans Golgi network: sorting at the exit site of the Golgi complex. Science 234:438-443.

Gros-Louis F, Lariviere R, Gowing G, Laurent S, Camu W, Bouchard JP, Meininger V, Rouleau GA, Julien JP (2004) A frameshift deletion in peripherin gene associated with amyotrophic lateral sclerosis. J Biol Chem 279:45951-45956.

Gruenberg J, Maxfield FR (1995) Membrane transport in the endocytic pathway. Curr Opin Cell Biol 7:552-563.

Gubbay SS, Kahana E, Zilber N, Cooper G, Pintov S, Leibowitz Y (1985) Amyotrophic lateral sclerosis. A study of its presentation and prognosis. J Neurol 232:295-300.

Guo W, Novick P (2004) The exocyst meets the translocon: a regulatory circuit for secretion and protein synthesis? Trends Cell Biol 14:61-63.

Hadano S, Hand CK, Osuga H, Yanagisawa Y, Otomo A, Devon RS, Miyamoto N, Showguchi-Miyata J, Okada Y, Singaraja R, Figlewicz DA, Kwiatkowski T, Hosler BA, Sagie T, Skaug J, Nasir J, Brown RH, Jr., Scherer SW, Rouleau GA, Hayden MR, Ikeda JE (2001) A gene encoding a putative GTPase regulator is mutated in familial amyotrophic lateral sclerosis 2. Nat Genet 29:166-173.

Haj FG, Verveer PJ, Squire A, Neel BG, Bastiaens PI (2002) Imaging sites of receptor dephosphorylation by PTP1B on the surface of the endoplasmic reticulum. Science 295:1708-1711.

Hanada K, Kumagai K, Yasuda S, Miura Y, Kawano M, Fukasawa M, Nishijima M (2003) Molecular machinery for non-vesicular trafficking of ceramide. Nature 426:803-809.

Harding HP, Zeng H, Zhang Y, Jungries R, Chung P, Plesken H, Sabatini DD, Ron D (2001) Diabetes mellitus and exocrine pancreatic dysfunction in perk-/- mice reveals a role for translational control in secretory cell survival. Mol Cell 7:1153-1163.

Hewett J, Gonzalez-Agosti C, Slater D, Ziefer P, Li S, Bergeron D, Jacoby DJ, Ozelius LJ, Ramesh V, Breakefield XO (2000) Mutant torsinA, responsible for early-onset torsion dystonia, forms membrane inclusions in cultured neural cells. Hum Mol Genet 9:1403-1413.

Hirschberg CB, Snider MD (1987) Topography of glycosylation in the rough endoplasmic reticulum and Golgi apparatus. Annu Rev Biochem 56:63-87.

Holthuis JC, Levine TP (2005) Lipid traffic: floppy drives and a superhighway. Nat Rev Mol Cell Biol 6:209-220.

Humeau Y, Doussau F, Grant NJ, Poulain B (2000) How botulinum and tetanus neurotoxins block neurotransmitter release. Biochimie 82:427-446.

Italiano JE, Jr., Roberts TM, Stewart M, Fontana CA (1996) Reconstitution in vitro of the motile apparatus from the amoeboid sperm of Ascaris shows that filament assembly and bundling move membranes. Cell 84:105-114.

Jamsa E, Simonen M, Makarow M (1994) Selective retention of secretory proteins in the yeast endoplasmic reticulum by treatment of cells with a reducing agent. Yeast 10:355-370.

Jiang A, Clark EA (2001) Involvement of Bik, a proapoptotic member of the Bcl-2 family, in surface IgM-mediated B cell apoptosis. J Immunol 166:6025-6033.

Kagiwada S, Hosaka K, Murata M, Nikawa J, Takatsuki A (1998) The Saccharomyces cerevisiae SCS2 gene product, a homolog of a synaptobrevin-associated protein, is an integral membrane protein of the endoplasmic reticulum and is required for inositol metabolism. J Bacteriol 180:1700-1708.

Kainu T, Enmark E, Gustafsson JA, Pelto-Huikko MP (1996) Localization of the Rev-ErbA orphan receptors in the brain. Brain Res 743:315-319.

Kaiser SE, Brickner JH, Reilein AR, Fenn TD, Walter P, Brunger AT (2005) Structural basis of FFAT motif-mediated ER targeting. Structure (Camb) 13:1035-1045.

Kano F, Kondo H, Yamamoto A, Tanaka AR, Hosokawa N, Nagata K, Murata M (2005) The maintenance of the endoplasmic reticulum network is regulated by p47, a cofactor of p97, through phosphorylation by cdc2 kinase. Genes Cells 10:333-344.

Katayama T, Imaizumi K, Sato N, Miyoshi K, Kudo T, Hitomi J, Morihara T, Yoneda T, Gomi F, Mori Y, Nakano Y, Takeda J, Tsuda T, Itoyama Y, Murayama O, Takashima A, St George-Hyslop P, Takeda M, Tohyama M (1999) Presenilin-1 mutations downregulate the signalling pathway of the unfolded-protein response. Nat Cell Biol 1:479-485.

Kato N, Lan KH, Ono-Nita SK, Shiratori Y, Omata M (1997) Hepatitis C virus nonstructural region 5A protein is a potent transcriptional activator. J Virol 71:8856-8859.

Kaufman RJ (2002) Orchestrating the unfolded protein response in health and disease. J Clin Invest 110:1389-1398.

Kimata Y, Kimata YI, Shimizu Y, Abe H, Farcasanu IC, Takeuchi M, Rose MD, Kohno K (2003) Genetic evidence for a role of BiP/Kar2 that regulates Ire1 in response to accumulation of unfolded proteins. Mol Biol Cell 14:2559-2569.

King PA, Horton ED, Hirshman MF, Horton ES (1992) Insulin resistance in obese Zucker rat (fa/fa) skeletal muscle is associated with a failure of glucose transporter translocation. J Clin Invest 90:1568-1575.

Kisby GE, Milne J, Sweatt C (1997) Evidence of reduced DNA repair in amyotrophic lateral sclerosis brain tissue. Neuroreport 8:1337-1340.

Klip A, Ramlal T, Bilan PJ, Cartee GD, Gulve EA, Holloszy JO (1990) Recruitment of GLUT-4 glucose transporters by insulin in diabetic rat skeletal muscle. Biochem Biophys Res Commun 172:728-736.

Kosinski M, McDonald K, Schwartz J, Yamamoto I, Greenstein D (2005) C. elegans sperm bud vesicles to deliver a meiotic maturation signal to distant oocytes. Development.

Kostova Z, Wolf DH (2003) For whom the bell tolls: protein quality control of the endoplasmic reticulum and the ubiquitin-proteasome connection. Embo J 22:2309-2317.

Kovacs WJ, Olivier LM, Krisans SK (2002) Central role of peroxisomes in isoprenoid biosynthesis. Prog Lipid Res 41:369-391.

Kreibich G, Freienstein CM, Pereyra BN, Ulrich BL, Sabatini DD (1978a) Proteins of rough microsomal membranes related to ribosome binding. II. Cross-linking of bound ribosomes to specific membrane proteins exposed at the binding sites. J Cell Biol 77:488-506.

Kreibich G, Czako-Graham M, Grebenau R, Mok W, Rodriguez-Boulan E, Sabatini DD (1978b) Characterization of the ribosomal binding site in rat liver rough microsomes: ribophorins I and II, two integral membrane proteins related to ribosome binding. J Supramol Struct 8:279-302.

Kruman, II, Pedersen WA, Springer JE, Mattson MP (1999) ALS-linked Cu/Zn-SOD mutation increases vulnerability of motor neurons to excitotoxicity by a mechanism involving increased oxidative stress and perturbed calcium homeostasis. Exp Neurol 160:28-39.

Kuge O, Dascher C, Orci L, Rowe T, Amherdt M, Plutner H, Ravazzola M, Tanigawa G, Rothman JE, Balch WE (1994) Sar1 promotes vesicle budding from the endoplasmic reticulum but not Golgi compartments. J Cell Biol 125:51-65.

Kunst CB, Mezey E, Brownstein MJ, Patterson D (1997) Mutations in SOD1 associated with amyotrophic lateral sclerosis cause novel protein interactions. Nat Genet 15:91-94.

Ladinsky MS, Mastronarde DN, McIntosh JR, Howell KE, Staehelin LA (1999) Golgi structure in three dimensions: functional insights from the normal rat kidney cell. J Cell Biol 144:1135-1149.

Lafont F, Verkade P, Galli T, Wimmer C, Louvard D, Simons K (1999) Raft association of SNAP receptors acting in apical trafficking in Madin-Darby canine kidney cells. Proc Natl Acad Sci U S A 96:3734-3738.

Lapierre LA, Tuma PL, Navarre J, Goldenring JR, Anderson JM (1999) VAP-33 localizes to both an intracellular vesicle population and with occludin at the tight junction. J Cell Sci 112 (Pt 21):3723-3732.

LeClaire LL, 3rd, Stewart M, Roberts TM (2003) A 48 kDa integral membrane phosphoprotein orchestrates the cytoskeletal dynamics that generate amoeboid cell motility in Ascaris sperm. J Cell Sci 116:2655-2663.

Levine T, Rabouille C (2005) Endoplasmic reticulum: one continuous network compartmentalized by extrinsic cues. Curr Opin Cell Biol 17:362-368.

Li Y, Prinz WA (2004) ATP-binding cassette (ABC) transporters mediate nonvesicular, raft-modulated sterol movement from the plasma membrane to the endoplasmic reticulum. J Biol Chem 279:45226-45234.

Li YC, Li YN, cheng CX, Sakamoto H, Kawate T, Shimada O, Atsumi S (2005) Subsurface cisterna-lined axonal invaginations and double-walled vesicles at the axonal-myelin sheath interface Neurosci Res 53:298-303.

Lindberg M, Bystrom R, Boknas N. Andersen PM, Oliveberg M (2005) Systematically perturbed folding patterns of amyotrophic lateral sclerosis (ALS)-associated SOD1 mutants. Proc Natl Acad Sci USA 102:9754-9759.

Liu X, Kim CN, Yang J, Jemmerson R, Wang X (1996) Induction of apoptotic program in cell-free extracts: requirement for dATP and cytochrome c. Cell 86:147-157.

Loewen CJ, Levine TP (2005) A highly conserved binding site in vesicle-associated membrane protein-associated protein (VAP) for the FFAT motif of lipid-binding proteins. J Biol Chem 280:14097-14104.

Loewen CJ, Roy A, Levine TP (2003) A conserved ER targeting motif in three families of lipid binding proteins and in Opi1p binds VAP. Embo J 22:2025-2035.

Loewen CJ, Gaspar ML, Jesch SA, Delon C, Ktistakis NT, Henry SA, Levine TP (2004) Phospholipid metabolism regulated by a transcription factor sensing phosphatidic acid. Science 304:1644-1647.

Lohmann V, Koch JO, Bartenschlager R (1996) Processing pathways of the hepatitis C virus proteins. J Hepatol 24:11-19.

Loo DT, Rillema JR (1998) Measurement of cell death. Methods Cell Biol 57:251-264.

Lund EG, Guileyardo JM, Russell DW (1999) cDNA cloning of cholesterol 24-hydroxylase, a mediator of cholesterol homeostasis in the brain. Proc Natl Acad Sci U S A 96:7238-7243.

Marques W, Jr., Davis MB, Abou-Sleiman PM, Marques VD, Silva Jr WA, Zago MA, Sobreira CS, Barreira AA (2004) Hereditary motor and autonomic neuronopathy 1 maps to chromosome 20q13.2-13.3. Braz J Med Biol Res 37:1757-1762.

Martinez-Arca S, Alberts P, Zahraoui A, Louvard D, Galli T (2000) Role of tetanus neurotoxin insensitive vesicle-associated membrane protein (TI-VAMP) in vesicular transport mediating neurite outgrowth. J Cell Biol 149:889-900.

Masu Y, Wolf E, Holtmann B, Sendtner M, Brem G, Thoenen H (1993) Disruption of the CNTF gene results in motor neuron degeneration. Nature 365:27-32.

Meriin AB, Zhang X, He X, Newnam GP, Chernoff YO, Sherman MY (2002) Huntington toxicity in yeast model depends on polyglutamine aggregation mediated by a prion-like protein Rnq1. J Cell Biol 157:997-1004.

Millecamps S, Gentil BJ, Gros-Louis F, Rouleau G, Julien JP (2005) Alsin is partially associated with centrosome in human cells. Biochim Biophys Acta 1745:84-100.

Miller MA, Ruest PJ, Kosinski M, Hanks SK, Greenstein D (2003) An Eph receptor sperm-sensing control mechanism for oocyte meiotic maturation in Caenorhabditis elegans. Genes Dev 17:187-200.

Miller MA, Nguyen VQ, Lee MH, Kosinski M, Schedl T, Caprioli RM, Greenstein D (2001) A sperm cytoskeletal protein that signals oocyte meiotic maturation and ovulation. Science 291:2144-2147.

Miyazaki E, Kida Y, Mihara K, Sakaguchi M (2005) Switching the sorting mode of membrane proteins from cotranslational endoplasmic reticulum targeting to posttranslational mitochondrial import. Mol Biol Cell 16:1788-1799.

Moser AB, Rasmussen M, Naidu S, Watkins PA, McGuinness M, Hajra AK, Chen G, Raymond G, Liu A, Gordon D, et al. (1995) Phenotype of patients with peroxisomal disorders subdivided into sixteen complementation groups. J Pediatr 127:13-22.

Mund T, Gewies A, Schoenfeld N, Bauer MK, Grimm S (2003) Spike, a novel BH3-only protein, regulates apoptosis at the endoplasmic reticulum. Faseb J 17:696-698.

Neutra M, Leblond CP (1966) Radioautographic comparison of the uptake of galactose-H and glucose-H3 in the golgi region of various cells secreting glycoproteins or mucopolysaccharides. J Cell Biol 30:137-150.

Ng FW, Nguyen M, Kwan T, Branton PE, Nicholson DW, Cromlish JA, Shore GC (1997) p28 Bap31, a Bcl-2/Bcl-XL- and procaspase-8-associated protein in the endoplasmic reticulum. J Cell Biol 139:327-338.

Nishimura AL, Mitne-Neto M, Silva HC, Oliveira JR, Vainzof M, Zatz M (2004a) A novel locus for late onset amyotrophic lateral sclerosis/motor neurone disease variant at 20q13. J Med Genet 41:315-320.

Nishimura AL, Mitne-Neto M, Silva HC, Richieri-Costa A, Middleton S, Cascio D, Kok F, Oliveira JR, Gillingwater T, Webb J, Skehel P, Zatz M (2004b) A mutation in the vesicle-trafficking protein VAPB causes late-onset spinal muscular atrophy and amyotrophic lateral sclerosis. Am J Hum Genet 75:822-831.

Nishimura Y, Hayashi M, Inada H, Tanaka T (1999) Molecular cloning and characterization of mammalian homologues of vesicle-associated membrane protein-associated (VAMP-associated) proteins. Biochem Biophys Res Commun 254:21-26.

Oka T, Ungar D, Hughson FM, Krieger M (2004) The COG and COPI complexes interact to control the abundance of GEARs, a subset of Golgi integral membrane proteins. Mol Biol Cell 15:2423-2435.

Oka T, Vasile E, Penman M, Novina CD, Dykxhoorn DM, Ungar D, Hughson FM, Krieger M (2005) Genetic analysis of the subunit organization and function of the conserved oligomeric golgi (COG) complex: studies of COG5- and COG7-deficient mammalian cells. J Biol Chem 280:32736-32745.

Okada T, Yoshida H, Akazawa R, Negishi M, Mori K (2002) Distinct roles of activating transcription factor 6 (ATF6) and double-stranded RNA-activated protein kinase-like endoplasmic reticulum kinase (PERK) in transcription during the mammalian unfolded protein response. Biochem J 366:585-594.

Ono S, Imai T, Igarashi A, Shimizu N, Nakagawa H, Hu J (1999) Decrease in the ciliary neurotrophic factor of the spinal cord in amyotrophic lateral sclerosis. Eur Neurol 42:163-168.

Ozcan U, Cao Q, Yilmaz E, Lee AH, Iwakoshi NN, Ozdelen E, Tuncman G, Gorgun C, Glimcher LH, Hotamisligil GS (2004) Endoplasmic reticulum stress links obesity, insulin action, and type 2 diabetes. Science 306:457-461.

Pahl HL, Baeuerle PA (1995) A novel signal transduction pathway from the endoplasmic reticulum to the nucleus is mediated by transcription factor NF-kappa B. Embo J 14:2580-2588.

Palade G (1975) Intracellular aspects of the process of protein synthesis. Science 189:347-358.

Pall GS, Wallis J, Axton R, Brownstein DG, Gautier P, Buerger K, Mulford C, Mullins JJ, Forrester LM (2004) A novel transmembrane MSP-containing protein that plays a role in right ventricle development. Genomics 84:1051-1059.

Partarnello T, Bargelloni L, Rossetto O, Schiavo G, Montecucco C (1993) Neurotransmission and secretion. Nature 364:581-582.

Pasinelli P, Belford ME, Lennon N, Bacskai BJ, Hyman BT, Trotti D, Brown RH, Jr. (2004) Amyotrophic lateral sclerosis-associated SOD1 mutant proteins bind and aggregate with Bcl-2 in spinal cord mitochondria. Neuron 43:19-30.

Peet DJ, Janowski BA, Mangelsdorf DJ (1998a) The LXRs: a new class of oxysterol receptors. Curr Opin Genet Dev 8:571-575.

Peet DJ, Turley SD, Ma W, Janowski BA, Lobaccaro JM, Hammer RE, Mangelsdorf DJ (1998b) Cholesterol and bile acid metabolism are impaired in mice lacking the nuclear oxysterol receptor LXR alpha. Cell 93:693-704.

Pennetta G, Hiesinger P, Fabian-Fine R, Meinertzhagen I, Bellen H (2002) Drosophila VAP-33A directs bouton formation at neuromuscular junctions in a dosage-dependent manner. Neuron 35:291-306.

Pfeffer S (2003) Membrane domains in the secretory and endocytic pathways. Cell 112:507-517.

Poch O, Sauvaget I, Delarue M, Tordo N (1989) Identification of four conserved motifs among the RNA-dependent polymerase encoding elements. Embo J 8:3867-3874.

Presley JF, Ward TH, Pfeifer AC, Siggia ED, Phair RD, Lippincott-Schwartz J (2002) Dissection of COPI and Arf1 dynamics in vivo and role in Golgi membrane transport. Nature 417:187-193.

Quan G, Xie C, Dietschy JM, Turley SD (2003) Ontogenesis and regulation of cholesterol metabolism in the central nervous system of the mouse. Brain Res Dev Brain Res 146:87-98.

Raabe T, Manley JL (1991) A human homologue of the Escherichia coli DnaJ heat-shock protein. Nucleic Acids Res 19:6645.

Raiteri L, Zappettini S, Stigliani S, Paluzzi S, Raiteri M, Bonanno G (2005a) Glutamate Release Induced by Activation of Glycine and GABA Transporters in Spinal Cord is Enhanced in a Mouse Model of Amyotrophic Lateral Sclerosis. Neurotoxicology. Oct;26(5):883-92.

Raiteri L, Stigliani S, Patti L, Usai C, Bucci G, Diaspro A, Raiteri M, Bonanno G (2005b) Activation of gamma-aminobutyric acid GAT-1 transporters on glutamatergic terminals of mouse spinal cord mediates glutamate release through anion channels and by transporter reversal. J Neurosci Res 80:424-433.

Reaume AG, Elliott JL, Hoffman EK, Kowall NW, Ferrante RJ, Siwek DF, Wilcox HM, Flood DG, Beal MF, Brown RH, Jr., Scott RW, Snider WD (1996) Motor neurons in Cu/Zn superoxide dismutase-deficient mice develop normally but exhibit enhanced cell death after axonal injury. Nat Genet 13:43-47.

Roy L, Bergeron JJ, Lavoie C, Hendriks R, Gushue J, Fazel A, Pelletier A, Morre DJ, Subramaniam VN, Hong W, Paiement J (2000) Role of p97 and syntaxin 5 in the assembly of transitional endoplasmic reticulum. Mol Biol Cell 11:2529-2542.

Russ WP, Engelman DM (2000) The GxxxG motif: a framework for transmembrane helix-helix association. J Mol Biol 296:911-919.

Ryu EJ, Harding HP, Angelastro JM, Vitolo OV, Ron D, Greene LA (2002) Endoplasmic reticulum stress and the unfolded protein response in cellular models of Parkinson's disease. J Neurosci 22:10690-10698.

Schweizer A, Fransen JA, Bachi T, Ginsel L, Hauri HP (1988) Identification, by a monoclonal antibody, of a 53-kD protein associated with a tubulo-vesicular compartment at the cis-side of the Golgi apparatus. J Cell Biol 107:1643-1653.

Shastry BS, Giblin FJ (1999) Genes and susceptible loci of Alzheimer's disease. Brain Res Bull 48:121-127.

Shi Y (2002) Mechanisms of caspase activation and inhibition during apoptosis. Mol Cell 9:459-470.

Shimura H, Hattori N, Kubo S, Mizuno Y, Asakawa S, Minoshima S, Shimizu N, Iwai K, Chiba T, Tanaka K, Suzuki T (2000) Familial Parkinson disease gene product, parkin, is a ubiquitin-protein ligase. Nat Genet 25:302-305.

Simmen T, Aslan JE, Blagoveshchenskaya AD, Thomas L, Wan L, Xiang Y, Feliciangeli SF, Hung CH, Crump CM, Thomas G (2005) PACS-2 controls endoplasmic reticulum-mitochondria communication and Bid-mediated apoptosis. Embo J 24:717-729.

Skehel PA, Fabian-Fine R, Kandel ER (2000) Mouse VAP33 is associated with the endoplasmic reticulum and microtubules. Proc Natl Acad Sci U S A 97:1101-1106.

Skehel PA, Martin KC, Kandel ER, Bartsch D (1995) A VAMP-binding protein from Aplysia required for neurotransmitter release. Science 269:1580-1583.

Snapp EL, Hegde RS, Francolini M, Lombardo F, Colombo S, Pedrazzini E, Borgese N, Lippincott-Schwartz J (2003) Formation of stacked ER cisternae by low affinity protein interactions. J Cell Biol 163:257-269.

Soderholm J, Bhattacharyya D, Strongin D, Markovitz V, Connerly PL, Reinke CA, Glick BS (2004) The transitional ER localization mechanism of Pichia pastoris Sec12. Dev Cell 6:649-659.

Sollner T, Bennett MK, Whiteheart SW, Scheller RH, Rothman JE (1993) A protein assembly-disassembly pathway in vitro that may correspond to sequential steps of synaptic vesicle docking, activation, and fusion. Cell 75:409-418.

Soussan L, Burakov D, Daniels MP, Toister-Achituv M, Porat A, Yarden Y, Elazar Z (1999) ERG30, a VAP-33-related protein, functions in protein transport mediated by COPI vesicles. J Cell Biol 146:301-311.

Sriburi R, Jackowski S, Mori K, Brewer JW (2004) XBP1: a link between the unfolded protein response, lipid biosynthesis, and biogenesis of the endoplasmic reticulum. J Cell Biol 167:35-41.

Stornaiuolo M, Lotti LV, Borgese N, Torrisi MR, Mottola G, Martire G, Bonatti S (2003) KDEL and KKXX retrieval signals appended to the same reporter protein determine different trafficking between endoplasmic reticulum, intermediate compartment, and Golgi complex. Mol Biol Cell 14:889-902.

Swash M (1999) An algorithm for ALS diagnosis and management. Neurology 53:S58-62.

Tabak HF, Murk JL, Braakman I, Geuze HJ (2003) Peroxisomes start their life in the endoplasmic reticulum. Traffic 4:512-518.

Tagami S, Eguchi Y, Kinoshita M, Takeda M, Tsujimoto Y (2000) A novel protein, RTN-XS, interacts with both Bcl-XL and Bcl-2 on endoplasmic reticulum and reduces their anti-apoptotic activity. Oncogene 19:5736-5746.

Tai CL, Chi WK, Chen DS, Hwang LH (1996) The helicase activity associated with hepatitis C virus nonstructural protein 3 (NS3). J Virol 70:8477-8484.

Takahashi R, Imai Y (2003) Pael receptor, endoplasmic reticulum stress, and Parkinson's disease. J Neurol 250 Suppl 3:III25-29.

Tamori Y, Kawanishi M, Niki T, Shinoda H, Araki S, Okazawa H, Kasuga M (1998) Inhibition of insulin-induced GLUT4 translocation by Munc18c through interaction with syntaxin4 in 3T3-L1 adipocytes. J Biol Chem 273:19740-19746.

Tanji Y, Kaneko T, Satoh S, Shimotohno K (1995) Phosphorylation of hepatitis C virus-encoded nonstructural protein NS5A. J Virol 69:3980-3986.

Tardif KD, Mori K, Siddiqui A (2002) Hepatitis C virus subgenomic replicons induce endoplasmic reticulum stress activating an intracellular signaling pathway. J Virol 76:7453-7459.

Tardif KD, Mori K, Kaufman RJ, Siddiqui A (2004) Hepatitis C virus suppresses the IRE1-XBP1 pathway of the unfolded protein response. J Biol Chem 279:17158-17164.

Tirasophon W, Welihinda AA, Kaufman RJ (1998) A stress response pathway from the endoplasmic reticulum to the nucleus requires a novel bifunctional protein kinase/endoribonuclease (Ire1p) in mammalian cells. Genes Dev 12:1812-1824.

Tobisawa S, Hozumi Y, Arawaka S, Koyama S, Wada M, Nagai M, Aoki M, Itoyama Y, Goto K, Kato T (2003) Mutant SOD1 linked to familial amyotrophic lateral sclerosis, but not wild-type SOD1, induces ER stress in COS7 cells and transgenic mice. Biochem Biophys Res Commun 303:496-503.

Tu H, Gao L, Shi ST, Taylor DR, Yang T, Mircheff AK, Wen Y, Gorbalenya AE, Hwang SB, Lai MM (1999) Hepatitis C virus RNA polymerase and NS5A complex with a SNARE-like protein. Virology 263:30-41.

van Herpen RE, Oude Ophuis RJ, Wijers M, Bennink MB, van de Loo FA, Fransen J, Wieringa B, Wansink DG (2005) Divergent mitochondrial and endoplasmic reticulum association of DMPK splice isoforms depends on unique sequence arrangements in tail anchors. Mol Cell Biol 25:1402-1414.

Vance JE (1990) Phospholipid synthesis in a membrane fraction associated with mitochondria. J Biol Chem 265:7248-7256.

Voelker DR (2000) Interorganelle transport of aminoglycerophospholipids. Biochim Biophys Acta 1486:97-107.

Wang HG, Pathan N, Ethell IM, Krajewski S, Yamaguchi Y, Shibasaki F, McKeon F, Bobo T, Franke TF, Reed JC (1999) Ca2+-induced apoptosis through calcineurin dephosphorylation of BAD. Science 284:339-343.

Wang HJ, Guay G, Pogan L, Sauve R, Nabi IR (2000) Calcium regulates the association between mitochondria and a smooth subdomain of the endoplasmic reticulum. J Cell Biol 150:1489-1498.

Wang XZ, Harding HP, Zhang Y, Jolicoeur EM, Kuroda M, Ron D (1998) Cloning of mammalian Ire1 reveals diversity in the ER stress responses. Embo J 17:5708-5717.

Waterman-Storer CM, Salmon ED (1998) Endoplasmic reticulum membrane tubules are distributed by microtubules in living cells using three distinct mechanisms. Curr Biol 8:798-806.

Watson P, Stephens DJ (2005) ER-to-Golgi transport: form and formation of vesicular and tubular carriers. Biochim Biophys Acta 1744:304-315.

Wei MC, Lindsten T, Mootha VK, Weiler S, Gross A, Ashiya M, Thompson CB, Korsmeyer SJ (2000) tBID, a membrane-targeted death ligand, oligomerizes BAK to release cytochrome c. Genes Dev 14:2060-2071.

Weir ML, Klip A, Trimble WS (1998) Identification of a human homologue of the vesicle-associated membrane protein (VAMP)-associated protein of 33 kDa (VAP-33): a broadly expressed protein that binds to VAMP. Biochem J 333 (Pt 2):247-251.

Weir ML, Xie H, Klip A, Trimble WS (2001) VAP-A binds promiscuously to both v- and tSNAREs. Biochem Biophys Res Commun 286:616-621.

Welihinda AA, Tirasophon W, Kaufman RJ (1999) The cellular response to protein misfolding in the endoplasmic reticulum. Gene Expr 7:293-300.

Wiebe MG, Karandikar A, Robson GD, Trinci AP, Candia JL, Trappe S, Wallis G, Rinas U, Derkx PM, Madrid SM, Sisniega H, Faus I, Montijn R, van den Hondel CA, Punt PJ (2001) Production of tissue plasminogen activator (t-PA) in Aspergillus niger. Biotechnol Bioeng 76:164-174.

Wootz H, Hansson I, Korhonen L, Napankangas U, Lindholm D (2004) Caspase-12 cleavage and increased oxidative stress during motoneuron degeneration in transgenic mouse model of ALS. Biochem Biophys Res Commun 322:281-286.

Wyles JP, Ridgway ND (2004) VAMP-associated protein-A regulates partitioning of oxysterol-binding protein-related protein-9 between the endoplasmic reticulum and Golgi apparatus. Exp Cell Res 297:533-547.

Wyles JP, McMaster CR, Ridgway ND (2002) Vesicle-associated membrane protein-associated protein-A (VAP-A) interacts with the oxysterol-binding protein to modify export from the endoplasmic reticulum. J Biol Chem 277:29908-29918.

Xu Q, Reed JC (1998) Bax inhibitor-1, a mammalian apoptosis suppressor identified by functional screening in yeast. Mol Cell 1:337-346.

Ye J, Rawson RB, Komuro R, Chen X, Dave UP, Prywes R, Brown MS, Goldstein JL (2000) ER stress induces cleavage of membrane-bound ATF6 by the same proteases that process SREBPs. Mol Cell 6:1355-1364.

Yoneda T, Imaizumi K, Oono K, Yui D, Gomi F, Katayama T, Tohyama M (2001) Activation of caspase-12, an endoplastic reticulum (ER) resident caspase, through tumor necrosis factor receptor-associated factor 2-dependent mechanism in response to the ER stress. J Biol Chem 276:13935-13940.

Yoshida H, Matsui T, Yamamoto A, Okada T, Mori K (2001) XBP1 mRNA is induced by ATF6 and spliced by IRE1 in response to ER stress to produce a highly active transcription factor. Cell 107:881-891.

Young J, Stauber T, del Nery E, Vernos I, Pepperkok R, Nilsson T (2005) Regulation of microtubule-dependent recycling at the trans-Golgi network by Rab6A and Rab6A'. Mol Biol Cell 16:162-177.

Zachowski A (1993) Phospholipids in animal eukaryotic membranes: transverse asymmetry and movement. Biochem J 294 (Pt 1):1-14.

Zhang J, Yamada O, Sakamoto T, Yoshida H, Iwai T, Matsushita Y, Shimamura H, Araki H, Shimotohno K (2004) Down-regulation of viral replication by adenoviral-mediated expression of siRNA against cellular cofactors for hepatitis C virus. Virology 320:135-143.

Zhang T, Hong W (2001) Ykt6 forms a SNARE complex with syntaxin 5, GS28, and Bet1 and participates in a late stage in endoplasmic reticulum-Golgi transport. J Biol Chem 276:27480-27487.

Zimmerberg J, Kozlov M (2006) How proteins produce cellular membrane curvature. Nature Reviews Mol Cell Biol 7: 9-19.

Zundel W, Giaccia A (1998) Inhibition of the anti-apoptotic PI(3)K/Akt/Bad pathway by stress. Genes Dev 12:1941-1946.